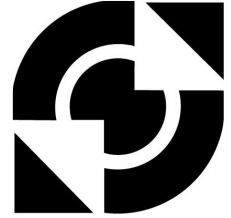


University of Twente

Department of
Mechanical Engineering



Chair of Structural Dynamics and Acoustics
Chair of Production Technology

Detection of delaminations based on dynamic behaviour

*Application of fibre bragg gratings for
dynamic damage detection*

Wouter Grouve
December 2006

CTW.06/TM-5543

Detection of delaminations based on dynamic behaviour

*Application of fibre bragg gratings for dynamic
damage detection*

W.J.B. Grouve

December 7, 2006

*Chair of Structural Dynamics and Acoustics,
Chair of Production Technology,
Department of Mechanical Engineering
University of Twente, Enschede*

SUMMARY / SAMENVATTING

English version

Nowadays, fibre reinforced plastics enjoy an increase in popularity. Their high specific strength and stiffness together with the high degree of design freedom have resulted in whole new variety of applications. However, due to their nature composites can suffer from complex damage types unknown to conventional materials. Common encountered examples include matrix cracking and delaminations. The detection of these damages can be a real challenge as it generally cannot be identified by visual inspection. The currently available non-destructive evaluation methods, such as ultrasonic evaluation, are time consuming and costly. In search for alternatives, part of the research concentrated on damage detection by monitoring changes in dynamic behaviour of structures. The first part of this thesis gives an overview of the existing literature on this subject. Various techniques and methods are discussed and compared.

The second part will underline the possibilities of damage detection based on dynamic behaviour. A theoretical analysis will show that delamination detection based on shifts in flexural resonance frequencies can give very accurate results. Also it is shown that measured frequency shifts of multiple modes can be used to locate the delaminations. The theory is experimentally validated with delaminated composite beam shaped test specimens.

Finally, an experimental programme is conducted to investigate the use of fibre bragg gratings for dynamic health monitoring. Fibre bragg grating have some advantages over conventional methods for capturing the response of a vibrating composite structure. The most notable is the fact that fibre bragg gratings can be embedded in composite structures, which protects them from environmental influences. More advantages can be found in the possibility of multiplexing, i.e. having multiple sensors on one fibre, and the strong resistance against fatigue. It is concluded that, despite the necessity of additional research, fibre bragg gratings will aid in the development of an applicable online health monitoring system.

Nederlandse versie

De populariteit van vezelversterkte kunststoffen groeit momenteel enorm. De hoge specifieke sterkte en stijfheid in combinatie met de grote mate van ontwerpvrijheid heeft geresulteerd in een heel nieuw scala van toepassingen. Echter, de complexe aard van composieten brengt ingewikkelde schadevormen met zich mee. Veel voorkomende voorbeelden kunnen worden gevonden in delaminaties of matrix cracking. Door middel van visuele inspectie kunnen deze schadevormen doorgaans niet worden herkend. In de huidige detectie methoden, zoals ultrasoon geluid, moet het gehele oppervlak gescand worden. Dit is een tijdrovende en dus kostbare bezigheid. De zoektocht naar alternatieve methoden heeft zich onder andere gericht op detectie van schade aan de hand van veranderingen in dynamisch gedrag van constructies. In het eerste deel van dit rapport worden de verschillende mogelijkheden op dit gebied vergeleken.

In het tweede deel worden de mogelijkheden van schade detectie op basis van veranderingen in dynamisch gedrag benadrukt. Een theoretisch model wordt gebruikt om aan te tonen dat delaminatie met grote nauwkeurigheid gedetecteerd kunnen worden op basis van gemeten eigenfrequenties. Daarnaast kan, door het meten van de verschuivingen van eigenfrequenties van verschillende trilmoden de delaminatie gelokaliseerd worden. Het theoretische model is experimenteel gevalideerd.

Als laatste wordt, aan de hand van een experimenteel programma, de mogelijkheid van het gebruik van fibre bragg gratings voor dynamische schade detectie onderzocht. Ten opzichte van meer conventionele sensoren hebben fibre bragg gratings enkele voordelen. Het feit dat the fibres ingebed kunnen worden in een composiet materiaal is de meest opvallende. De sensor wordt hierdoor beschermd tegen invloeden van buitenaf. Ook de mogelijkheid van multiplexing, dat wil zeggen het plaatsen van meerdere sensoren op een vezel, en de grote weerstand tegen vermoeiing kunnen worden gezien als voordelen. Ondanks het feit dat er nog veel onderzoek nodig is, kan geconcludeerd worden dat fibre bragg gratings een positieve invloed zullen hebben op de ontwikkeling van een toepasbaar online schade detectie systeem.

TABLE OF CONTENTS

Summary / Samenvatting	i
Preface	v
1 Introduction	1
1.1 General introduction	1
1.2 Thesis lay-out	2
1.3 Background information	2
1.3.1 Composites	3
1.3.2 Vibration based structural health monitoring	6
1.3.3 Fibre bragg gratings	7
2 Literature survey	9
2.1 General information	9
2.1.1 Factors to consider	10
2.1.2 Classification	11
2.1.3 Monitoring modal parameters	11
2.2 Frequency based detection methods	12
2.2.1 Literature on damage detection methods based on shifting resonance frequencies	12
2.2.2 Factors to consider when using resonance frequencies for health monitoring	18
2.3 Damping based detection methods	18
2.3.1 Literature on damage detection methods based on changes in damping	19
2.4 Other methods worth mentioning	22
2.5 Summary and concluding remarks	23
3 Theoretical modelling	27
3.1 Flexural vibration of delaminated beams	27
3.1.1 Basic assumptions and modelling	27
3.1.2 Static solution	29
3.1.3 Dynamic solution: Bernoulli-Euler beam equations	32
3.1.4 Dynamic Solution: Governing equations	34

3.1.5	Dynamic solution: Boundary and continuity conditions . . .	37
3.1.6	Dynamic solution: Analytical results	38
3.2	Application of the model for composite beams	42
3.2.1	Determination of flexural rigidity	42
3.2.2	Static solution	44
3.2.3	Dynamic solution	46
3.3	Finite element analysis	48
3.3.1	Beam elements with node coupling	48
3.3.2	Contact elements in combination with brick elements . . .	49
3.3.3	Results	49
3.4	Summary and concluding remarks	50
3.5	Nomenclature	52
4	Experimental validation	53
4.1	Programme outline	53
4.2	Experimental set-up	54
4.3	Stage A: Validation of the experimental set-up and sensor evaluation	55
4.3.1	Specimen preparation	56
4.3.2	Evaluation of the experimental results	57
4.3.3	Conclusions	64
4.4	Stage B: Application of fibre bragg gratings for health monitoring	65
4.4.1	Goals and proposed testing scheme	65
4.4.2	Experimental set-up for static testing	66
4.4.3	Specimen preparation	67
4.4.4	Evaluation of the experimental results	68
4.4.5	Discussion	71
4.4.6	Conclusions and recommendations	73
4.5	Stage C: Validation of theoretical analysis	74
4.5.1	Testing scheme	74
4.5.2	Evaluation and discussion	75
4.5.3	Conclusions and recommendations	78
5	Discussion and application	81
5.1	Discussion	81
5.2	Application	83
6	Conclusions and recommendations	85
6.1	Conclusions	85
6.2	Recommendations	87
A	Data acquisition and used hardware equipment	93
B	Specimen fabrication scheme	97
C	Specimen dimensions and delamination parameters	99

PREFACE

"After exhaustive research it can confidentially be concluded that the cow indeed got killed."

-WOUTER, Oct. 2006

The work reported in this thesis forms the climax of my study Mechanical Engineering at the University of Twente and provides a free pass to a sedulous and civil life. Curious for the time to come, I realize that the last six tedious years of education and personal development will inevitable be missed in the future.

The accomplishment of this thesis has been aided by a number of people. First, I want to thank Laurent Warnet for his infectious enthusiasm and great assistance during this research. I also want to thank the company FOS&S for providing the tested fibre bragg gratings and for their hospitality and helpfulness during our stay in Belgium. An honourable mention is deserved by Bert Wolbert, for his assistance during the validation programme, and Andre de Boer, for his supervision of this project. Last, but certainly not least, I want to thank my girlfriend for her support and continuous encouragement.

Exam committee:

- Prof. dr. ir. De Boer
- Dr. ir. Warnet
- Dr. ir. Van der Hoogt
- Dr. ir. Vlekken

INTRODUCTION

In this chapter the reader is provided with the background information necessary to understand the theme of this thesis. The first two sections give a general problem description and the lay-out of this thesis. In the third section general information about composites and fibre bragg gratings is presented.

1.1 General introduction

An increase in quality together with the development of new production methods have resulted in a growth of demand in composite materials. This goes especially for aerospace applications. Airbus and Boeing, for example, both have plans to manufacture an airplane in which a substantial part consists of fibre reinforced plastics. This is because composites combine high strength and stiffness with low weight. The application of composites however is also a cause of concern in the field of maintenance. The complexity of fibre reinforced plastics results in unconventional types of damage, like transverse cracking or delaminations. These damages can severely influence the mechanical properties of the composite materials, which in the past even resulted in catastrophic failure with loss of life.

Present methods which are able to detect these damage types are laborious and expensive. The lack of a cheap and effective damage detection system can be seen as a hindrance in the application of composite materials. Research in alternative non-destructive detection methods has increased enormously over the past decades. A part of this research concentrated on the development of an online detection system based on changes in dynamic behaviour. This idea is based on the fact that dynamic properties, like resonance frequencies or damping values, are directly related to the structural properties. A change in these mechanical properties, due to damage, results therefore in a change in dynamic behaviour. An advantage is that some dynamic characteristics can easily and cheaply be obtained by response

measurements at a single point on the structure, which implies that only a part of the structure needs to be accessible. Furthermore it is proved in this thesis that dynamic damage detection can give very good and reliable results.

1.2 Thesis lay-out

The first part of this thesis concentrates on the investigation of the possibilities and advantages of health monitoring based on dynamic behaviour. A literature survey is conducted in which the various possibilities on this subject are discussed and compared. A broad overview of different techniques is given and conclusions are drawn on present and future applicability. An analytical model is presented in which the flexural resonance frequencies of delaminated beams can be determined. It is shown that damage detection based on shifts of resonance frequencies is able to detect smaller delaminations than a similar static analysis. It is also proved that laminate lay-up plays an important role. As an addition two finite element models, describing a delaminated beam, are also presented. The theoretical findings are experimentally validated in a testing programme.

Furthermore the possibilities of fibre bragg gratings for damage detection based on dynamic behaviour are investigated experimentally. Fibre bragg gratings consist of a glass fibre with sensors for strain measurements and can be used to capture the response of vibrating structures. Fibre bragg gratings possess some advantages over conventional sensing systems. The first and most notable lies in the fact that the glass fibre can be embedded in the composite structure, which allows strain measurements inside the host material. Also embedding the fibres can be preferred over gluing strain gauges or accelerometers for practical reasons. The fact that strain can be measured at multiple location with only one fibre can be an advantage as well. Various tests are conducted to investigate the applicability of these fibre bragg gratings for health monitoring purposes.

1.3 Background information

Today, composites are widely used in all kind of fields. Generally, modern composite materials combine high strength and stiffness with low density. This makes them extremely useful in applications where weight plays an important role. First, the reader is provided with basic background information about composites. In the second part background information about vibration based health monitoring and fibre bragg gratings is provided. Knowledge of this section is desired to fully understand theme of this thesis. Readers with experience in these fields can skip this section and continue with the next chapter on page 9.

1.3.1 Composites

By the broadest definition, a composite material is one in which two or more materials that are different are combined to form a single component. It has to be stipulated that the constituents retain their identity; that is, they can still be physically identified and do not merge or dissolve in one another. Composites combine the material properties of its components in order to obtain properties, unavailable in natural occurring materials. The constituent materials can be divided in two categories: matrix and reinforcement. At least one fraction of both is required. Due to the enormous variety in available matrix and reinforcement materials the potential is tremendous.

One commonly used composite in the modern world is reinforced concrete. This building material combines concrete and steel. Concrete is a hard material with a very high compressive strength. In contrast, steel has a very high tensile strength. Combining these materials results in a composite with superior mechanical properties. However when speaking about composite materials or composites today, few refer to reinforced concrete, instead one often refers to the highly engineered combinations of polymers and fibre materials such as graphite, carbon or glass. This type of composite is ordinarily known as *fibre reinforced plastic* or FRP.

Fibre reinforced plastics

Fibre reinforced plastics are widely used in aerospace, automotive and marine industries. They comprise a polymer matrix reinforced with fibres. The fibres in these composites are, in most cases, used for their high strength and stiffness, while the matrix transfers loads, binds the fibres together and protects them from harsh environmental influences. Given the nature of FRP's there are virtually infinite ways of combining matrix and fibres. Every composite material can be tailored specifically for a certain application. Fibre reinforced materials have some great advantages over ordinary natural occurring materials. These advantages may be summarized as:

- **High specific strength and stiffness:** Most fibre reinforced plastics combine a high stiffness and high strength with a low weight. Compared to steel and aluminium, fibre reinforced plastics have a much higher specific stiffness and strength.
- **High durability:** Fibre reinforced plastics possess a high resistance against corrosion. Besides FRP's also have a fair resistance against fatigue. These properties make fibre reinforced plastics extremely useful for applications in harsh environments.
- **Design flexibility:** The anisotropic character of composites opens new possibilities for designers. Material properties can be tailored, in some extend,

to meet certain design demands, which allows the designer to save material amounts. Furthermore, fibre reinforced plastics can be formed into many complex shapes during the manufacturing process.

- **Cost-effective:** Using fibre reinforced plastics can effectively reduce manufacturing costs. Parts that formerly consisted of several smaller steel components can, with composites, be manufactured into one larger part. Also, compared to steel tooling bodies, the initial investment in manufacturing equipment is relatively low.

The benefits of fibre reinforced plastics over steel are notable. The research in composites has flourished over the past decades and composites are more and more employed over a variety of applications.

Carbon fibre reinforced plastic

Carbon fibre reinforced plastic (CFRP or CRP), is a strong, light and very expensive composite material or fibre reinforced plastic. As with most composites, the material is commonly referred to by the name of its reinforcing fibres.

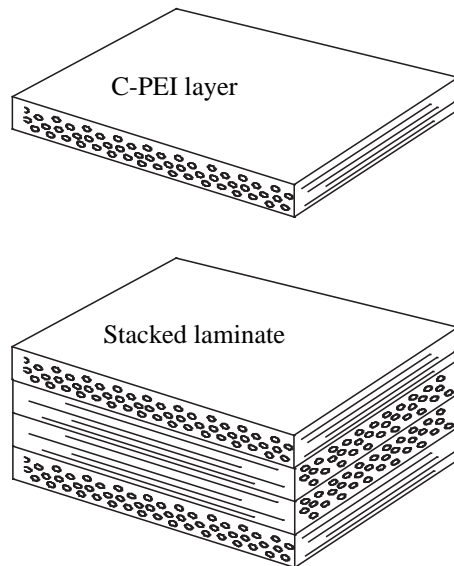


Figure 1.1: Carbon-polyetherimide layer and stacked laminate.

Carbon fibres possess high strength and stiffness. The plastic is most often an epoxy, but other plastics, such as polyester, vinylester but also some thermoplastics, are also used. All these plastics have a low density. As stated before the plastic binds and protects the fibres and transfers loads between them. The high specific strength and stiffness causes carbon fibre reinforced plastics to have many applications in aerospace and automotive fields. The production process of fibre reinforced plastic is based on the bonding of fibres and matrix and obtaining the purposed product shape. Vital step in this process is to impregnate the matrix material in order to enclose the fibres and to obtain the product shape. The process in which most CFRP is made varies, depending on the piece being created and how many of this particular product are going to be produced.

The used processes vary from traditional autoclave pressing to liquid composite

moulding. An overview of these methods can be found in [37]. Test specimens used in this thesis were all fabricated by hot pressing prepreg carbon reinforced polyetherimide, the production scheme is given in appendix B. In this process layers consisting of pre-impregnated carbon fibres in one direction are stacked in the desired laminate lay-up, this is illustrated in figure 1.1. The pile of prepreg material is then placed in a heated press in which the polyetherimide matrix is melted. Pressure is applied to ensure good consolidation of the laminate. After the cooling process, in which the pressure is preserved, a laminated plate is manufactured.

FRP damage types: transverse cracking and delaminations

Due to their complex nature and the required production process, FRPs suffer from various damage types unknown to conventional materials. One of the first damage mechanisms to occur is known as transverse cracking or matrix cracking. This type of crack grows parallel to the fibre and in the thickness direction of the laminate. The formation of transverse cracks does rarely mean the total fracture of a laminate, as it does not affect the load carrying capacity of the fibres. However, transverse cracking influences the mechanical and thermal properties of the laminate. Most importantly, this type of cracking forms a trigger for further damage mechanisms. Figure 1.3 shows a simple illustration of a transverse crack. In figure 1.2 it can be seen that the crack runs between the fibre interfaces. Transverse cracks can be caused by in-service loading, e.g. due to impact. Also the difference in thermal expansion coefficient between fibre and matrix can, in the production phase, be a cause of matrix cracking.

Delamination is a damage type that generally is preceded by transverse cracking. The term delamination is directly related to the process of laminating. Just in the same way as producing a laminate is about bonding different layers to each other, delaminating is about debonding the layers. It is therefore a crack, which again runs in a plane parallel to the fibres, but at the interface between two layers. Chronologically, it is recognized that a delamination mostly initiates from the tip of a transverse crack. Figure 1.3 also shows a delamination at the interface between the 0° and the 90° layer. Figure 1.4 shows a micrograph of a cross-section

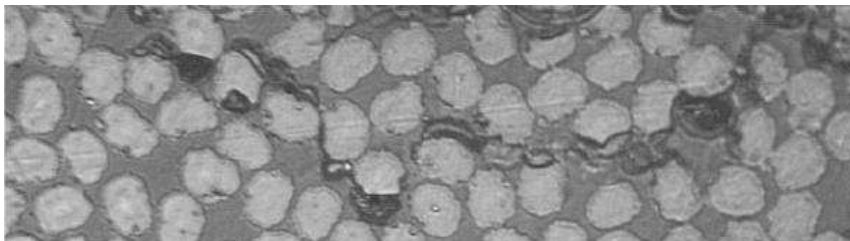


Figure 1.2: Micrograph of cross-sectioned 90° layer in the region of a transverse crack.

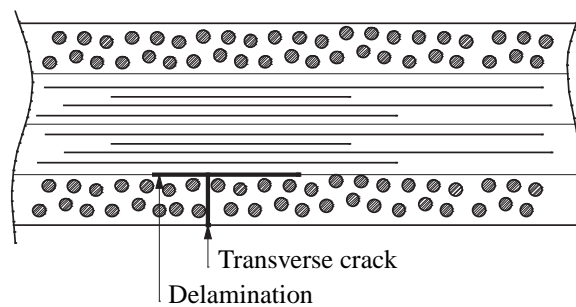


Figure 1.3: Schematic representation of transverse crack and delamination in a laminate.

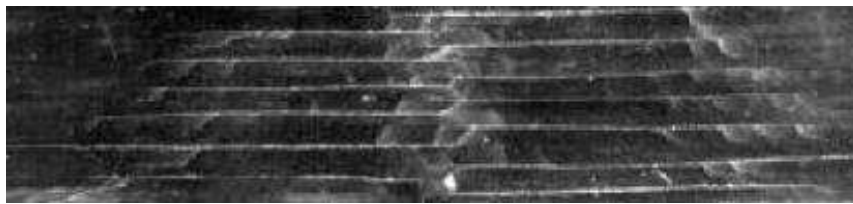


Figure 1.4: Cross-section of a laminate with transverse cracks and delaminations.

of a laminate with both transverse cracks and delaminations. Delaminations can seriously affect the thermo-mechanical properties of the laminate.

1.3.2 Vibration based structural health monitoring

Health monitoring consist of the continuous assessment of the condition of a structural of mechanical system. Ideally, a health monitoring system is able to detect damage at the moment it originates. A working system should then be able to replace current expensive maintenance routines. The idea to monitor dynamic parameters is based on the fact that modal parameters are function of the physical properties, e.g. Youngs modulus or geometry, of the structure. Changes in these physical properties will therefore result in detectable changes in modal parameters. The process of modal based damage detection reduces eventually to some form of pattern recognition problem [10]. In practice the structure under consideration is excited, either forced or by environmental forces. The response is captured and dynamic properties, like mode shapes, resonance frequencies or damping values, are determined. The obtained modal data is compared to either a healthy reference model or to some form of mathematical model. Deviations are used as a damage indicator.

1.3.3 Fibre bragg gratings

A fibre bragg grating is a segment of an optical fibre that reflects particular wavelengths of light. This is achieved by altering parts of the fibre core so that their index of refraction is slightly higher than normal. As a result, the structure will transmit most wavelengths of light, but will reflect certain specific wavelengths. This is illustrated in figure 1.5. The grating is created by burning a periodic variation in the index of refraction into the core of an optic glassfibre. The reflected wavelength is related to the refractive index of the material and the grating period. The basis of a fibre bragg grating based sensor system lies in the variation of this grating period as a result of stretching or compressing of the optical fibre. Monitoring the shifts of wavelengths can be used to determine the strain of the grating. By embedding fibre bragg gratings in a host structure the strain inside the host material can be determined. This embeddability is an advantage over conventional strain gauges. Other advantages can be found in the possibility of multiplexing, the strong resistance against fatigue and the fact that no electric signal is required. Multiplexing uses several bragg gratings with different reflective wavelengths on one fibre. This way the strain at different locations can be obtained with only one fibre. By coupling the strain measurements to material properties like thermal expansion coefficient or Youngs modulus other parameters, like temperature or stress, can be acquired. However in this thesis only the pure strain measurements are used.

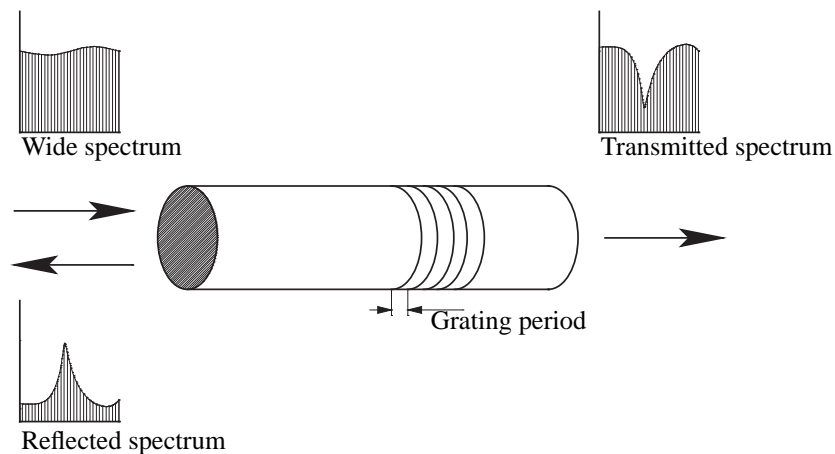


Figure 1.5: Working principle of fibre bragg gratings.

LITERATURE SURVEY: HEALTH MONITORING BASED ON DYNAMIC BEHAVIOUR

A combination of failure of equipment, technological advancements and economic considerations have resulted in an increase in research and publications on the subject of health monitoring over the past few decades. Especially the prospect of reducing costs on maintenance has been a major motive in health monitoring research. A fully operating and reliable monitoring system could replace expensive routine checks. A large part of this research concentrates on the application of health monitoring based on dynamic behaviour. This section gives an overview of the available literature on this subject.

2.1 General information

The general concept of dynamic health monitoring is based on the fact that modal parameters, like natural frequencies, modal damping or mode shapes, are a function of physical properties like mass, stiffness or geometry. A change in structural integrity, induced by damage, will therefore result in a change in modal parameters. Of course the opposite is also true. A measured change in modal parameters might be preceded by a change in structural integrity and geometry. This fact could be used in practice by subjecting the structure under consideration to a modal analysis and compare the results with some sort of healthy reference model. Every deviation in modal parameters (resonance frequency, modal damping or mode shapes) from the model signifies some form of damage. This means that in fact, as stated in [10], the process of modal-based damage detection reduces to some form of pattern recognition problem.

Cawley and Adams [4] noted in 1979 that the measurement of dynamic characteristics of a structure as a form of structural health monitoring had a promising future. The dynamic characteristics (e.g. resonance frequencies or damping values) of a structure can be measured at a single point on the structure and are independent of the chosen position, with exception of nodal points of modes of interest. This means that dynamic testing does not require access to the whole structure, which is an advantage over conventional 'scanning' types of health monitoring, like the use of ultrasound. Salawu [28] added that modal parameters can easily and cheaply be obtained. A transducer monitors structural responses to artificially or environmentally induced excitations. In general low input excitation levels are required since the input energy is dynamically amplified.

2.1.1 Factors to consider

Besides the obvious advantages, Farrar and Doebling [10] listed some factors to consider when applying modal data for health monitoring. The first, and most important, is that standard modal data represents some form of data compression, which effectively results in loss of data. The main reason of this loss can be found in the fact that for a linear system the modal parameters are independent of excitation signal characteristics (amplitude and frequency) and excitation location, while the time histories are not. Furthermore the sampling parameters may limit the ability to resolve the higher frequencies, which effectively also results in loss of data.

Identifying different modes contributing to the response can in practice also prove to be difficult because of coupling between modes that are closely spaced in frequency. Especially at higher frequencies this problem is often encountered, as modal density tends to be greater. Also, the introduction of systematic errors from windowing data or those that arise from changing environmental conditions during the test, will tend to make the identified modal parameters less representative. A practical issue to take seriously into account concerns the fact that damage is generally a local phenomenon. In order to detect these local integrity changes one is particularly interested in the local response of the structure. The fact that local responses are generally captured by higher frequency modes causes difficulties [28]. In order to produce measurable responses from a high frequency excitation more energy is required in comparison with lower frequency excitation. Together with the loss of information these factors form the major difficulties in current modal based health monitoring. One logical solution would be to use the time-history data for damage detection. However, despite the difficulties that arise with detection based on modal data, it is far more difficult to detect changes in material properties directly based on measured time histories.

2.1.2 Classification

Health monitoring or damage identification methods can be classified in different ways. Two of them are commonly known and widely used. The first classification distinguishes two approaches, namely *non-model* and *model* based techniques. In a *non-model* based technique the results are compared with the results of a measurement prior to setting the structure in service. Deviances in modal parameters indicate the presence of damage. In a *model* based technique the modal analysis is compared with some form of mathematical model. This can either be an analytical or finite element model. The advantage of using model based techniques is that these could well be extended to give information about the location and severity of the detected damage. General model based techniques imply that the damage on the structure can be classified as linear. This means that an initially linear-elastic structure remains linear-elastic after damage. The response of the structure can still be modelled using linear equations of motion. However, when a structure behaves non-linear after damage, the effect is classified as non-linear damage. An example is the opening and closing of a formed delamination, see figure 2.3. Linear equations of motion do not hold any longer and modeling the behaviour of the structure becomes problematic. However the observation of nonlinear behaviour in a supposedly linear-elastic structure can be a strong indicator for damage.

Another classification system for health monitoring is given by Rytter [27]. Rytter defines four levels of damage identification.

- Level 1: Determination that damage is present in the structure.
- Level 2: Level 1 plus determination of the geometric location of the damage.
- Level 3: Level 2 plus quantification of the severity of the damage.
- Level 4: Level 3 plus prediction of the remaining service life of the structure.

In order to obtain level 3 damage detection a mathematical model is required, this makes level 3 and 4 a model based technique. Non-model based techniques can only provide health monitoring up to level 2 [27].

2.1.3 Monitoring modal parameters

There exists a wide variety of literature about modal based health monitoring. The earliest literature studies the relation between changes in resonance frequencies or modal damping and structural damage. Adams and Cawley [1, 2, 3, 4, 5] were among the first to actively research this subject. A part of the available literature about these methods will be summarized in the following two sections. Subsequently research concentrated also on other parameters. Zou *et al.* [40] and Farrar

and Doebling [10] mention several options like mode shape changes, curvature changes or thermography. The most promising techniques will be mentioned in section 2.4.

2.2 Frequency based detection methods

Damage can influence mass, Young's modulus or the second moment of area, which in turn can result in a change in resonance frequencies. By monitoring these frequencies it should be possible to acquire information about structural health. Salawu [28] noted that shifts in resonance frequencies are probably the most useful for detecting damage in structures. An additional advantage, besides the general ones for dynamic measurements mentioned before, can be found in the fact that resonance frequencies show less statistical variation from random error sources than other modal parameters. Also the knowledge on resonance frequencies is relative great.

2.2.1 Literature on damage detection methods based on shifting resonance frequencies

Adams *et al.* [1] found that damage could be roughly located by examining frequency shifts of multiple vibration modes. This is based on the fact that the stress distribution through a vibrating structure is non-uniform and different for each mode. This means that every mode will be influenced differently by local changes in dynamic stiffness and thus damage. If the damage is located at a point with minimum stress for some mode, the effect on the natural frequency for this mode will be minimal. Naturally, the opposite is also true. The effect of damage on natural frequencies is maximal in case the damage is located at points with maximum stress. Adams also added that the size of the frequency changes may be related to the severity of the damage.

Cawley and Adams [5] used this to develop a method to locate and roughly quantify damage in fibre reinforced composite structures by using shifts of natural frequencies only. For determining the location and severity of the damage, which is in fact a level 3 problem, a mathematical model is required. Cawley and Adams based damage location on the fact that the ratio, $\delta\omega_i/\delta\omega_j$, of the frequency changes due to damage in two modes i and j is only a function of the position of damage within the structure. The ratio $\delta\omega_i/\delta\omega_j$ for different damage locations is theoretically determined. Positions where the calculated ratio equals the experimentally measured value are then possible damage sites. The theoretical frequency changes as a result of the damage were determined by performing a sensitivity analysis. The analysis of one mode pair gives a locus of possible damage sites. In order to achieve a unique solution, several mode pairs have to be used. In the case of symmetry a

minimum number of solutions equal to the degree of geometric symmetry can be found. The most likely damage site is calculated with an error function.

Cawley and Adams [3] used this method to detect different types of damage inflicted on composite structures, which were representative of those encountered in aerospace. Damage types included holes, saw cuts, crushing, impact and local heating. The lower resonance frequencies of various structures were determined by Cawley and Adams. It was shown that it was possible to detect, locate and roughly quantify all these types of damage. The testing showed that it was possible to detect damage equivalent to the removal of approximately 0.1% of the area of a shell structure.

Hassiotis and Jeong [14] noted that this method has the disadvantage that a sensitivity analysis of all the individual elements has to be carried out. This is a time consuming activity and calls for a large data storage capacity for complex structures. Also, the possibility of damage in more than one location is excluded. Instead Hassiotis and Jeong [14] tried to reconstruct the element stiffness matrices from changes in natural frequencies. A first-order perturbation of the eigenvalue problem is used to yield the relation between the variation in global stiffness matrix and eigenvalues. Then, the variation of the stiffness matrix is expressed as the summation of changes proportional to the element stiffness matrices. The result is a set of simultaneous equations that relate changes in eigenvalues to those of elements stiffnesses. Using only a small number of resonance frequencies, Hassiotis and Jeong were able to successfully detect simulated damage of a cantilever beam and an iron frame. Damage, in the order of 10% reduction in stiffness, was identified extremely accurately when exact data was used. However, when the data was corrupted with random noise it proved very difficult to successfully detect damage. This was because the changes in eigenvalues due to damage was sometimes less than the change due to noise. If the data was corrupted with random white noise it was only possible to detect damage equal to a reduction of 40% of the stiffness.

Transverse cracks or notch detection

The articles discussed above all describe methods for damage detection based on a general decrease in stiffness due to damage. These methods could well be applied to all types of damage. However, a wide variety of literature is dedicated to the investigation of the relation between resonance frequencies and specific types of damage, for example notches or delaminations. These damage types are often, for research purposes, inflicted on simplified structures, like cantilevered beams. The following three articles comprise a damage type that can be quantified as a notch or transverse crack.

Gudmundson [11] presented a method which predicts changes in resonance frequencies resulting from cracks, notches or other general geometric changes. Chang-

es in resonance frequencies are shown to be dependant on the strain energy of a static solution. Patil and Maiti [24] explained that the strain energy of a beam containing a crack reduces because the beam can deform easier to the same extent as the uncracked beam. The reduction is found to equal the extend of energy stored in a fictitious bending spring, which represents the crack. See figure 2.1. Gudmundson couples this reduction of strain energy with changes in resonance frequencies. The proposed technique was checked on three different cases. In the first case analytical data was compared with experimental data gathered by Wendtland [38]. The two other cases compared the analytical results with a finite element analysis. In all cases the analytical results compared well with the experimental results.

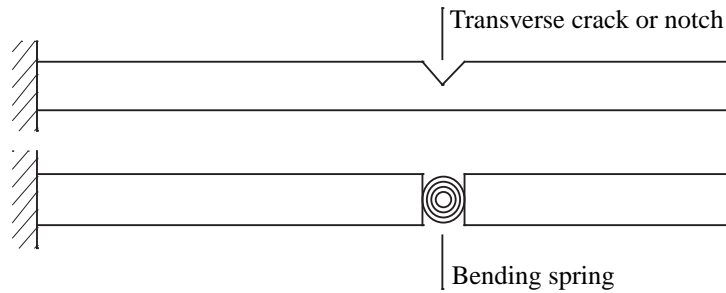


Figure 2.1: Bending spring representing a transverse crack or notch.

Salawu [28] noted that through width transverse cracks could well be represented by bending springs. The local spring stiffness can be computed from the strain energy function and depends on crack depth and beam thickness. The beam is divided in segments separated by bending springs. For every segment the Bernoulli-Euler beam equations are solved for appropriate boundary and continuity conditions. Ostachowicz and Krawczuk [22] determined a flexibility function which describes the equivalent spring stiffness for both single and double sided cracks. Chondros *et al.* [7] developed a similar function, with slight differences.

Tomasel *et al.* [33] carried out some experiments in order to compare both [22, 7] methods for determining equivalent spring stiffness. The measurements determined resonance frequencies using an optical experimental set-up. Both methods showed good agreement with measured values for crack depths up to 80% of the total height of the beam. It was, however, evident that the best approach was given by Chondros *et al.* [7].

Delamination detection

Delaminations are another damage type. In fact this damage type can be seen as the most commonly observed form of damage. Delaminations may originate during fabrication, due to incomplete wetting or entrapped air pockets, or may

be service induced, such as by impact or fatigue loading. The difficulties with delaminations can be found in the fact that they arise inside the laminate. This type of damage is therefore difficult to identify by visual inspection. However the resulting degradation in strength and stiffness can be disastrous. There is a wide variety of literature available on the subject of detecting delaminations through dynamic analysis of structures.

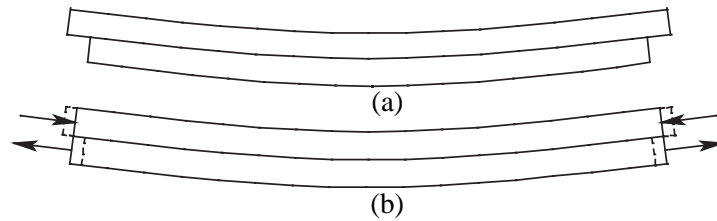


Figure 2.2: Delaminated layers without (a) and with (b) coupling effects.

Ramkumar *et al.* [26] were among the first to present a simplified analysis to estimate the free flexural vibration frequencies of a laminated beam with an interlaminar delamination. The through width delamination can exist at an arbitrary axial location. The flawed beam is analyzed as four separate beams that are joined together with the appropriate boundary and continuity conditions. However the theory did not match experimental results very well. The analytical prediction was found to underestimate the flexural stiffness.

Wang *et al.* [35] proposed a similar delaminated beam theory. An analytical model was proposed based on the classical beam theory. However Wang did, in contrast with Ramkumar, include the coupling effects between longitudinal and flexural motion, see figure 2.2. The calculated results did now show good agreements with the experimental results. However, Mujumdar and Suryanarayan [21] found that the theory proposed by Wang *et al.* could lead to mode shapes that are not physically admissible, as in figure 2.3. They extended the theory with the assumption that the delaminated layers of the beam are constrained to have identical transverse displacement. Results of an experimental study on vibration of beams with mid-plane as well as off-midplane delaminations verified the validity of the analytical model over a wide range of values of the delamination parameters. In both studies the basic assumption is that in vibration the delamination always remains either open [35] or closed [21].

Lee attempted [20] to include the interaction between opening and closing vibration modes of the delaminated region. The opening and closing of the delamination can be classified as non-linear motion which causes considerable difficulties. To overcome these problems, Lee assumed that the period of motion can be split in two states of mode shapes which are considered separately; one in which a delamination opens and one in which delamination closes. He stated that, assuming

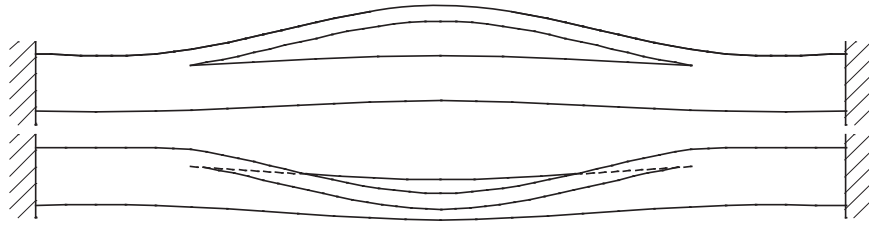


Figure 2.3: Example of a mode shape that is physically not admissible.

that both layers have the same velocity and deflection at the transition between the two modes, the total period T can be approximated by:

$$T = \frac{1}{2}(T_{open} + T_{closed})$$

As result, from the relation between period and resonance frequency, the resonance frequencies can be estimated as follows:

$$\omega = \frac{2 \cdot \omega_{open} \cdot \omega_{closed}}{\omega_{open} + \omega_{closed}}$$

In which ω_{closed} and ω_{open} represent the resonance frequencies for a particular mode in the case of constrained or free delaminated layers. Lee noted that the velocity matching assumption is somewhat inappropriate for longer, i.e. 60% of the specimens length, delaminations. This is because the first vibration mode for delamination opening show almost pure local vibration of the thin upper layer, while delamination opening-suppressed mode is global. The result is a substantial difference between the two cases. For the case of large delaminations a more rigorous approach, which can predict interaction between open and closed delamination states accurately, is necessary.

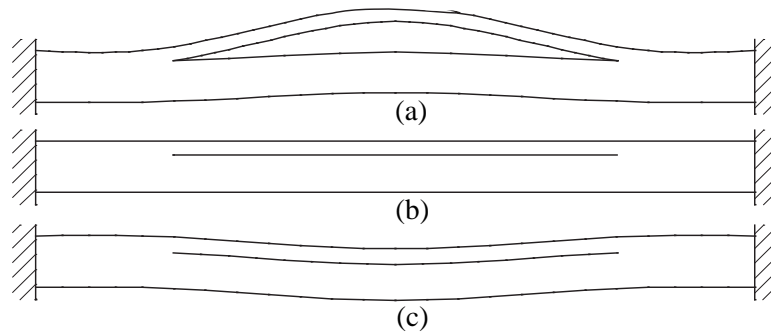


Figure 2.4: Vibration mode change during the period of motion for a clamped beam.

Diaz Valdes and Soutis [34] measured the effect of enlarging a small delamination in a cantilevered beam on natural frequencies. The measurements were taken in the frequency range from 8 to 13 kHz, because it was expected that the effects of small delamination are more significant at higher modes. A sharp scalpel was used to enlarge an artificial introduced delamination. Every time the size of the delamination was increased a modal analysis was conducted in order to monitor changes in natural frequency and damping. In this fashion the delamination was gradually grown from 0.23% to 3.84% of the total surface area. This type of artificial delamination is thought to better represent damage patterns observed in fatigue loading than through width delaminations with sizes covering 5% to 60% of the total surface area. The results show clearly that all resonance frequencies shift to lower values with increasing damage size. The absolute frequency changes are quite large and detectable, i.e. in the order of ten to a few hundred Hz. There is also a small attenuation of the peak level and sharpness as damage grows, which indicates an increase in damping. More on this subject can be found in section 2.3.

Tenek *et al.* [32] studied the effect of delaminations on the natural frequencies of plates. A finite element method was adopted for this purpose. The method showed good comparison with experimental results for the case of cantilever laminated plates. The results for delaminated plates indicated that even for large flaw sizes, the first few resonance frequencies are not significantly affected. However, for higher frequencies an overall reduction proportional to the delamination size was observed. There is a possibility that at certain excitation frequencies, delaminations exhibit independent dynamic plate behaviour and vibrate out of phase with the rest of the structure. Tenek *et al.* also studied the possibilities of utilizing thermographic and thermoelastic non-destructive evaluation techniques. They found that at particular frequency regions, local flaw vibration causes dissipation of mechanical energy into heat, which in turn can be detected. This is further discussed in section 2.4.

Chrysochoidis and Saravanos [8] found an apparent linear relation between the number of resonance peaks in a frequency response plot and the size of a delamination. Experiments show a clear increase in resonance peaks between 0 and 2kHz. This phenomenon can be partially attributed to the appearance of additional opening and sliding mode shapes in the delaminated region, which vibrate either individually or coupled with the bending modes of the beam. Also the shifting of resonance frequencies to lower values as the delamination increases contributes to the increased modal density.

The methods described above all concern a linear damage effect. The structures all behave linearly after the inflicted damage. In reality however, it's questionable whether this assumption will hold. One can easily imagine that an originated crack will open and close under varying load. Damage detection can in this case reduce to identifying non-linear behaviour.

2.2.2 Factors to consider when using resonance frequencies for health monitoring

In some of the techniques mentioned above the damage is modelled as either a bending spring or delamination. Changes in resonance frequencies are calculated for these damage types. A fundamental limitation of these methods is that it should be possible to represent the actual damage with these models. This will not always be the case. Salawu [28] lists other factors to consider when using shifts in resonance frequencies for damage detection. For successful application of vibration data, measurements should be taken at points where all the modes of interest are well represented. The simplest way of achieving this is to perform a theoretical vibration analysis prior to testing in order to identify the desired measurement points.

A full understanding of the effect of damage on resonance frequencies is vital. Also an idea of the sensitivity of changes in support or environmental, such as temperature or humidity, conditions is required. Changes in resonance frequencies of about 5% are measured as a result of changes in ambient conditions only. Quantitative relationships between resonance frequencies and environmental factors are rare. This is because many variables are involved, which makes it difficult to assign numerical factors. The effect of pre-loading and residual stress on frequency response was tested by Kawiecki [16]. From the various tests it can be concluded that changes in loading conditions or residual stresses can cause resonance frequencies to shift. As a result of these external influences, the changes in frequencies should be considerable in order to detect damage with confidence.

Other factors to consider are the consistency and reliability of measuring procedures. Besides, Doebling *et al.* [9] mention that the somewhat low sensitivity of the lower resonance frequency shifts to damage requires very precise measurements or large levels of damage. Currently, using frequency shifts to detect damage appears to be more practical in applications where such shifts can be measured very precisely in a controlled environment, such as for quality control in manufacturing.

2.3 Damping based detection methods

There is little literature available on the effect of damage on damping. Zou *et al.* [40] mention that damping is more sensitive to damage than stiffness or mass. This makes damping a potential interesting parameter to monitor for damage detection. Chandra *et al.* [6] give two types of damping due to damage. The first consists of frictional damping, which is a result of slip in the unbound regions between fibre and matrix interface or delaminations. The other type is damping due to dissipation of energy as a result of visco-elastic deformation in the area of matrix cracks, broken fibres etc. In the following section a part of the available literature is reviewed.

2.3.1 Literature on damage detection methods based on changes in damping

Guild and Adams [12] described a method in which the measurements of specific damping capacity (SDC) are used to detect very small cracks in unidirectional glass-fibre reinforced polyester. The specific damping capacity is defined as the ratio of the energy absorbed by the beam during one cycle to the total strain energy stored by the beam during that cycle. The energy stored can be calculated from the power input to the exciting coils. The total strain energy absorbed by the beam can be calculated from the deflection measured at a point, together with the theoretical mode shape. A change of SDC is based on the principle that cracks will cause a significant loss of energy. Guild and Adams extended a method proposed by Adams and Bacon [2] in which measurements of SDC of composite materials could provide relative insight into their lay up. Previous result in the article by Adams and Bacon indicated that the method could be used for the detection of cracks. Guild and Adams developed an apparatus that is able to excite beams in a free-free flexural vibration, the apparatus is described in [13]. Guild and Adams [12] introduced cracks in the central region of glass fibre reinforced plastic beams using four-point flexural loading. The growth of a crack was monitored using acoustic emission. The beams were excited and the specific damping capacity was determined. With the proposed method Guild and Adams were able to successfully detect small cracks in glass fibre reinforced plastic beams. The measurements indicated a notable change in SDC after cracking was observed by acoustic emission. These cracks were small and not visible by naked eye.

Kyriazoglou *et al.* [18] measured the specific damping capacity of different types of composite beams in flexural vibration. An experimental set-up similar to the one used by Guild and Adams [13] was used. Tests have been conducted before and after damage was introduced. Homogeneous damage was induced using quasi-static loading in tension or as a result of cyclic loading. The results showed that the specific damping capacity is more sensitive to damage than resonance frequencies. Transverse cracks in continuous GFRP as a result of quasi-static loading were clearly measurable. Also for damaged cross-ply GFRP specimens a clear change in SDC was noticed. It should be mentioned however that the change in SDC is dependant on laminate lay-up. The cracks in the transverse layer have far greater effect on the SDC when they are in the outer plies of the beam. The explanation for this behaviour is believed to arise from the constraint imposed on the crack opening by the outer plies. However, a change in specific damping capacity was also measured when cracking occurred in the inner plies. The changes in SDC for woven GFRP laminates were not so consistent. When, in quasi-static loading, the applied strain exceeded 0.6% a significant increase in SDC was observed. However, no consistent change was measured after application of higher levels of strain. As for the cyclic loading, the specific damping capacity clearly increases with an increasing number of cycles. It is concluded by Kyriazoglou *et al.* that damping

properties are sensitive to the presence of cracks. By monitoring the specific damping capacity damage can successfully be detected.

Lee *et al.* [19] measured damping coefficients with use of an impulse technique developed by Sun *et al.* [31]. Specimens are cantilevered and excited by a hammer blow. A non-contact motion transducer monitored the displacement of the free end. Signals acquired by the motion transducer and hammer were fed into a FFT analyzer which displayed a frequency response function. Damping was derived from this function. Lee *et al.* utilized the technique to measure the influence of different types of damage on damping. The following conclusions were drawn from the measurements:

- For notches, the experimental results show that the changes in damping for different modes depend on the location of notches. That is, the change in damping may be significant in one mode and may not be in another mode. A similar phenomenon was encountered earlier in section 2.2 where it is explained that the ratio of frequency change for two modes could also be used to predict damage location. The same technique could be employed with damping changes for two modes.
- Rather disappointing results were obtained when Lee *et al.* tried to measure damping changes as a result of matrix cracking. Cracks were introduced in specimens by means of a three point bending test. Even for the specimen which was bend with a force equal to 90% of the maximum bending force, before failure, no significant increase in damping was observed. Lee *et al.* believed that the changes in damping due to matrix cracking may be overwhelmed by the changes due material imperfections. In addition it was noticed that the damping measurement was strongly dependent on clamping conditions.
- For artificial induced delaminations the increase in damping is proportional with the size of the delaminated area. Generally speaking it seemed that the damping measurements of the second and the third modes show significant changes while the first mode has the lowest sensitivity.
- In order to analyze the effect of material imperfections, specimens with inclusions were studied. The measurements show little change in damping. This is probably due to the fact that the inserts are well bonded with the laminate, so that there is no real friction between insert and laminate.

Overall Lee *et al.* concluded that the impulse technique is quite capable of detecting both severity and location of the notches. Also for delamination the technique is quite promising. For matrix cracks and material imperfections however, the changes of damping are insignificant. Lee *et al.* suggested that in order to detect microdamage the wave length of the impulse should be in the same order or less than that of microdamage.

Kawiecki [16] used piezotransducers to record a frequency transfer function of specimens. The modal damping magnitudes were determined using the halfpower point approach. Damage was simulated with viscoelastic patches. All measurements show that changes in damping are clearly visible and detectable. Kawiecki concludes that the results are an important complement to monitoring methods based on detection of changes in stiffness.

Although sufficient literature is available on crack or delamination prediction and propagation, the theoretical work on damping behaviour in delaminated composite structures is almost non-existent [6]. Saravanos and Hopkins [30] developed a laminate theory which predicts resonance frequencies and modal damping. Analytical results of modal damping in graphite epoxy composite beams with a central delamination are compared with experimental measurements. The analytical results show reasonable comparison for modal damping for small and medium, i.e. smaller than 30% of the specimens length, delaminations. However, the effects of delaminations on the dynamic characteristics (resonance frequencies or damping) are very dependent on laminate configuration.

Diaz Valdes and Soutis [34] measured the effect of enlarging a small delamination on the modal damping of a cantilevered composite beam. The measurements were conducted in the frequency range of 8 to 13kHz, because it was expected that the effects of small delamination are more significant at higher modes. It was shown that damping increases with increasing delamination length.

Chrysochoidis and Saravanos [8] also carried out some experiments in order to investigate the effect of delaminations on modal damping. It is found that damping seems to increase with the size of delamination. However the relation seems less apparent than the relation between resonance frequencies and delamination size. Also the effect becomes more notable at higher modes. Chrysochoidis and Saravanos concluded that, for the time being, modal damping may not be effectively used for delamination detection.

The fact that damping is more sensitive to damage [40] makes it an interesting parameter for health monitoring. However there is not much literature available on the subject, which calls for an increase in research. The effects of damage on material damping have to be investigated more thoroughly, in order to successfully use changes in damping for damage detection. Also there are some factors to consider. Most of the ones mentioned in section 2.2.2 apply as well for the case of damping. For the external effects for example, Kyriazoglou mentioned that air damping has been found to significantly affect damping measurements [18]. Kawiecki [16] also investigated the effect of pre-loading and residual stress on damping and found that these factors also influence measured modal damping.

2.4 Other methods worth mentioning

Considerable effort has been spent in obtaining a relation between resonance frequencies or damping values and the presence and location of damage. However, a part of the research investigated alternative techniques. The techniques worth mentioning are discussed in this section.

Yuen [39] investigated the influence of damage on the mode shapes of a cantilever beam. A finite element programme was used and damage was modelled by a reduction in elasticity. Yuen expected that the mode shapes representing each of the degrees of freedom would be affected differently by the presence of damage. Also it was expected that the changes in the mode shapes would reflect the location and extend of the damage. The damage zone should behave like a spring allowing a greater degree of motion for points beyond the damage zone. The mode shapes of a cantilever beam with varying damage location were calculated. Results indicate that there is a systematic change in the first mode shape with respect to the damage location. However for higher modes this does not apply. The mode shapes of higher modes are too complex and further investigation is needed in order to use these modes for damage location.

Pandey *et al.* [23] extended this research and introduced a new parameter called *curvature mode shape*. Curvature mode shapes are related to the flexural rigidity of a beam. Curvature is defined by $\nu'' = M/(EI)$, in which ν'' is the curvature, M is the bending moment and EI is the flexural rigidity. In case of damage the flexural rigidity EI will reduce in that region, as a result the curvature will increase there. As curvature is a function of EI one could easily relate the change in curvature to the severity of damage. Finite element experiments were carried out on both a cantilevered and a simply supported beam. Differences between curvature mode shapes of damaged beams and intact ones were analyzed. The largest difference could be found at damage regions. The differences in curvature are relatively small outside the damage region, which makes it easy to identify damage. This is an advantage over the method proposed by Yuen [39], in which it proved difficult to identify the exact damage location. Also the method of Pandey is not restricted to the first vibration mode. The fact that curvature is proportional to the bending strain, makes it an interesting parameter. Curvature mode shapes can be easily obtained by measuring strains instead of displacement or acceleration.

Sampaio *et al.* [29] extended the theory given by Pandey [23] and developed the frequency response function curvature method. This method uses the curvature on all frequencies in the measurement range and not just the modal frequencies. In order to obtain the curvature for each frequency, responses at different locations of the damaged structure are needed. The curvature is given by

$$\alpha''(\omega)_{i,j} = \frac{\alpha(\omega)_{i+1,j} - 2\alpha(\omega)_{i,j} + \alpha(\omega)_{i-1,j}}{h^2},$$

where $\alpha_{i,j}$ is the receptance measured at location i for a force input at location j and h is the step size. Positions where the difference between intact and damaged FRF curvature maximizes, can be identified as probable damage locations. Two tests show that the FRF curvature method performed well in detecting and locating damage. Its main advantage is its simplicity the fact that no modal analysis needs to be performed for the identification of mode shapes or resonance frequencies.

In an article by Kim [17], damage identification is based on reconstructed frequency response functions (FRF). The possibility of using the residual FRF, i.e. the difference between intact and damaged FRFs, as a damage indicator is investigated. Also changes of the area under the FRF-curve are used as damage indicator. Kim concluded that use of changes in area under the FRF-curves cannot be used as a decisive damage detection parameter. However in combination with changes in resonance frequencies and damping it can prove reliable information on the detection of damage.

Hu *et al.* [15] used mode shapes, obtained from a modal analysis, from both experimental and finite element analysis of laminated plates. The mode shapes were then used to calculate strain energy using a technique known as the differential quadrature method. The local strain energies of both intact and damaged plates were used to identify surface crack location. Experimental results showed that surface crack location in various composite laminates can successfully be detected.

A different technique was proposed by Pye and Adams [25]. Infra-red thermography was used to give an indication of variation in the surface temperature of the structure under test. As the structure is subjected to cyclic stresses, as a result of resonance, temperature variations are caused by local increase in energy dissipation which then again is a result of damage. Testing showed that this can be an effective technique for location damage. Temperature differences in the order of 0.5°C were measured. However for CFRP materials this technique might cause difficulties because of the high thermal conductivity of carbon.

2.5 Summary and concluding remarks

Several techniques and methods for damage detection based on dynamic behaviour have been discussed. Most of them consisted of monitoring shifts in resonance frequencies or changes in modal damping. An overview of the advantages and disadvantages is given in this section.

In section 2.2 health monitoring based on frequency shifts are discussed. The articles discussed can be summarized:

- Resonance frequencies show less statistical variation compared to other modal parameter, this is large advantage over other methods [28].

- Resonance frequencies can be used as a damage indicator. As a result of changes in stiffness or second moment of area, resonance frequencies tend to shift [1, 3, 5, 14]. Since stress distribution is non-uniform during vibration every mode will be affected differently by damage location. As a result shifts of multiple modes can be used for locating damage [3, 5].
- The influence of several damage types on resonance frequencies shifts have been modelled in the past. The models concerned transverse cracks and notches [7, 11, 22, 33] or delaminations [8, 20, 21, 26, 32, 34, 35]. These methods could be used as a basis for level 3 damage detection [27]. From these models it is shown that laminate configuration has a large influence on resonance frequency shifts. A fundamental limitation, however, of these methods is that it should be possible to represent the actual damage with these models. This will not always be the case.
- Exogenic effect can influence measurements, resonance frequency shifts exceeding 5% have been recorded as a result of environmental changes only [28, 16]. Also the low sensitivity of resonance frequency changes to certain damage can cause difficulties [9]. Successful damage detection, based on resonance frequency shifts only, calls for either very precise measurements or severe damage.

Section 2.3 discussed health monitoring based on changes in modal damping:

- Experiments showed that damping is more sensitive to damage than resonance frequencies [40]. Measurements showed that changes in damping are highly related to laminate lay-up [30]. Despite the sensitivity, the relation between damage and changes in damping seems not very apparent [8].
- Damping seems to increase with damage [12, 18]. However for matrix cracking or material imperfections, changes in modal damping are rather small [19].
- Also for damping it applies that exogenic effect has an influence on measurements. It has been reported that air damping can be found to significantly affect damping measurements [18]. Also pre-loading and residual stress can influence the measured modal damping values [16].

There are other methods available for dynamic measurement based damage detection, these are discussed in section 2.4. Changes in mode shapes [39] or curvature mode shapes [23, 29] were shown to be promising parameters for damage detection. Especially, results obtained with help of the curvature mode shapes were encouraging. A disadvantage of these methods is that several measurement points are required to qualify the different mode or curvature mode shapes.

Authors	Year	Ref.	Frequency based	Damping based	Model based	Predefined damage	Remarks
REVIEW ARTICLES							
Farrar, Doebling, Prime and Shevitz	1997	[10]	yes	yes	na	na	
Salawu	1997	[28]	yes	no	na	na	
Zou, Tong and Steven	2000	[40]	yes	yes	na	na	
THEORETICAL MODELS FOR DAMAGE DETECTION							
Cawley and Adams	1978	[5]	yes	no	yes	no	
Wang, Liu and Gibby	1982	[35]	yes	no	yes	yes	models delaminations
Gudmundson	1982	[11]	yes	no	yes	yes	
Yuen	1985	[39]	no	no	yes	no	uses mode shape changes
Mujumdar and Suryanarayan	1988	[21]	yes	no	yes	yes	models delaminations
Pandey, Biswas and Samman	1991	[23]	no	no	yes	no	uses curvature changes of beams
Hassiotis and Jeong	1993	[14]	yes	no	yes	no	
Tenek, Henneke and Gunzburger	1993	[32]	yes	no	yes	yes	
Saravanos and Hopkins	1996	[30]	no	yes	no	no	
Chondros, Dimarogonas and Yao	1998	[7]	yes	no	yes	yes	models notches
Sampaio, Maia and Silva	1999	[29]	no	no	yes	no	uses curvature changes of beams
Lee	2000	[20]	yes	no	yes	yes	models delaminations
EXPERIMENTS ON DAMAGE DETECTION							
Cawley and Adams	1978	[3]	yes	no	yes	no	
Cawley and Adams	1981	[1]	no	yes	no	no	
Lee, Sun and Liu	1987	[19]	no	yes	no	no	
Tomasel, Larrondo and Laura	1999	[33]	yes	no	yes	yes	notch detection
Diaz Valdes and Soutis	1999	[34]	yes	yes	no	yes	delamination detection
Kawiecki	2001	[16]	yes	yes	no	no	
Kyriazoglou, Page and Guild	2004	[18]	no	yes	no	no	

Table 2.1: A selection of literature on damage detection based on dynamic behaviour.

DETERMINING THE RESONANCE FREQUENCIES OF A DELAMINATED BEAM

In the following chapter the model presented by Mujumdar and Suryanarayan [21] is outlined. This model determines the resonance frequencies of a beam containing one 'through width' delamination. To provide some insight into the mechanics of the model a solution to the static problem is added. In the second section the model is modified to make it applicable for composite materials. Finally two finite element models are presented.

3.1 Flexural vibration of delaminated beams

Delamination is a common detected type of damage in composite components and can have a great influence on mechanical properties. As stated in previous sections delaminations may originate during fabrication or from in-service loading. The notion that delaminations not only affect strength but also cause a reduction in bending stiffness the basis of the model described by Mujumdar and Suryanarayan [21]. The model is an extension of the theory proposed by Ramkumar *et al.* [26] and provides an analytical solution to the eigenvalue problem and determines the resonance frequencies of delaminated beams in flexural vibration.

3.1.1 Basic assumptions and modelling

The model presented by Mujumdar and Suryanarayan [21] describes a beam with an arbitrarily located through-width delamination. Figure 3.1 shows a delaminated beam subdivided in three separate sections, namely two integral sections and one

delaminated section. The delaminated region is then again subdivided in component segments above and below the delamination plane. The four segments are each treated as Bernoulli-Euler beams. The solution for the whole beam is obtained in terms of the solutions of all the separate sections by satisfying the appropriate boundary and continuity conditions. For the sake of simplicity, Mujumdar and Suryanarayan assumed the beam to be homogeneous and isotropic. Also only a single delamination is considered, though the analysis can be easily extended to multiple delaminations. It is further assumed that there exists no gap between the delaminated layers.

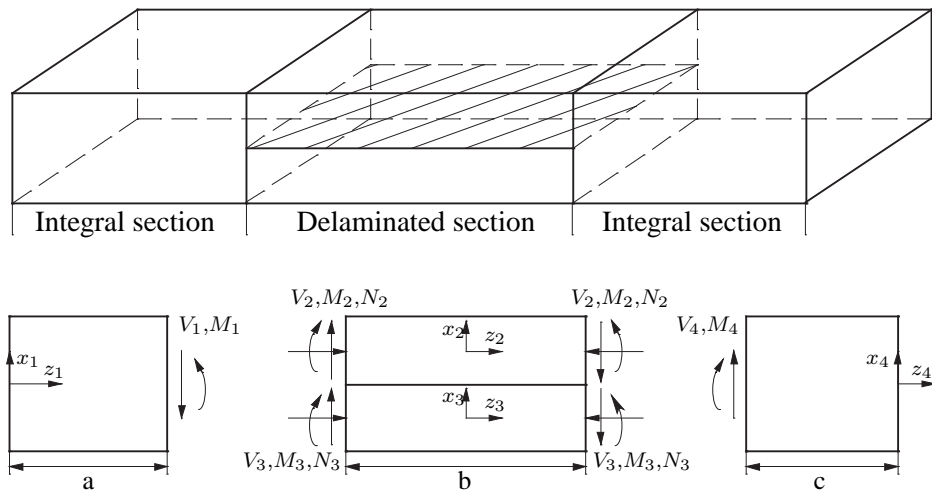


Figure 3.1: Geometry, co-ordinate system and modelling of a beam with a delamination.

The basic theory is based on variations in the distribution of shear stress. In a beam that is in nonuniform bending both normal and shear stress is developed. In a beam without delamination the shear stress is distributed as shown in figure 3.2a. However, in case a delamination is present, the layers are free to slide and the shear stress on the delaminated surface therefore equals zero per definition. The shear stress distribution for this case is shown in figure 3.2b. This discontinuity in shear stress results in a decrease of bending stiffness which then again will cause the flexural resonance frequencies to shift to lower values.

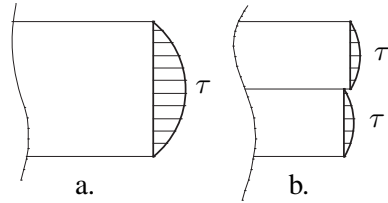


Figure 3.2: Distribution of shear stress in (a) an intact beam section and (b) a delaminated beam section.

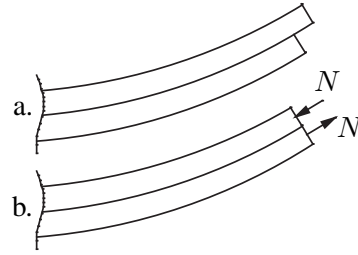


Figure 3.3: Different continuity conditions at junction between delaminated and integral section.

The difference between this model and the one proposed by Ramkumar *et al.* [26] lies in the axial continuity conditions at the junctions between integral and delaminated section. Ramkumar, as opposed to Mujumdar and Suryanarayan [21], neglected the coupling effects between axial and flexural deformation. This is best illustrated in figure 3.3. Mujumdar and Suryanarayan demand that the free ends of the delaminated segments stay in the same plane. In order to realize this the normal force N is introduced, as in figure 3.3b. Figure 3.3a shows the situation as proposed by Ramkumar *et al.* The absence of normal force N results in a discontinuity at the end plane. The delaminated section acts entirely equivalent to a beam with a step reduction in flexural rigidity corresponding to a reduced second moment of area equal to $(I_2 + I_3)$. It was already shown by Ramkumar *et al.* [26] that the flexural rigidity of a delaminated beam is considerable underestimated this way. The compatibility condition used by Mujumdar and Suryanarayan introduces an axial load system of equal and opposite forces. These normal forces compress one segment and stretch the other such that their ends lie in the same plane. This load system results in an internal bending moment, which contributes to the total bending stiffness of the beam.

3.1.2 Static solution

In order to gain insight in the theory proposed by Mujumdar and Suryanarayan a solution to the static problem is presented first. The results are compared with results obtained by the model proposed by Ramkumar *et al.* [26]. As stated above, Mujumdar and Suryanarayan included the coupling effects between longitudinal and flexural motion. For this static analysis, the delaminated section is clamped at one end, as is shown in figure 3.4, and a force F_0 and bending moment M_0 are applied to the free end. Figure 3.5 show the forces that act on each separate beam segment. The normal forces N_2 and N_3 stretch one beam segment and compress the other such that their free ends lie in the same plane.

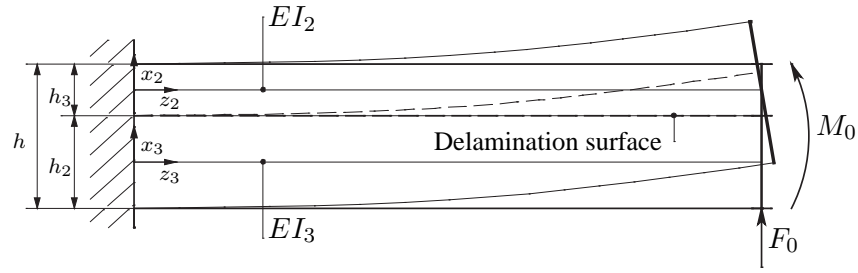


Figure 3.4: Geometry, co-ordinate system and modelling of a delaminated beam section.

Equilibrium of force in both z - and x -direction and bending moment give the following equations:

$$\begin{aligned} N_2 + N_3 &= 0 \\ D_2 + D_3 &= F_0 \\ M_2 + M_3 - N_2 \frac{1}{2}h &= M_0 \end{aligned} \quad (3.1)$$

The bending moment is taken with respect to the junction between delamination surface and endplane.

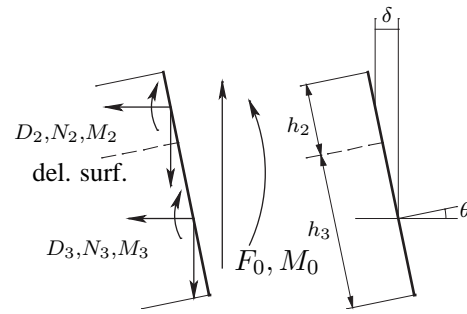


Figure 3.5: Free body diagram of end plane.

In case the deflection is assumed to be small the slope and displacement in x -direction at the free end for the separate beams follow from the bending moment equation and are given by

$$\begin{aligned} u'_i(L) = \varphi_i(L) &= \frac{M_i L}{EI_i} + \frac{D_i L^2}{2EI_i} \\ u_i(L) &= \frac{M_i L^2}{2EI_i} + \frac{D_i L^3}{3EI_i} \end{aligned} \quad (3.2)$$

with $i = 2, 3$. The displacement in axial direction is calculated by:

$$w_i(L) = \frac{N_i L}{EA_i} \quad (3.3)$$

The Young's modulus is represented by E , the second moment of area by I_i and the cross sectional area by A_i . Continuity of x -displacement and slope of both beam segments at the free end is demanded. Also the free end of both beams should remain in the same plane. This results, with figure 3.5, in the following continuity

conditions:

$$\begin{aligned}\varphi_2(L) &= \varphi_3(L) \\ u_2(L) &= u_3(L) \\ w_3 &= w_2 + \delta = w_2 + \frac{1}{2}h\varphi_2(L)\end{aligned}\quad (3.4)$$

Substituting equations 3.1, 3.2 and 3.3 in the continuity conditions 3.4 the following system of equations is found:

$$\begin{aligned}M_2\left(\frac{L}{EI_2} + \frac{L}{EI_3}\right) + D_2\left(\frac{L^2}{2EI_2} + \frac{L^2}{EI_3}\right) - N_2\frac{hL}{2EI_3} &= M_0\frac{L}{EI_3} + F_0\frac{L^2}{2EI_3} \\ M_2\left(\frac{L^2}{2EI_2} + \frac{L^2}{2EI_3}\right) + D_2\left(\frac{L^3}{3EI_2} + \frac{L^3}{3EI_3}\right) - N_2\frac{hL^2}{4EI_3} &= M_0\frac{L^2}{2EI_3} + F_0\frac{L^3}{3EI_3} \\ M_2\frac{hL}{2EI_2} + D_2\frac{d_1L^2}{4EI_2} + N_2\left(\frac{L}{EA_2} + \frac{L}{EA_3}\right) &= 0\end{aligned}$$

From this set of equations the three unknown parameters M_2 , D_2 and N_2 can be derived and the transversal displacement and slope at $z = L$ can be determined by substituting these in equations 3.2. For a fictive beam the results are obtained and listed in table 3.1. The table also shows the results for a beam without a delamination and in case the delamination is treated as a step in second moment of area, as proposed by Ramkumar [26]. The delamination is located at a fraction h_2/h of the beams thickness.

It can be seen from table 3.1 that, in both models, the effect of the delamination increases as it is positioned closer to the neutral line. The solution of both displacement and slope approach the intact case when alpha approaches zero or one. The differences between the results obtained with Ramkumar *et al.* and Mujumdar and Suryanarayan are significant. In the model used by Mujumdar and Suryanarayan the loss of flexural rigidity is compensated by the additional bending moment caused by the stretching and compressing of the layers.

h_2/h	F_0	M_0	No delamination		Ramkumar <i>et al.</i>		Mujumdar Suryanarayan	
			$u(L)$	$\varphi(L)$	$u(L)$	$\varphi(L)$	$u(L)$	$\varphi(L)$
0.2	1	0	.5	.75	1.0	1.4	.615	.75
0.2	0	1	.75	1.5	1.4	2.9	.75	1.5
0.4	1	0	.5	.75	1.8	2.7	.821	.75
0.4	0	1	.75	1.5	2.7	5.4	.75	1.5
0.5	1	0	.5	.75	2.0	3.0	.875	.75
0.5	0	1	.75	1.5	3.0	6.0	.75	1.5

Table 3.1: Comparison of static solutions

In case the beam is in pure bending the deflection and slope equal the intact case. This makes sense, since no shear stress is developed in the beam and therefore no sliding of the layers occurs. On the other hand when a shear force is applied the layers will slide and the effect of a delamination is noticed. The normalized shape of a delaminated beam subjected to a shear force at the free end is given in figure 3.6. It can be seen that only the deflection at the free end is influenced, the slope equals the intact case.

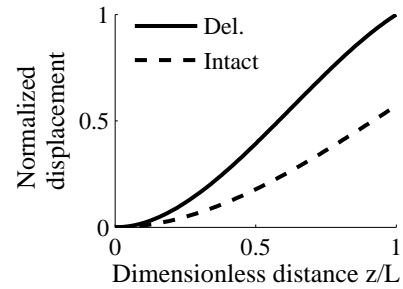


Figure 3.6: Shape of a beam subjected to a shear force.

It seems, from figure 3.6, that the delamination has a huge effect on the total displacement of the beam. However normally only a fraction of the beam will be delaminated and the influence on the total displacement will be minimal. This is illustrated in figure 3.7 where the normalized shape of a delaminated beam under a shear force is plotted. The dimensionless length of the delamination is varied. Even for delaminations with a length up to 40% of the beam span the increase in displacement is negligible.

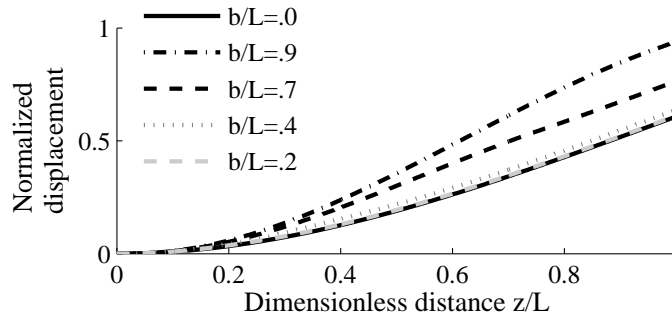


Figure 3.7: Shape of beams with varying midplane delamination lengths.

3.1.3 Dynamic solution: Bernoulli-Euler beam equations

The model proposed by Mujumdar and Suryanarayan uses Bernoulli-Euler beam equations for every beam section. In this paragraph the equations of motion for such a beam section are derived. Figure 3.8¹ shows a beam under uniform loading,

figure 3.9¹ displays the free-body diagram corresponding to a beam element of length dz . The transverse displacement at point z and time t is denoted by $x(z, t)$ and the force per unit length is $p(z, t)$. The parameters involved are mass per unit length $m(z)$ and the flexural rigidity $EI(z)$, where $I(z)$ is the second moment of area about the y -axis and $E(z)$ is Young's modulus of elasticity. It is assumed that the rotation of the beam is negligible compared to the vertical displacement. For this to be true the ratio between length and height should be relatively large and the beam should not become too 'wrinkled', with other words only the lower modes of vibration should be considered.

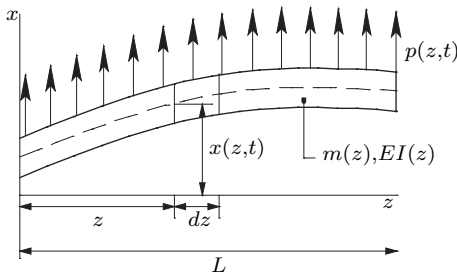


Figure 3.8: Beam in flexure under uniform loading.

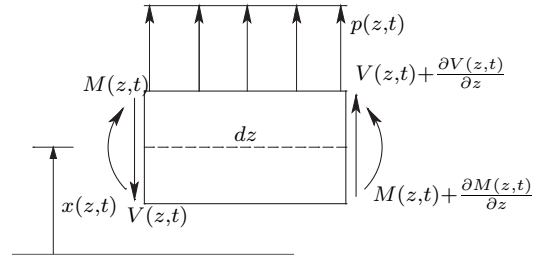


Figure 3.9: Free body diagram of a beam element.

First, from figure 3.9, the force equation of motion in x -direction is derived:

$$\left[V(z, t) + \frac{\partial V(z, t)}{\partial z} dz \right] - V(z, t) + p(z, t) dz = m(z) dz \frac{\partial^2 x(z, t)}{\partial t^2} \quad (3.5)$$

Since the rotation induced inertia torque is ignored the following equation holds for the moment about the center of the left edge:

$$\left[M(z, t) + \frac{\partial M(z, t)}{\partial z} dz \right] - M(z, t) + \left[V(z, t) + \frac{\partial V(z, t)}{\partial z} dz \right] dz + p(z, t) dz \frac{1}{2} dz = 0 \quad (3.6)$$

Canceling appropriate terms and discarding terms involving second or higher powers in dz , equation 3.6 reduces to:

$$-\frac{\partial M(z, t)}{\partial z} = V(z, t) \quad (3.7)$$

¹Figures are taken from: L. Meirovitch. *Elements of Vibration analysis*, 1986.

$$M(z, t) = \frac{EI(z)\partial^2 x(z, t)}{\partial z^2} \quad (3.8)$$

Substituting equation 3.7 into 3.5 and using the bending moment equation 3.8 the following differential equation for the flexural vibration of a beam is found:

$$-\frac{EI(z)\partial^4 x(z, t)}{\partial z^4} + p(z, t) = m(z)\frac{\partial^2 x(z, t)}{\partial t^2} \quad (3.9)$$

Separation of variables $x(z, t) = u(z)f(t)$ and letting $p(z, t) = 0$, give:

$$\begin{aligned} -\frac{EI(z)}{m(z)} \frac{1}{u(z)} \frac{d^4 u(z)}{dz^4} &= -\omega^2 \\ \frac{1}{f(t)} \frac{d^2 f(t)}{dt^2} &= -\omega^2 \end{aligned} \quad (3.10)$$

Rearranging the first of equation 3.10 the eigenvalue problem formulation reduces to the following differential equation (3.11), with solution (3.12):

$$\frac{d^4 u(z)}{dz^4} - \frac{\omega^2 m(z)}{EI(z)} u(z) = \frac{d^4 u(z)}{dz^4} - \beta^4 u(z) = 0 \quad (3.11)$$

$$u(z) = A \sin(\beta z) + B \cos(\beta z) + C \sinh(\beta z) + D \cosh(\beta z) \quad (3.12)$$

The solution depends on the constants of integration A, B, C and D , these can be found by applying the four boundary conditions. For finding a solution to the eigenvalue problem, the value of the constants is not needed. The boundary conditions can be written as a set of simultaneous linear homogeneous algebraic equations in the unknown constants. A non-trivial solution is only found when the determinant of the coefficient matrix vanishes. All the components of the matrix are functions of the unknown fundamental frequency β , which can thus be solved.

3.1.4 Dynamic Solution: Governing equations

In section 3.1.1 it was explained that Mujumdar and Suryanarayan [21] modelled a delaminated beam as four separate Bernoulli-Euler beams. Since the integral beam regions, with lengths a and c in figure 3.1, have the same loading as the beam segment explained above, the equation and solution derived there will be used. However, the equation will be written in a dimensionless form,

$$\frac{d^4 \bar{u}_i(\bar{z}_i)}{d\bar{z}_i^4} - \beta^4 \bar{u}_i(\bar{z}_i) = 0, \quad i = 1, 4 \quad (3.13)$$

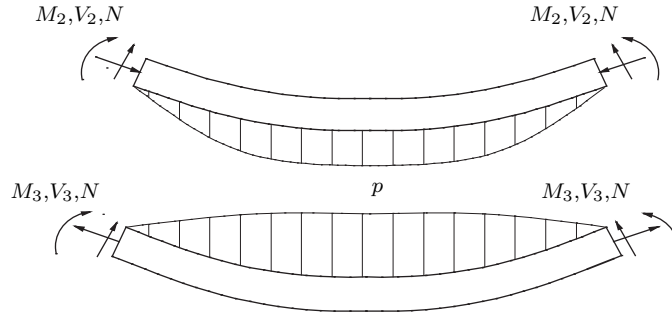


Figure 3.10: Free body diagrams of the layers above and below a delamination.

in which:

$$\beta^4 = \frac{\omega^2 mL^4}{EI} \quad (3.14)$$

The dimensionless axial coordinate and transverse displacement are defined as $\bar{z}_i = z_i/L$ and $\bar{u}_i = u_i/d$. A full list of the used notation can be found in section 3.5. Since it is assumed that the delaminated layers remain in contact a pressure, $p(z, t)$, exists between the two layers, see figure 3.10 and 3.11. The equations of motion for both segments can be written as:

$$\begin{aligned} \frac{EI_2 \partial^4 x_2(z_2, t)}{\partial z_2^4} - N \frac{\partial^2 x_2(z_2, t)}{\partial z_2^2} - \frac{m_2 \partial^2 x_2(z_2, t)}{\partial t^2} + p &= 0 \\ \frac{EI_3 \partial^4 x_3(z_3, t)}{\partial z_3^4} + N \frac{\partial^2 x_3(z_3, t)}{\partial z_3^2} - \frac{m_3 \partial^2 x_3(z_3, t)}{\partial t^2} - p &= 0 \end{aligned} \quad (3.15)$$

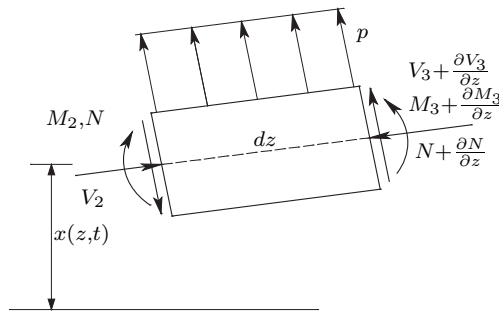


Figure 3.11: Free body diagram of a delaminated beam element.

As stated before the delaminated layers remain in contact with each other, this means that the displacement in the x -direction of segment 2 equals the displacement of segment 3, or $u_2(z, t) = u_3(z, t)$. Furthermore it follows from the origins shown in figure 3.1 that z_2 equals z_3 . Replacing u_3 and z_3 by u_2 and z_2 respectively

in the last of equation 3.15 and adding this to the first of equation 3.15, the governing differential equation describing the dynamic behaviour of de delaminated section is obtained:

$$\frac{E(I_3 + I_2)\partial^4 x_2(z_2, t)}{\partial z_2^4} - \frac{(m_2 + m_3)\partial^2 x_2(z_2, t)}{\partial t^2} = 0$$

After separation of variables and writing the solution in a dimensionless form one obtains:

$$\frac{d^4 \bar{u}_2(\bar{z}_2)}{d\bar{z}_2^4} - \beta_2^4 \bar{u}_2(\bar{z}_2) = 0 \quad (3.16)$$

in which:

$$\beta_2^4 = \frac{\omega^2(m_2 + m_3)L_i^4}{E(I_2 + I_3)} \quad (3.17)$$

Introducing the dimensionless variables $\bar{h}_2 = h_2/h$ and $\bar{h}_3 = h_3/h$, with h_2 and h_3 the thickness of the upper and lower delaminated beam segments respectively and h the total thickness, equation 3.17 can be rewritten using equation 3.14:

$$\beta_2^4 = \frac{\omega^2(m_2 + m_3)L^4}{E(I_2 + I_3)} = \frac{\beta^4}{\bar{h}_2^3 + \bar{h}_3^3} \quad (3.18)$$

Recapitulating, a general differential equation is found for two integral sections and one combined delaminated section,

$$\frac{d^4 \bar{u}_i(\bar{z}_i)}{d\bar{z}_i^4} - \beta_i^4 \bar{u}_i(\bar{z}_i) = 0, \quad i = 1, 2, 4 \quad (3.19)$$

in which:

$$\beta_1^4 = \beta_4^4 = \frac{\omega^2 m L^4}{EI}$$

$$\beta_2^4 = \frac{\omega^2(m_2 + m_3)L^4}{E(I_2 + I_3)} = \frac{\beta^4}{\bar{h}_2^3 + \bar{h}_3^3} \quad (3.20)$$

The general solution, which describes the displacement for each section ($i = 1, 2, 4$) is found to be:

$$\bar{u}_i(\bar{z}_i) = A_i \sin \beta_i \bar{z}_i + B_i \cos \beta_i \bar{z}_i + C_i \sinh \beta_i \bar{z}_i + D_i \cosh \beta_i \bar{z}_i \quad (3.21)$$

3.1.5 Dynamic solution: Boundary and continuity conditions

The solution presented in the last section contains 12 unknown coefficients, these are determined by the boundary and continuity conditions. The beam, presented in figure 3.1, has two boundaries ($z_1 = 0$) and ($z_4 = 0$); for every boundary two conditions are obtained. In table 3.2 several ways of supporting a beam are listed along with the resulting boundary conditions.

Support	Boundary conditions	
Clamped	$u_i(0) = 0$	$u_i'(0) = 0$
Simply supported	$u_i(0) = 0$	$u_i''(0) = 0$
Free	$u_i''(0) = 0$	$u_i'''(0) = 0$

Table 3.2: Boundary conditions

A total of four boundary conditions is found; another eight conditions are needed to solve the twelve unknown constants in equation 3.21. These follow from the conditions of continuity at the two junctions ($z_1 = \bar{a}$) and ($z_4 = -\bar{c}$). Continuity of displacement and slope:

$$\begin{aligned} \bar{u}_1(\bar{a}) &= \bar{u}_2(-\bar{b}/2) & \bar{u}_4(-\bar{c}) &= \bar{u}_2(\bar{b}/2) \\ \bar{u}'_1(\bar{a}) &= \bar{u}'_2(-\bar{b}/2) & \bar{u}'_4(-\bar{c}) &= \bar{u}'_2(\bar{b}/2) \end{aligned} \quad (3.22)$$

The remaining four conditions follow from the continuity in shear force and bending moment at the two junctions. Continuity of shear force between the integral and delaminated section gives $V_i = V_2 + V_3$, with $i = 1, 4$. In terms of displacement this results in

$$EI_1 \frac{d^3 u_i}{dz_i^3} = (EI_2 + EI_3) \frac{d^3 u_2}{dz_2^3}$$

writing this in a dimensionless form one obtains:

$$\frac{d^3 \bar{u}_i}{d\bar{z}_i^3} = (\bar{h}_2^3 + \bar{h}_3^3) \frac{d^3 \bar{u}_2}{d\bar{z}_2^3}, \quad i = 1, 4 \quad (3.23)$$

The equilibrium of bending moments about the midplane of section 1 or 4 can be found to be $M_i = M_2 + M_3 + N(h/2)$, with again $i = 1, 4$. This also can be written in terms of displacements:

$$EI_1 \frac{d^2 u_i}{dz_i^2} = (EI_2 + EI_3) \frac{d^2 u_2}{dz_2^2} + N(h/2)$$

In dimensionless form:

$$\frac{d^2 \bar{u}_i}{d\bar{z}_i^2} = (\bar{h}_2 + \bar{h}_3) \frac{d^2 \bar{u}_2}{d\bar{z}_2^2} + NL^2/2EI_1, \quad i = 1, 4 \quad (3.24)$$

The force N on the left of equation 3.24 depends on the stretching and compressing of the segments 2 and 3. This was also shown in the static solution. Force N is given in a dimensionless form by:

$$N = \frac{EI}{L^2} (6\bar{h}_2\bar{h}_3/\bar{b}) \left[-\frac{d\bar{u}_1(\bar{a})}{d\bar{z}_1} + \frac{d\bar{u}_4(-\bar{c})}{d\bar{z}_4} \right] \quad (3.25)$$

A derivation of this term can be found in [21]. The resulting equation for continuity of bending moment is obtained, with $i = 1, 4$:

$$\frac{d^2 \bar{u}_i}{d\bar{z}_i^2} = (\bar{h}_2 + \bar{h}_3) \frac{d^2 \bar{u}_2}{d\bar{z}_2^2} - (3\bar{h}_2\bar{h}_3/\bar{b}) \left[-\frac{d\bar{u}_1(\bar{a})}{d\bar{z}_1} + \frac{d\bar{u}_4(-\bar{c})}{d\bar{z}_4} \right] \quad (3.26)$$

A total of 12 boundary and continuity conditions are formulated. These conditions can be written as a matrix vector equation in twelve unknown constants. The system possesses a non-trivial solution when the determinant of the matrix equals zero. All components in the matrix are functions of the unknown fundamental frequency β , which can thus be solved.

3.1.6 Dynamic solution: Analytical results

Analytical results for a cantilevered beam, obtained with the model described above, are shown in figures 3.12 to 3.15. The figures show the influence of the delamination parameters like delamination length \bar{b} and both axial \bar{a}_c and thickness-wise

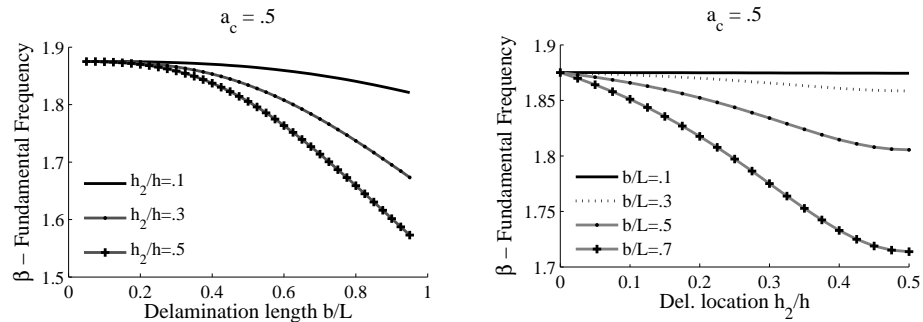


Figure 3.12: Influence of delamination length b and thickness-wise location h_2 on first vibration frequency.

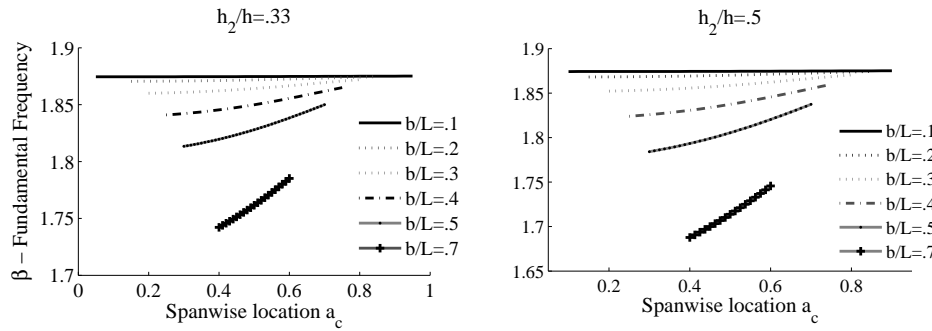


Figure 3.13: Effect of axial position \bar{a}_c of a delamination on the first vibration frequency.

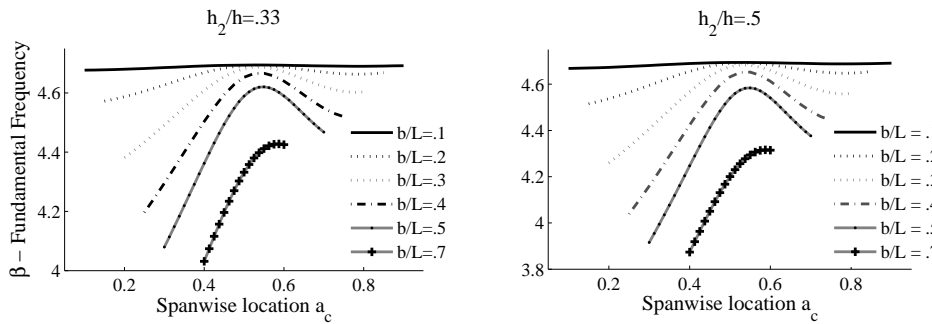


Figure 3.14: Effect of axial position \bar{a}_c of a delamination on the second vibration frequency.

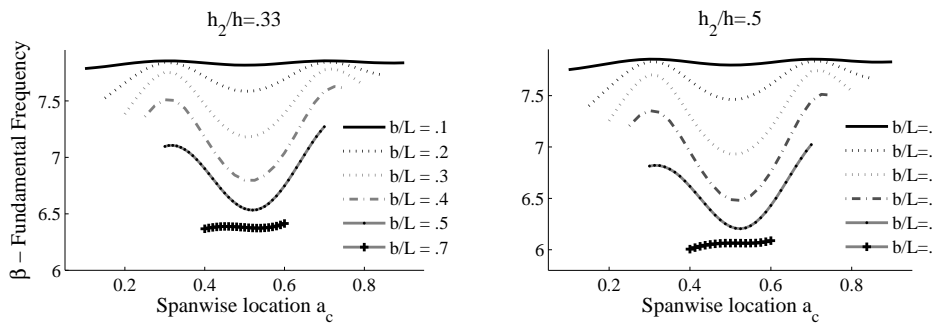


Figure 3.15: Effect of axial position \bar{a}_c of a delamination on the third vibration frequency.

\bar{h}_2 location on the fundamental frequencies β of the delaminated beam. The fundamental frequency can be substituted in equation 3.14 to determine the resonance frequencies of the delaminated beam.

Figure 3.12 shows that both the delamination length and thickness-wise location have a big influence on the first fundamental frequency. In these cases the delamination is located at half the total length of the beam. For an intact beam the first

fundamental frequency equals 1.875. It can be seen that the solution converges to this value in case h_2 approaches zero and the delamination shifts to the surface of the beam. Furthermore it is observed that the effect is maximal for a delamination near the midplane ($\bar{h}_2 = .5$). This was also observed in the static analysis. However it has to be mentioned that only for relatively large delaminations ($\bar{b} > .3$) the effect on the first mode is noticeable. This can also be seen in figure 3.13 where the influence of the axial location on the first fundamental frequency is shown. It is shown that the delamination has the greatest influence when it is positioned near the clamped end. However, a delamination with a length of $\bar{b} = .3$ only causes a reduction of the first resonance frequency ω of 2.6 %, which is probably not enough to detect it with confidence. Figure 3.14 shows that the second fundamental frequency is influenced more by the delamination. The second fundamental frequency for an intact beam equals 4.694. The greatest effect again is observed when the delamination is positioned close to the clamped end. The peak near $a_c = .55$ attracts the attention and indicates that the effect of a delamination is negligible in case it is located at .55 times the beams length. In figure 3.15, which shows the effect on the third fundamental frequency, similar peaks are observed; in this case however these are located at approximately $a_c = .32$ and $a_c = .73$. The third fundamental frequency for an intact beam equals 7.855.

As mentioned in the static solution the effect of the delamination is a combination of two effects: one is the reduction in flexural stiffness over the beams thickness, the other is the stretching and compressing of the delaminated beam segments. The first effect results in a reduction of flexural rigidity, while the second effect tends to compensate this. It was pointed out in section 3.1.2 that the weakening effect of a delamination is only noticed in case a shear force is applied. This means that the effect of a delamination can be neglected if the delamination is located in regions where the shear force approaches zero. The shear force can be expressed as a function of the third derivative of the displacement:

$$V = EI \frac{\partial^3 u(z)}{\partial z^3}$$

The displacement $u(z)$ of an intact cantilever beam at location z is given by:

$$u(z) = A_r \left[(\sin\beta L - \sinh\beta L)(\sin\beta z - \sinh\beta z) + \cos\beta L + \cosh\beta L (\cos\beta z - \cosh\beta z) \right] \quad (3.27)$$

In figure 3.16 the displacement $u(z)$ and third derivative $\partial^3 u(z)/\partial z^3$ for the second mode of vibration of an intact beam is plotted. Figure 3.17 plots the result for the third vibration mode. Both the displacement and third derivative are normalized to the maximum value. As can be seen from both figures, $\partial u(z)^3/\partial z^3$ equals zero where the influence of the delamination vanishes. Also the delamination has the biggest influence where $\partial u(z)^3/\partial z^3$ maximizes, which is in fact near the clamped end.

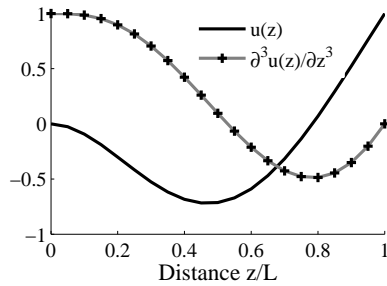


Figure 3.16: Mode shape and third derivative for second vibration mode.

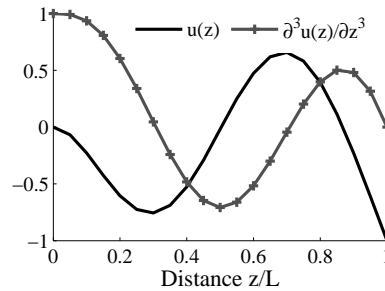


Figure 3.17: Mode shape and third derivative for third vibration mode.

This influence on spanwise location also shows up in the vibration mode shapes. Figure 3.18 shows the mode shapes for the second vibration mode of an intact and delaminated beam. It can be seen that the effect of the delamination is minimal in case it is located at $a_c = .55$. For $a_c = .3$ a clear difference between the delaminated and intact case is observed. Figure 3.19 shows similar results for the third vibration mode. The mode shapes of an intact or delaminated beam do not differ much in case the delamination is located near regions of minimum shear stress. If its located near regions of high shear stress a clear difference is observed.

Overall it can be concluded from figure 3.12 to 3.15 that the influence of a delamination increases with mode number. The third vibration mode is clearly more affected than the first. It is also observed that the influence increases in case the delamination shifts to the midplane ($\bar{h}_2 = .5$) and vanishes at the surface ($\bar{h}_2 = 0$). Also the spanwise location has a great influence. An arbitrary located delamination affects each mode differently depending on the location. This is caused by the nonuniform distribution of shear stress. This effect was used by Cawley and Adams [3] to locate delaminations.

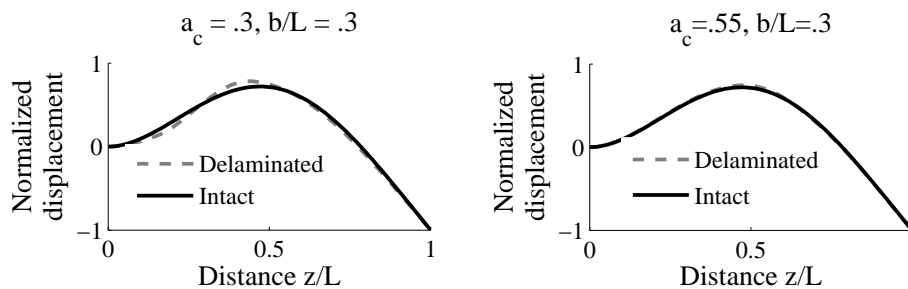


Figure 3.18: Mode shapes for second mode of vibration for delaminated and intact beam.

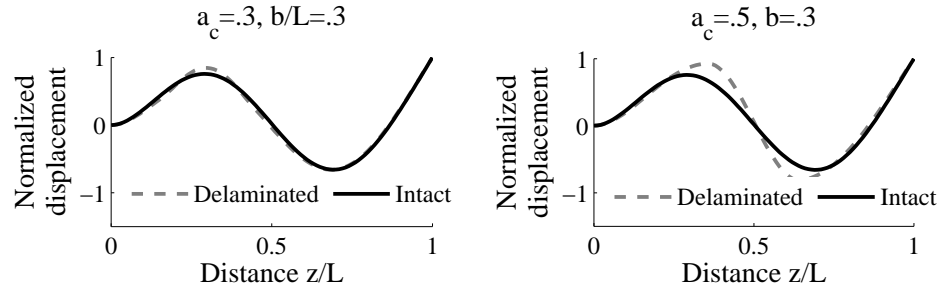


Figure 3.19: Mode shapes for third mode of vibration for delaminated and intact beam.

3.2 Application of the model for composite beams

The model by Mujumdar and Suryanarayan [21] can easily be applied to composite beams. Unlike isotropic materials, the Young's modulus of composites varies along the thickness. This is caused by changes in fibre orientation over the thickness. Mujumdar and Suryanarayan simplified their model for application with homogeneous materials. This simplification however, can easily be undone. To do so the ratio $(EI_2 + EI_3)/EI_1$ in the continuity equations for shear force, bending moment and normal force cannot be rewritten in terms of dimensionless beam thickness, as in equations 3.23, 3.24 and 3.25. This is because this ratio is now also a function of laminate lay-up, and not only of the thickness anymore. Also the moment caused by the stretching and compressing of the layers depends now on lay-up. In the following section it is shown how this laminate lay-up influences both the static and dynamic behaviour of a delaminated composite beam.

3.2.1 Determination of flexural rigidity

The flexural rigidity of the segments can be determined by calculating the internal bending moment and combining this with the bending moment equation. Before calculating the flexural rigidity, the location of the neutral surface has to be determined. This is done by subjecting the beam to a normal force F which causes the beam to compress, as shown in figure 3.20. In case the force is applied at the neutral surface the separate layers will all deform equally with ϵ_l . To determine this location the sum of moments is taken about the bottom-left point of the laminate. The force generated by each layer can be derived from the strain of the laminate:

$$\epsilon_l = \frac{\sigma_l}{E_l} = \frac{F}{EA_l}$$

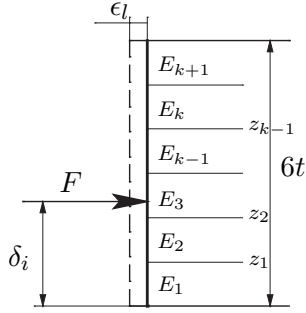


Figure 3.20: Determination of neutral surface.

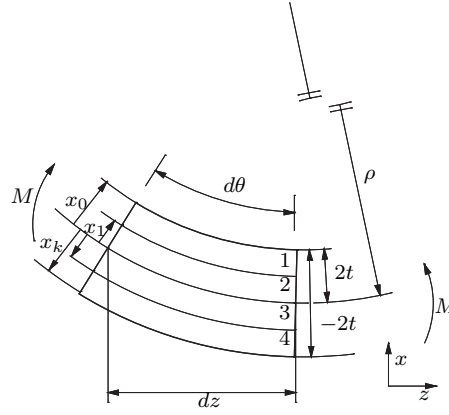


Figure 3.21: Composite beam under bending moment.

In which σ_l represent the stress in the laminate and E_l the Youngs modulus of the laminate. $E A_l$ can be determined as follows:

$$E A_l = b \sum_{k=1}^N E_k (x_{k-1} - x_k) \quad (3.28)$$

With E_k representing the Youngs modulus of a layer and x_k the distance of the layer edge to the delaminated surface. The summation of the moment exerted by each layer should equal the moment caused by F multiplied by the distance δ_i from the delaminated surface.

$$F \delta_i = \sum_{k=1}^N d_k \sigma_k b t = \sum_{k=1}^N d_k \epsilon_l E_k b t = \sum_{k=1}^N d_k \frac{F}{E A_l} E_k b t$$

In which $d_k = z_{k-1} + (1/2)(z_k - z_{k-1})$ represents the distance from delaminated surface to the midplane of the layer. This results in:

$$\delta_i = \sum_{k=1}^N \frac{d_k E_k b t}{E A_l} \quad (3.29)$$

To calculate the flexural rigidity figure 3.21 is considered. A laminated beam is subjected to a bending moment M which results in a radius of curvature of ρ . The normal stress at a distance x from the neutral line in a beam in flexure is calculated from the normal strain

$$\sigma_z(x) = E_k \frac{x}{\rho}$$

in which ρ is the radius of curvature of the laminate and E_k the local Young's modulus. The resulting bending moment can be determined by:

$$M = \int_{-2t}^{2t} \sigma_z(x) b x dx$$

With x_k and x_{k-1} the distances from the neutral surface the following is obtained:

$$M = \sum_{k=1}^N \int_{z_{k-1}}^{z_k} E_k \frac{-bx^2}{\rho} dx = \frac{-b}{3\rho} \sum_{k=1}^N E_k (x_{k-1}^3 - x_k^3) \quad (3.30)$$

The bending moment equation can be used to express the bending moment as a function of the elasticity modulus of the laminate E_2^l :

$$E_l I_y u'' = M \rightarrow E_l I_y = M \rho \quad (3.31)$$

Combining the last two equations gives the flexural rigidity of the laminate as a whole:

$$EI_l = \frac{-b}{3} \sum_{k=1}^N E_k (x_{k-1}^3 - x_k^3) \quad (3.32)$$

This relation can be used to determine the bending stiffness of each beam segment. The distances x_k and x_{k-1} then relate to the neutral line of every separate beam segment. As an example the ratio $(EI_2 + EI_3)/EI_1$ of a $[90_3/0/90_4]_s$ laminate, with material properties as in table 3.3, is plotted against delamination location. For comparison the ratio for an isotropic beam is also plotted. From figure 3.22 it is seen that laminate lay-up plays an important role.

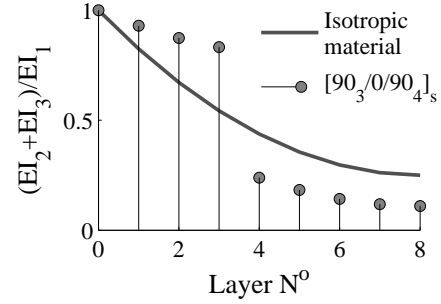


Figure 3.22: Influence of delamination location on flexural rigidity.

The ratio $(EI_2 + EI_3)/EI_1$ shows a great jump in case the delamination is located after the fourth layer. This is caused by the fact that the stiff fourth layer now belongs to the upper laminate. The effective distance from the neutral line is reduced which results in a reduction of the total flexural rigidity.

carbon-PEI	E_0 (GPa)	E_{90} (GPa)	G_{12} (GPa)	ν_{12}	ν_{23}	ρ (kg/m ³)
	120	8.1	3.5	0.32	0.45	1580

Table 3.3: Mechanical properties of carbon-polyetherimide layer.

3.2.2 Static solution

The flexural rigidity of the delaminated segments derived above can be substituted in the static solution presented in section 3.1.2. Besides this, also the location

where force N_i is applied has changed. Force N_i causes either a shortening or an elongation of the delaminated layers. In order to prevent nonuniform strain this force should be applied at the neutral surface. This distance was also calculated in the paragraph above.

Figure 3.23 shows the free body diagram of the endplane. Equilibrium of force in both x - and z -direction and bending moment about the junction between delamination and end plane give now:

$$\begin{aligned} N_2 + N_3 &= 0 \\ V_2 + V_3 &= 0 \\ M_2 + M_3 + N_2(\delta_2 + \delta_3) &= 0 \end{aligned}$$

A similar change is observed in the continuity conditions:

$$\begin{aligned} \varphi_2(L) &= \varphi_3(L) \\ u_2(L) &= u_3(L) \\ w_3(L) &= w_2(L) + (\delta_2 + \delta_3)\varphi_2(L) \end{aligned}$$

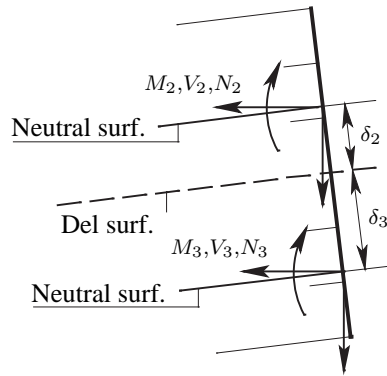


Figure 3.23: Free body diagram of end plane.

As was observed in section 3.1.2, also in case of composites only the displacement as result of a shear force is affected. Figure 3.24 shows the displacement at the free end in case a shear force is applied as function of delamination location. The graph shows a considerable increase of deflection after the delamination is located under the fourth layer. The stiff fourth layer becomes part of the upper segment, as a result its distance to the neutral surface is reduced which decreases the flexural rigidity of the delaminated segment.

In figure 3.25 the effect of delamination location on the displacement is shown for

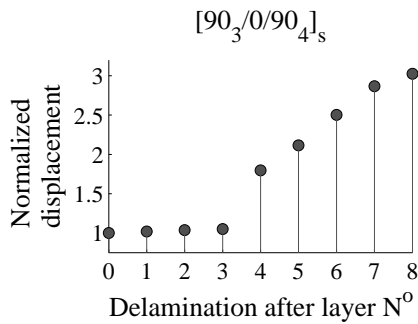


Figure 3.24: Effect of delamination location on displacement.

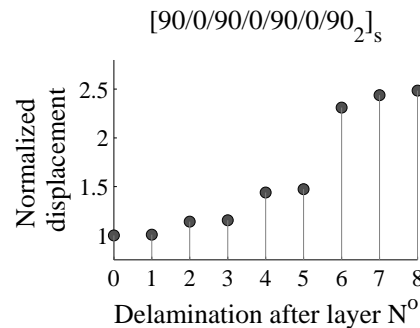


Figure 3.25: Effect of delamination location on displacement.

a $[90/0/90/0/90/0/90_2]_s$ laminate. Every time a stiff zero degree layer is shifted to the upper segment a jump in displacement is observed. From the figures 3.22, 3.24 and 3.25 it can be concluded that in case of laminates the decrease in flexural rigidity is heavily influenced by the delamination location and laminate lay-up.

3.2.3 Dynamic solution

As stated above the flexural rigidity of the delaminated section depends on laminate lay-up. The general solution for the delaminated segment was found to be:

$$\bar{u}_2(\bar{z}_i) = A_2 \sin \beta_2 \bar{z}_2 + B_2 \cos \beta_2 \bar{z}_2 + C_2 \sinh \beta_2 \bar{z}_2 + D_2 \cosh \beta_2 \bar{z}_2 \quad (3.33)$$

In this equation β_2 cannot be rewritten in the dimensionless transversal delamination location h_2 anymore. For β_2 the following relation is found:

$$\beta_2^4 = \frac{\omega^2(m_2 + m_3)L^4}{EI_2 + EI_3} = \frac{\beta^4 EI_1}{EI_2 + EI_3}$$

Furthermore the continuity conditions for shear force, bending moment and normal force, equations 3.23, 3.24 and 3.25, have to be rewritten. These cannot be simplified to the dimensionless transversal delamination location anymore. The continuity equations for shear force and bending moment become:

$$\frac{\partial^3 \bar{u}_i}{\partial \bar{z}_i^3} = \left(\frac{EI_2 + EI_3}{EI_1} \right) \frac{\partial^3 \bar{u}_2}{\partial \bar{z}_2^3}, \quad i = 1, 4 \quad (3.34)$$

$$\frac{\partial^2 \bar{u}_i}{\partial \bar{z}_i^2} = \left(\frac{EI_2 + EI_3}{EI_1} \right) \frac{\partial^2 \bar{u}_2}{\partial \bar{z}_2^2} + \frac{PL^2(\delta_2 + \delta_3)}{dEI_1}, \quad i = 1, 4 \quad (3.35)$$

The force P can be determined from the extend of stretching of the delaminated layers, as shown in static analysis. From [21] it follows that P equals:

$$P = \frac{\bar{d}(\delta_2 + \delta_3)}{\bar{b}L} \left[\frac{1}{EA_2} + \frac{1}{EA_3} \right]^{-1} \left[-\frac{\partial \bar{u}_1(\bar{a})}{\partial \bar{z}_1} + \frac{\partial \bar{u}_4(-\bar{c})}{\partial \bar{z}_4} \right] \quad (3.36)$$

In which EA_i is determined above and given in equation 3.28. The twelve conditions are again written as a matrix vector equation. The fundamental frequency β is found by the requirement for the determinant of the matrix to equal zero.

For a $[90_3/0/90_4]_s$ laminate the influence of delamination location on the first and second fundamental frequency is respectively shown in figure 3.26 and 3.27. The delamination length equals 20% of the total beam length. The delamination has almost no effect if it's located anywhere between the first or fourth layer. However in case it's located after layer number four a considerable influence is noticed. These results correspond well with the static solution presented above. There also

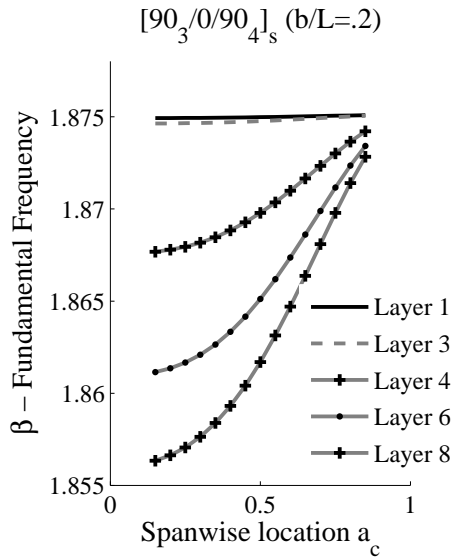


Figure 3.26: Effect of delamination location on first resonance frequency.

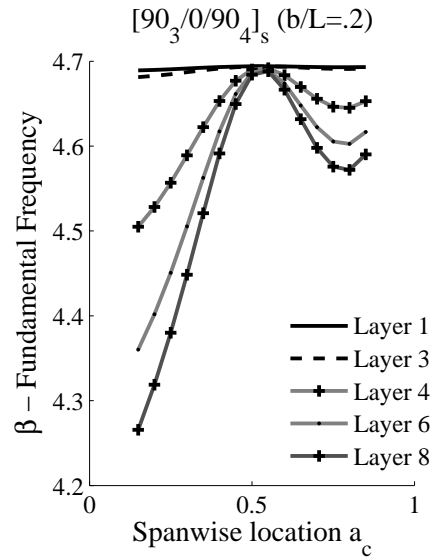


Figure 3.27: Effect of delamination location on second resonance frequency.

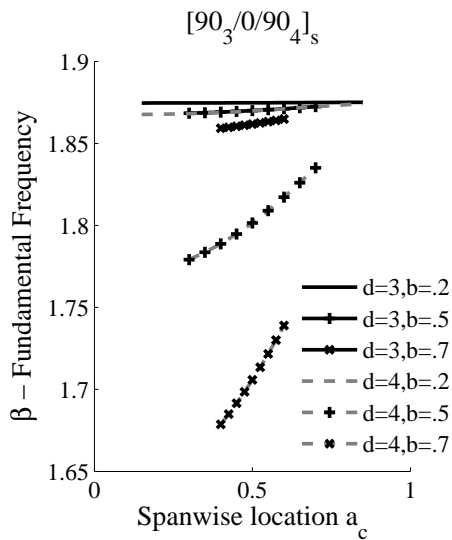


Figure 3.28: Effect of delamination location on first resonance frequency.

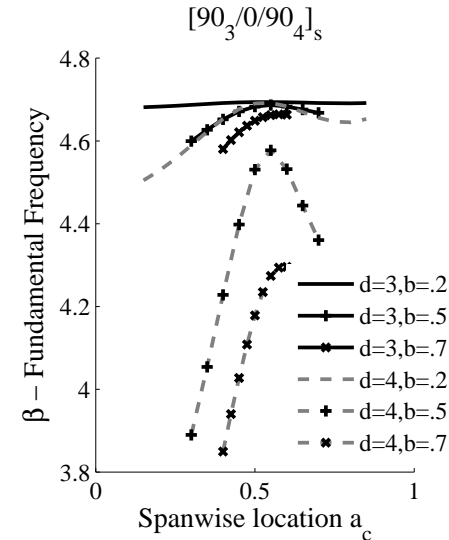


Figure 3.29: Effect of delamination location on second resonance frequency.

a sudden decrease in flexural rigidity was observed in case the delamination was located after the fourth layer. In figure 3.28 and 3.29 the effects of delamination length for different transversal and longitudinal locations on the first and second fundamental frequency is shown. Again the effect of delamination location on flexural rigidity is underlined. The parameter d indicates after which layer the delamination is located.

3.3 Finite element analysis

Two finite element models, representing a delaminated beam, are described in this section. Finite element models provide an easy way of investigating the effect of delaminations in more complex structures. In this section two models are proposed. In the first model the delaminated beam is modelled with two node beam elements. As in the analytical model this model consists of four separate beam segments. The second model uses contact elements in combination with four node 2D brick elements. The contact elements in this last model could be used in the future for modelling more complex delaminated structures.

3.3.1 Beam elements with node coupling

This model is based on 2D two node beam elements. As stated above four segments can be distinguished in this model, this is illustrated in figure 3.30. The transversal displacement of axially corresponding nodes in the delaminated layers are coupled:

$$u_{a^n} = u_{b^n} \quad (3.37)$$

This effectively means that the delaminated layers stay in contact during the vibration of the beam. However because the axial displacement and rotation are not coupled the layers are free to slide with respect to each other. At the junction between integral and delaminated segments all degrees of freedom are coupled. For the transversal displacement and rotation of the nodes at the junction the following holds:

$$\begin{aligned} \phi_i &= \phi_j = \phi_k \\ u_i &= u_j = u_k \end{aligned}$$

For the axial displacement of nodes i, j, k in figure 3.30 one obtains:

$$\begin{aligned} w_i &= w_j - \phi_j \delta_2 \\ w_k &= w_j + \phi_j \delta_3 \end{aligned}$$

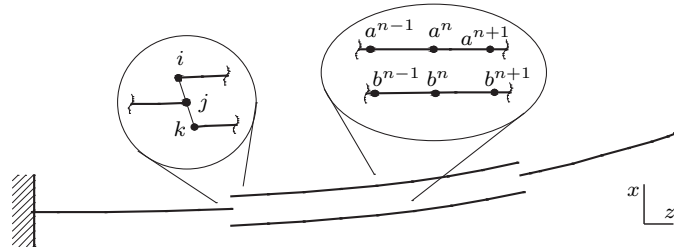


Figure 3.30: Representation of a delaminated beam with 2-node beam elements.

In which δ_i represents the distance of the neutral plane of segment i to the neutral plane of the first or last beam segment. The beam is modelled in ANSYS using BEAM3 elements to represent the separate segments. The elements are created on the neutral axis of the beam segments.

3.3.2 Contact elements in combination with brick elements

A two dimensional finite element model was created in ANSYS. The beam was modelled using PLANE42 elements. This brick element is mainly used for 2D modelling of solid structures. The element is defined by four nodes, all having two degrees of freedom: translations in nodal x and y . A plane strain situation was assumed. The delaminated surface was created using contact elements. For this purpose two elements were needed, namely a contact element CONTA171 and a target element TARGE169. It was assumed that the delaminated layers stay in contact and only slide, without friction, in relation to each other. Figure 3.31 shows the finite element representation of a delaminated section of the beam.

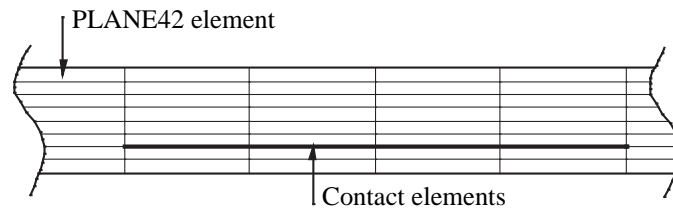


Figure 3.31: Representation of a section of a delaminated beam with contact elements and 2D-brick plane elements.

A common problem encountered using four node plane elements in bending analysis, is that the flexural rigidity can be overestimated. This effect is minimized by taking more elements over the beam thickness. A study showed that the extend of this overestimation, compared with results obtained by using eight node 2D brick elements, is found to be less than .3% for resonance frequencies near 1200Hz.

3.3.3 Results

A modal analysis of both models was carried out to extract the resonance frequencies of the first five modes of vibrations for an isotropic cantilevered beam. The material properties used are listed in table 3.3. The beams length and width were respectively 400mm and 20mm, the thickness was 2.0mm. In table 3.4 the resonance frequencies obtained by the analytical analysis are compared with the results obtained by these finite element analysis. It can be seen that the results from the finite element models correspond well with the analytical case. Both the coupling of nodes and the use of contact elements are very suitable for representing sliding

delaminations. In more complex structures, however, it might be hard to represent a delamination by coupling nodes. Contact elements provide, as can be seen in table 3.4, an excellent alternative. Also contact elements can be used to introduce friction between the layers or allow the delamination to open and close during vibration.

DELAMINATION PARAMETERS						
$\bar{a}_c = .4, \bar{b} = .6, \bar{h}_2 = .25$				$\bar{a}_c = .5, \bar{b} = .2, \bar{h}_2 = .5$		
Mode	Analytical	BEAM3	PLANE42	Analytical	BEAM3	PLANE42
1	16.52	16.52	16.51	17.56	17.56	17.56
2	94.25	94.25	94.06	110.46	110.46	110.40
3	241.53	241.53	241.07	279.41	279.39	278.92
4	484.34	484.33	483.89	596.70	596.63	595.68
5	801.05	801.12	800.93	821.93	821.79	821.17

Table 3.4: Comparison between analytical and FEM results.

3.4 Summary and concluding remarks

The influence of a delamination on the resonance frequencies of a cantilever beam was studied in this chapter. For this purpose an analytical model, introduced by Mujumdar and Suryanarayan [21], was investigated and modified for use with composite structures. Furthermore two finite element models were presented which both could be used to investigate the dynamic behaviour of delaminated structures. The results of the two finite element models compared extremely well with the analytical analysis.

Regarding the effects of a single 'through width' delamination on an isotropic, homogeneous beam the following general conclusions can be drawn:

- A static analysis, subjecting a delaminated beam to a shear force, showed that the influence of a delamination on bending shape or displacement of free end can be neglected. Only for large delaminations, over 40% of the beams length, a detectable change in displacement is observed.
- The axial, in contrast with transversal, location of the delamination has no influence on static bending behaviour. Transversally, however, the effect of a delamination maximizes in case it is located on the neutral plane of the beams thickness.
- The influence of a delamination on resonance frequencies is significant and increases with mode number. In all cases resonance frequencies shift to lower values as result of a delamination.

- As in the static case, resonance frequencies are influenced most in case the delamination is located at half the thickness.
- Each mode is affected differently by the axial location of the delamination. This fact results from the fact that the shear force is distributed non-uniformly across the beam's length and can be used to locate the delamination.

An investigation of the influence of a delamination on the resonance frequencies of composite beams showed that, laminate lay-up plays an important role.

From this theoretical analysis it can be concluded that shifts in resonance frequencies can very well be used as a damage indicator. Monitoring resonance frequencies provides a more accurate way for detecting delaminations than a static analysis.

3.5 Nomenclature

A_i, B_i, C_i, D_i	constants in mode shape expression
a	length of first integral segment
b	delamination length
β	fundamental frequency
c	length of third integral segment
$\bar{a}, \bar{b}, \bar{c}$	dimensionless delamination parameters, $a/L, b/L, c/L$
\bar{a}_c	dimensionless spanwise delamination location
h	thickness of beam
h_i	thickness of segment i
\bar{h}, \bar{h}_i	dimensionless thickness h/L , dimensionless transversal delamination location h_i/h
EI_i	flexural rigidity of segment i
i	subscript representing each segment
L	beam length
M_i	bending moment in each segment
m	mass per unit length
N_i	normal force in each segment
p	contact pressure between each segment
t	time
u_i	transversal displacement
\bar{u}_i	dimensionless transversal displacement u_i/d
V_i	shear force in each segment
w_i	axial displacement
\bar{w}_i	dimensionless axial displacement w_i/d
\bar{z}_i	dimensionless axial co-ordinate z_i/L
ω	radian frequency of vibration

EXPERIMENTAL VALIDATION

In the following section the validation programme will be described. Both static and dynamic tests have been conducted. Two goals will be pursued in this programme. The first consists of validating the analytical and finite element models provided in chapter 3. The second goal is to investigate the potential of fibre bragg gratings for dynamic health monitoring based on dynamic behaviour.

4.1 Programme outline

The validation programme consists of three stages, of which a detailed outline is given below. The programme is aimed at validating the statements found in the theoretical analysis. A modal analysis is performed on cantilevered beam shaped specimens with varying delamination parameters. The experimental set-up is discussed in section 4.2. Delaminated specimens are easily manufactured by inserting a thin sheet of kapton foil between two pre-impregnated carbon-polyetherimide plies prior to the consolidation of the laminate. The foil prevents the two plies to melt together and thus a delamination is formed. The size and position of the delamination is highly controllable which is an advantage over other artificially induced damage types.

Stage A: Validation of the experimental set-up and sensor evaluation

In order to validate the conclusions drawn in the theoretical analysis a reliable testing approach should be adopted. The main goal of this stage therefore is to check the testing approach in terms of reproducibility and to study the influence of external parameters like clampforce and tension in the spring, supporting the shaker. The set-up is shown in figure 4.1. Various literature state that it is difficult to achieve exact cantilever vibration in practice. It is checked to what extent this might cause problems during this experimental programme. The secondary goal is to evaluate different types of sensors to capture the response of the beam specimens. In this

stage an accelerometer, strain gauge and a microphone are evaluated. Furthermore results obtained from the models derived in section 3.1 are validated. To achieve these goals, nine beam-shaped specimens are fabricated. Three of these specimens are labeled as intact and contain no delamination. The other six are divided in two groups, of which three specimens have a delamination at 50% of the beam thickness and the remaining three have a delamination at 25% of the thickness.

Stage B: Application of fibre bragg gratings for health monitoring

Despite the encountered difficulties, stage A proved that strain measurements could be used to determine the dynamic properties of a structure. This stage will investigate the application of fibre bragg gratings for strain measurements in composite structures. These measurements are used to derive the dynamic properties of the specimens. The main problem concerning strain measurements lied in the fact that for higher vibration modes the strains became too small to measure. The laminate lay-up for the different specimens will be tailored in order to maximize the strain for higher modes. Static tests will be conducted to investigate the resolution and accuracy of the fibre bragg gratings. The data acquisition system is tested in order to evaluate the sampling rate.

Stage C: Validation of theoretical results

In this stage the analytical and finite element models will be validated. The resonance frequencies of beam specimens containing varying delamination parameters are obtained. Stage A demonstrated that the experimental set-up, as described in section 4.2, did not satisfy the requirements. Test specimens are therefore excited by hammer-impact. The delaminations have a length of 30% of the beam span at most. Also the effect of a growing delamination is closely monitored. For this purpose a specimen containing a small delamination is used. Between several modal analyses the delamination is extended by using a sharp razorblade.

4.2 Experimental set-up

In figure 4.1 the experimental set-up is outlined. Beam shaped specimens are cantilevered and excited using a shaker. In order to reduce the influence of environmental vibrations the shaker is hung from a spring connected to the fixed world. The force excited by the shaker on the specimen is recorded with a force transducer. The response of the beam is measured using accelerometers, strain gauges and fibre bragg gratings. Also the sound radiated from the vibrating beam is recorded by microphone. The signals are amplified before these are fed in to a data analyser, see appendix A. With help of a computer the gathered time responses are analysed and transformed by means of a fast fourier transformation (FFT). In appendix A the used hardware is also listed.

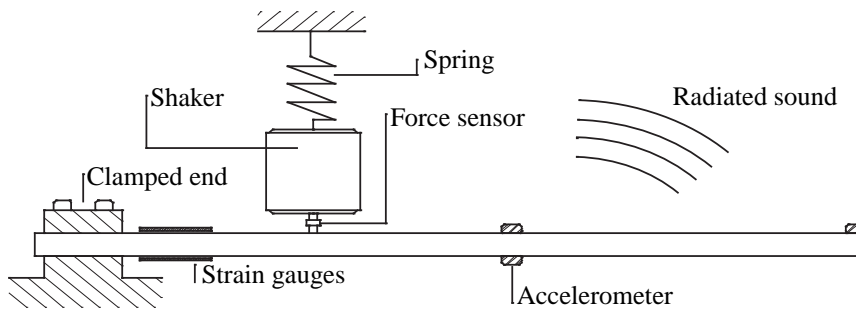


Figure 4.1: Experimental set-up (shaker) for modal analysis.

4.3 Stage A: Validation of the experimental set-up and sensor evaluation

The main goal of stage A was to validate the test approach and the experimental set-up in terms of reproducibility and robustness. Also the use of accelerometers, strain gauges and a microphone were evaluated for capturing the responses of the beam. At last the effects of delaminations on the frequency response of beams were obtained and compared to the theoretical analysis. The following testing scheme was adopted to pursue these goals.

1. Validation of the testing approach

- **Effect of clamping conditions** The effect of clamping conditions on the frequency response plot was studied. The conditions were systematically varied.
- **Influence of spring force** The effect of the tension in the spring was investigated. The spring force was varied by means of changing the deflection of the spring in rest. Three cases were examined, the deflection was varied between 0, 7 and 15mm.
- **Reproducibility** The reproducibility was studied by performing separate tests with constant conditions at distinct times. The specimen was removed after each test. The resulting variations gave an indication of the reproducibility of the testing method.

All these tests were performed using an intact specimen. The shaker excited the beams with a chirp signal from 0 to 2kHz. The response of the beam was captured with an accelerometer attached to the free end of the specimen.

2. **Evaluation of used sensors** The response of the beam specimens was obtained by means of different sensors. In this stage measurements were obtained using an accelerometer, strain gauges and a microphone. The data obtained by the different sensors was compared and conclusions were drawn

on their applicability for dynamic health monitoring. The information gathered by the strain gauges was used to gain insight in the application of fibre bragg gratings in later research. The tests were performed using the same specimen as used above.

3. **Evaluation of the effect of delaminations** Two series of three specimens contained a through width delamination at 50% and 25% of the thickness. The effect of these delaminations on the resonance frequencies was investigated. The theoretical study indicates a shift of resonance frequencies to lower values. The obtained resonance frequencies were compared to theoretical values.

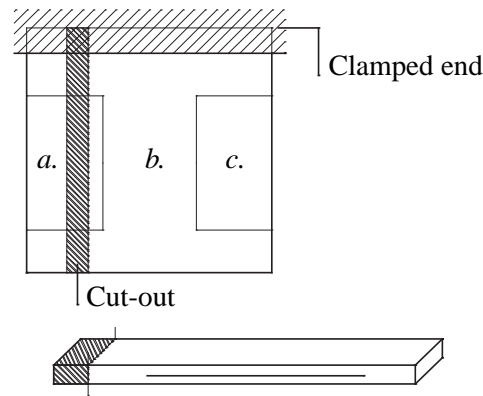


Figure 4.2: Specimen cut-outs.

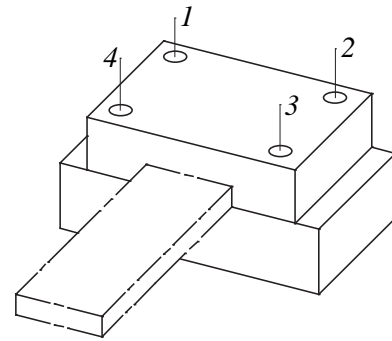


Figure 4.3: Clamping construction.

4.3.1 Specimen preparation

A unidirectional plate was fabricated from 12 layers of prepreg C-PEI. The fabrication process is documented in appendix B. The resulting plate had a thickness of approximately 1.6mm and a fibre mass fraction of 40% [36]. The material properties are listed in table 4.1. By using 16 μm thick kapton foil two delaminations at different thickness-wise locations were created. The delaminations, indicated in figure 4.2 by *a* and *c*, were located on respectively 25% and 50% of the thickness and measured 60% of the beams total length. The region indicated by *b* contained no delamination. The large delaminations were thought to have a great influence on the beams dynamic behaviour and the effect will be easy to note. Three beams,

carbon-PEI	E_1 (GPa)	E_2 (GPa)	G_{12} (GPa)	ν_{12}	ν_{23}	ρ (kg/m^3)
	120	8.1	3.5	0.32	0.45	1580

Table 4.1: Mechanical properties of carbon-polyetherimide layer.

with a length of 336mm and a width of 20mm , were cut from every section. The axial direction of the beam shaped cut-outs corresponded with the fibre direction of the laminated plate. Table 4.2 and appendix C list the specimen dimensions and delamination parameters. An explanation of the delamination parameters can also be found in appendix C.

Specimen ID	Specimen size			Del. parameters		
	L (mm)	w (mm)	h (mm)	\bar{a}_c	\bar{b}	\bar{h}_2
U1.00.000	320	20.1	1.67	na.	na.	na.
U1.06.025	320	20.1	1.66	.5	.6	.25
U1.06.050	320	19.9	1.67	.5	.6	.5

Table 4.2: Specimen dimensions and configuration stage A.

4.3.2 Evaluation of the experimental results

Validation of the experimental set-up

The experimental set-up was validated on two distinct points: the reproducibility of the experiments and the influence of external parameters like clamping conditions or spring tension.

The influence of the clamp, see figure 4.3, was studied by performing several tests under varying clamping conditions. In figure 4.4 four obtained frequency response functions are plotted. The conditions are listed in the table 4.3. The results represent worst case scenarios. Tests with other variations in clamping conditions showed less or no deviation at all in frequency response plots compared to the fixed case.

Condition	Description
Fixed	Fully bolted
Condition 1	Six layers of scotch tape added between the two clamp parts
Condition 2	Left side (bolt 1 and 4) ^{β} of the clamp bolted
Condition 3	Back side (bolt 1 and 2) ^{β} of the clamp bolted

^{β} See figure 4.3

Table 4.3: Clamping conditions.

The results indicate that only in the case of condition 4 the frequency response plot shows a large deviation compared to the fixed clamp. A significant shift in resonance frequencies is observed. However, since the clamp was only bolted at the back side, this case hardly represents cantilever vibration. For the remaining conditions the resonance frequencies do not vary significantly. Based on the results obtained it may be concluded that a small variation in clamping conditions has a

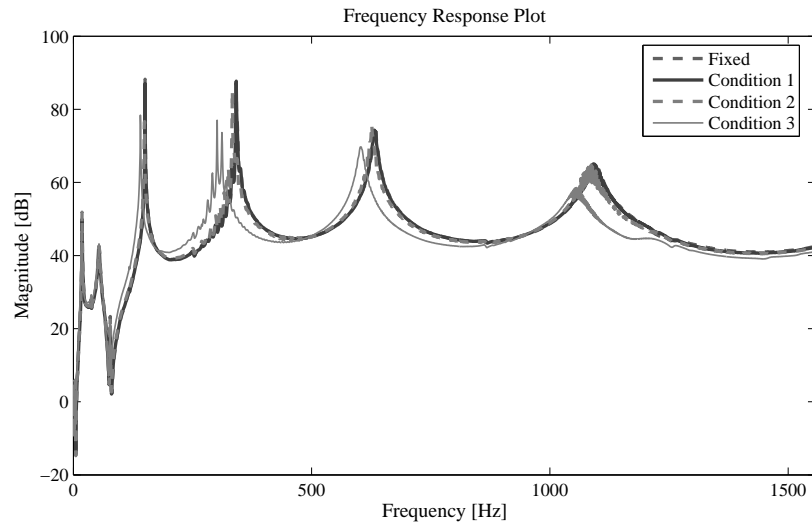


Figure 4.4: Frequency response plots of intact specimen U1.00.000 with varying clamping conditions.

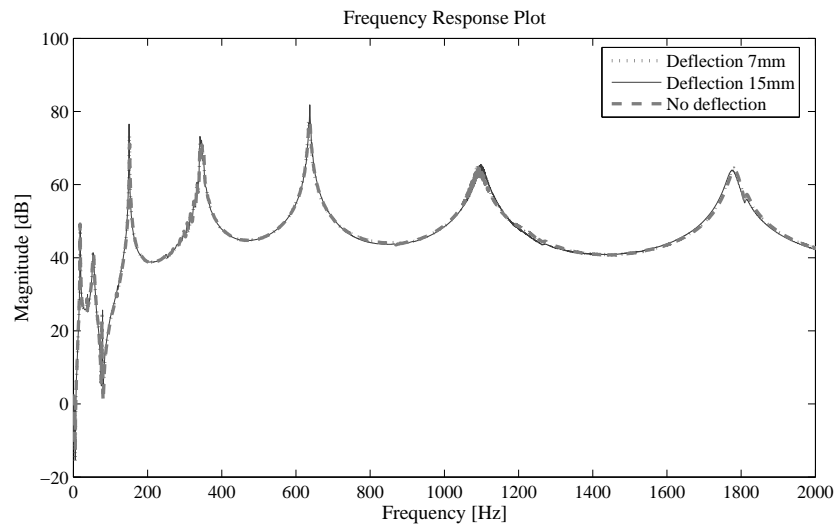


Figure 4.5: Frequency response plots of intact specimen U1.00.000 with varying spring tension.

negligible influence on the obtained frequency response functions. The clamp can therefore safely be used in this experimental programme and does not need any refinement.

The influence of the tension in the spring on the obtained result was also investigated. Similar conditions concerning excitation and response capturing were used as for the tests above. The tension was varied by changing the spring deflection

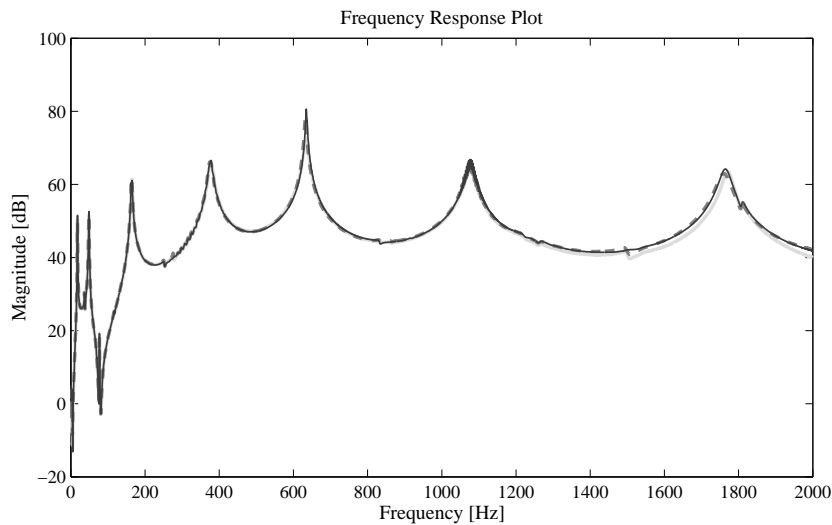


Figure 4.6: Frequency response plots of specimen U1.00.000 at similar conditions, but at distinct times.

in rest between 0, 7 and 15mm. Figure 4.5 shows the frequency response plots for three different cases. As can be seen from the figure this has no influence on the obtained frequency response plots.

The reproducibility of the experimental set-up was tested by performing three tests under constant conditions at distinct times. An intact specimen was used. The beam was after each test removed from the clamp. Figure 4.6 shows three measured frequency response plots for an intact specimen, at different times. As can be seen the different curves compare very well. The highest standard deviation over the three tests was found to be .35% for the last peak. The averaged standard deviation over all peaks equalled 0.2%. Similar results were obtained for the other beam specimens. It is therefore concluded that the experimental set-up and method satisfies the demands in terms of reproducibility. In literature the small statistical variation of resonance frequencies was already mentioned [28]. The small standard deviation allows the detection of very small shifts of resonance frequency and thus the detection of small delaminations.

Recapitulating, the following conclusions are drawn:

- The influence of external parameters can be neglected. However, the clamped end should be used with care. Small deviations in clamping conditions have no influence on the obtained results, while erroneous usage can influence the results heavily.
- The experiments are easy to reproduce and the obtained results show negligible differences.

- The experimental set-up and method suffices the conditions in terms of reproducibility and influence of external parameters and can therefore be used in this programme.

Evaluation of different sensors

The second part of stage A evaluated different sensors for capturing the beams response. Besides the accelerometers used in the first part of this stage, the response of the beam was also captured by strain gauges and a microphone. The strain gauges were fixed near the clamped end of the beam in order to capture all flexural vibration modes. Radiated sound from the vibrating beam was captured by a microphone. The obtained time signals were fed into a data analyser and transformed by means of FFT.

Figures 4.7 and 4.8 show respectively the frequency transfer plots obtained by an accelerometer and strain gauges. The upper graph in both figures shows the coherence of the measurement. The coherence is a guide to the quality of the transfer function measurement. The coherence measures in what extend the power of the response of the beam is caused by the driving power of the excitator. For a good measurement the coherence equals 1 over the whole frequency spectrum. As can be seen from figure 4.7 the quality of the measurement obtained by the accelerometer is very good. For the measurements obtained by the strain gauges, figure 4.8, however the coherence is poor. Only at resonance frequencies the coherence tends to equal 1. The beam vibrates heavily in its resonance frequency, allowing the

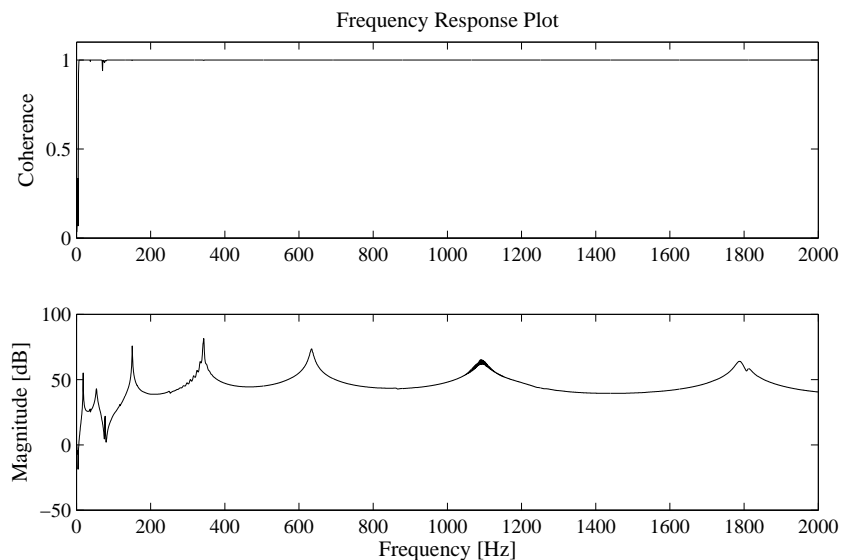


Figure 4.7: Frequency response plots of specimen U1.00.000 obtained by an accelerometer attached to the free end of the beam specimen.

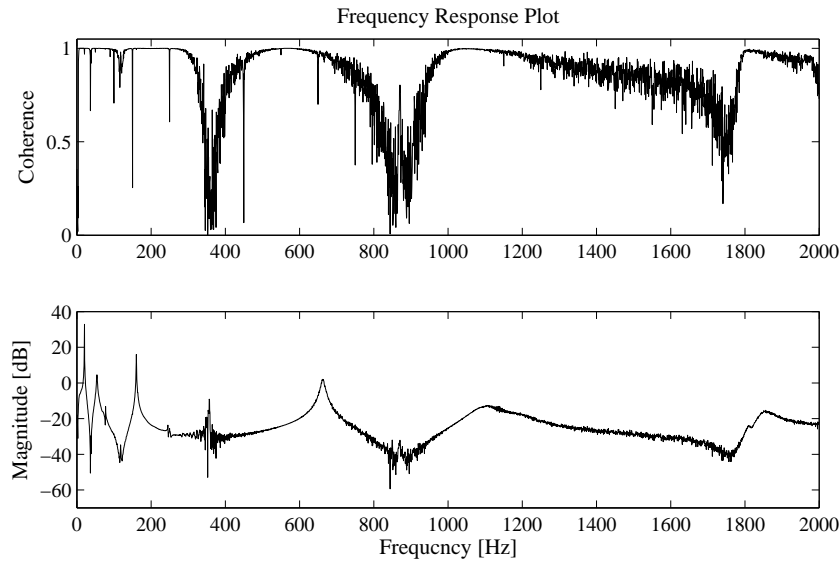


Figure 4.8: Frequency response plots of specimen U1.00.000 obtained by strain gauges glued near the clamped end of the beam specimen.

strain sensor to distinguish the induced strain from the noise level. Outside these resonance frequencies the strain becomes very small, resulting in a poor signal to noise ratio. For the higher modes with frequencies over 2kHz, the strain gauges were unable to provide any signal at all. It is also noted that the resonance frequencies obtained by the accelerometer are slightly lower than the ones obtained by the strain gauges. This can be explained by the fact that the accelerometer adds mass to the system.

Also the use of a microphone for capturing the response of vibrating structures was investigated. Figure 4.9 shows the frequency response plot, up to 10kHz, of an intact specimen. In the upper graph the signal was captured by the accelerometer. The lower graph gives the frequency response plot as obtained by the microphone. The frequency response function obtained by the microphone shows more peaks and also a more erratic profile. The additional peaks can be caused by the fact that a microphone is also able to capture torsional vibration modes, while the accelerometer is located in the middle of the beams width to prevent this. Furthermore the surrounding noise can be the reason for the erratic profile shown in the graph. To prevent the influence of surrounding noise, measurements with a microflown can be considered. Nevertheless the general profile of the two measurements compare reasonably.

Recapitulating, the following conclusions are drawn:

- Accelerometers provide good results for obtaining the response of the cantilevered specimens. The measurements show good coherence and resonance

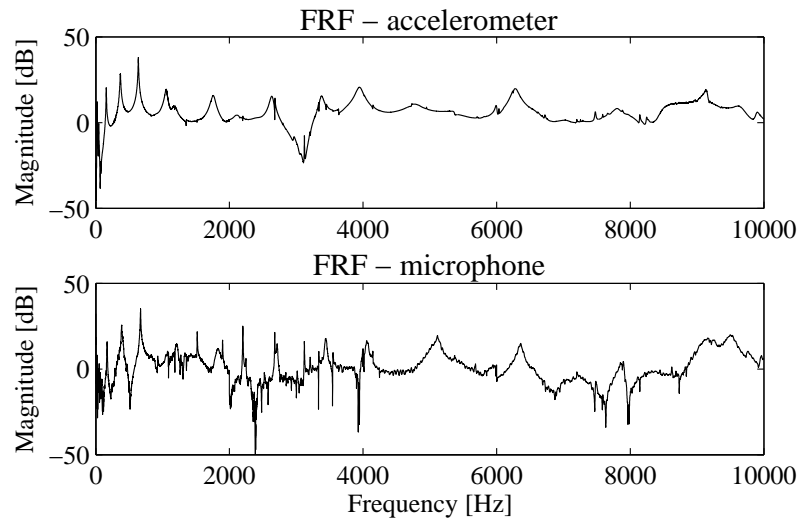


Figure 4.9: Frequency response plots of intact specimen U1.00.000 obtained by an accelerometer and by capturing the radiated pressure waves with a microphone.

peaks are easy to identify.

- The strain gauges showed bad coherence outside the resonance frequencies. This can be explained by the poor signal to noise ratio. The occurring strain becomes too small to distinguish it from the noise level. This problem plays a bigger role for higher vibration modes, as the strain will become smaller. Tailoring the specimens in terms of laminate lay-up might prove useful in an attempt to increase the measured strains.
- Obtaining the frequency response function by means of a microphone looks quite good. At higher frequencies the obtained coherence was still good. The influence of surrounding noise however can limit the applicability of a microphone for capturing responses.

The effect of a single 'through width' delamination

Three types of specimens were cut-out from the fabricated unidirectional plate. Two types contained a delamination; one type at 50% of the thickness and one type at 25% of the thickness. The response of these specimens was measured.

Figure 4.10 shows the frequency response plots of the three specimens. It can clearly be seen that the resonance frequencies of the delaminated beams are much lower than for the intact beam. This qualitatively corresponds well with literature [21, 8, 20, 26, 32, 34, 35]. It can be observed that the reduction in resonance frequencies is the greatest for the specimen with a delamination at 50% of the thickness. This was also determined using the model by Mujumdar and Suryanarayan [21], described in chapter 3. The closer the delamination plane lies to the neutral

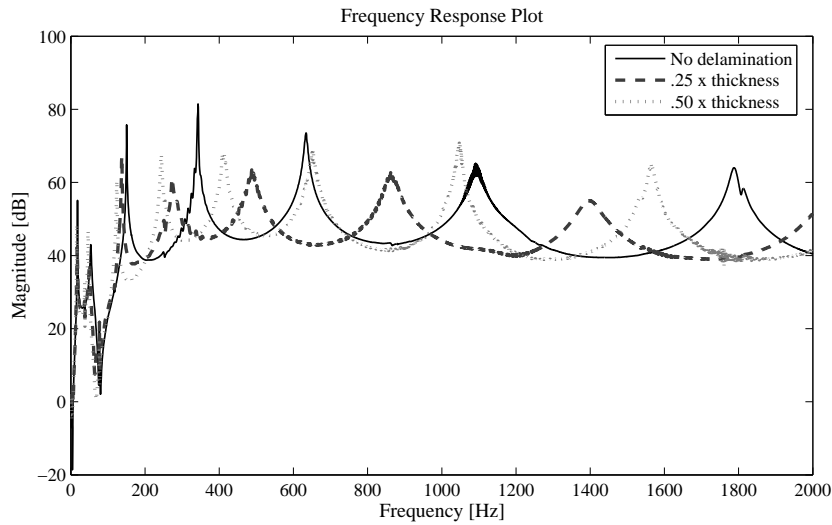


Figure 4.10: Frequency response plots of three specimens with varying delamination parameters.

line the larger the reduction in resonance frequencies. This is explained by the fact that the flexural rigidity of the delaminated region ($EI_2 + EI_3$) decreases as the plane moves to this neutral line.

In table 4.4 the obtained resonance frequencies are compared with the theoretical values calculated with the beam element model. This model is used as reference since it provides an easy way of adding the mass for the accelerometer. The differences between theory and validation for the intact specimen stand out. These differences question the reliability of the used experimental set-up. In order to investigate this theory, the shaker was removed from the set-up and the specimens were excited by a hammer impact, as can be seen in figure 4.11. The accelerometer again was used to record the response of the excited beam. The hammer-impact was applied at the same location the shaker was fixed to make sure all modes of interest were excited. The obtained results, listed in table 4.5, show for the intact

Mode	U1.00.000		U1.06.025		U1.06.050	
	Theory	Val.	Theory	Val.	Theory	Val.
1 st	18.7	18.1	18.6	17.5	17.5	16.3
2 nd	121.3	150.6	116.6	175.5	108.3	124.4
3 rd	339.8	343.6	262.8	273.8	216.3	243.8
4 th	671.1	634.4	530.1	488.1	440.4	413.1
5 th	1118.1	1073.1	909.0	862.5	744.1	653.8

Table 4.4: Comparison between theoretical and validated (shaker) resonance frequencies [Hz].

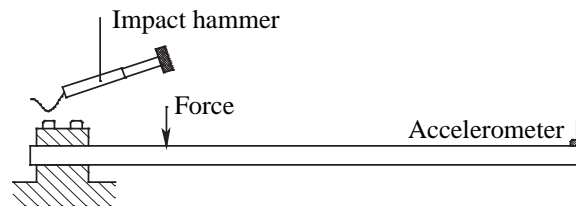


Figure 4.11: Experimental set-up (hammer-impact) for modal analysis.

beam far better comparison with the theoretical values. From this is concluded that the hammer-impact is a reliable way of obtaining the resonance frequencies. For the delaminated specimens the results show reasonable comparison with theory. The differences observed can be explained by the fact that the delaminations had a length of 60% of the beams length. The analytical model required the delaminated segments to stay in contact and slide among each other. With delaminations this size it is practically impossible to satisfy this requirement. Also if there exists contact between the layers there probably occurs some friction, which can also influence the results.

Mode	U1.00.000			U1.06.025			U1.06.050		
	Theory	%	Val.	Theory	%	Val.	Theory	%	Val.
1 st	18.7	.5	18.8	18.6	6.3	17.5	17.5	3.6	16.9
2 nd	121.3	0	121.3	116.6	10.3	130	108.3	9.3	119.4
3 rd	339.8	.8	342.6	262.8	1.1	260.0	216.3	2.6	210.8
4 th	671.7	.2	673.1	532.8	.5	530.1	440.4	4.4	421.9
5 th	1118.1	.7	1110.0	909.0	1.3	910.2	744.1	5.5	705.6

Table 4.5: Comparison between theoretical and validated (hammer-impact) resonance frequencies [Hz].

4.3.3 Conclusions

In this first testing stage the experimental set-up was validated in terms of reproducibility and robustness. Furthermore different sensors for capturing the response of vibrating test specimens have been evaluated. At last the obtained resonance frequencies of specimens, with varying delamination parameters, have been compared with the theoretical analysis in section 3.1. From this the following conclusions can be drawn:

- In terms of reproducibility and robustness the experimental set-up does satisfy the requirements for scientific research. However, the shaker has a significant influence on the found resonance frequencies, especially for the lower modes. For experiments in which the results are to be compared with a

theoretical analysis this set-up can therefore not be used. The resonance frequencies can in this case be obtained by an impact analysis. The specimen is excited by a hammer-impact and the response is captured by an accelerometer. Results obtained this way show better comparison with theory.

- Capturing the response by an accelerometer gives the best results; the measurements showed good coherence and the resonance frequencies can easily be identified. It is harder to measure the beams response with strain gauges. This is caused by a poor signal to noise ratio. Only for low vibration modes the strain is large enough to distinguish it from the noise level. Capturing the response of a vibrating beam by means of recording the radiated noise seems a reasonable alternative. It might be difficult, however, to identify torsional or flexural vibration modes. Also the surrounding noise has a large influence on the obtained frequency response function.
- The results obtained by the hammer-impact for the intact beam specimens correspond well with theory. For the delaminated specimens differences were found. However these discrepancies were small and are probably caused by the size of the delaminations. Theory requires that the delaminated segments stay in contact and slide amongst each other. However, since the delaminations measured 60% of the beams length, it can be argued whether this requirement can be satisfied. The experimental programme needs to be extended to validate the theoretical models.

4.4 Stage B: Application of fibre bragg gratings for health monitoring

The goal of this stage was to investigate the possibility of using the fibre bragg gratings for dynamic health monitoring. Fibre bragg gratings can be embedded in composite structures and are able to measure strain at different positions, this makes them a potential interesting monitoring technique. Also the fact that fibre bragg gratings show good resistance against corrosion and fatigue is an advantage over conventional strain gauges. Various tests were conducted and finally conclusions were drawn on future applicability of fibre bragg gratings for dynamic health monitoring.

4.4.1 Goals and proposed testing scheme

The accuracy of the strain measurements with fibre bragg gratings was evaluated with a static test. Beam specimens containing the sensing fibres were cantilevered and a force was applied at the free end. The strain near the clamped region was measured by an embedded fibre bragg grating and compared with theory. The goal

of these tests was to determine the general accuracy of the gratings. Both displacement and applied force were measured at the free end. The validity of the obtained data was checked by the calculated flexural rigidity. The laminate lay-up of the beam specimens was tailored to ensure that the fibres stayed on their desired location during production. In order to investigate the applicability of fibre bragg gratings for dynamic health monitoring dynamic experiments were also conducted. These tests also determined the suitability of the data acquisition system for dynamic signal processing. The following testing programme was adopted:

1. Static testing

- **Force-displacement** Beam shaped specimens were cantilevered. A force cell pushed the free end of the specimen down. The applied force and displacement at the free end were captured. The results were analysed and the flexural rigidity of the beam specimens was obtained.
- **Strain measurements** The strain near the clamped end was measured with the fibre bragg gratings. The results were compared with the theoretical case. Conclusions were drawn on the accuracy of the strain measurements.

2. **Dynamic testing** For the dynamic experiments the set-up provided in stage A was used. The resonance frequencies of the beam were obtained with help of the accelerometer. The shaker was then used to excite the beam in a number of these resonance frequencies. The strain near the clamped end was obtained by the fibre bragg gratings. The quality of the response was visually investigated. The data was captured by a data acquisition system with a sampling rate of 50kHz. The system only allowed a record time of one second. The time signal for various driving frequencies were transformed by means of a fast fourier transform. These tests gave insight in the maximum frequency up to which the data acquisition system is still able to capture the beams response.

4.4.2 Experimental set-up for static testing

In figure 4.12 the experimental set-up is outlined. A force cell is used to push the cantilevered specimen down. The displacement of the free end is recorded by means of a laser distance measurement device. Both the force and displacement at the free end are recorded. The data acquisition scheme is shown in appendix A. The maximum delamination length in the test specimens in this experimental stage equals 30% of the beams length. As was shown in section 3.1 the influence of such small delaminations on stiffness can be neglected. No real difference in bending stiffness between a delaminated and intact beam is thus expected. The

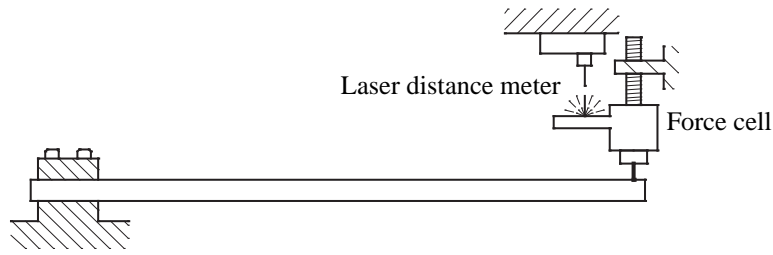


Figure 4.12: Experimental set-up for static tests.

flexural rigidity of the specimens can be determined as follows:

$$EI = \frac{F L^3}{u \cdot 3}$$

In which F/u represents the beam stiffness and is obtained from the experimental set-up and L represents the beams length. The theoretical flexural rigidity of laminated beams is derived in section 3.2.1.

4.4.3 Specimen preparation

A total of six beam specimens, of which five contained a sensing fibre, were sawn from a laminated CFRP plate. In order to maximize the measured strain, the fibre bragg gratings were positioned far from the neutral bending surface. To make sure the fibre gratings stayed on their desired distance from the neutral surface during the manufacturing process, the fibres were placed between two 90° layers. This is illustrated in figure 4.13. The carbon fibres in the 90° layers will prevent the layers to move in the melted matrix material during production. Space was created in the 0° to minimize deformation of the sensing fibres. However, as can be seen from the figure the fibre diameter (approx. $195\mu m$) is larger than the thickness of the individual layers (approx. $150\mu m$). During production the sensing fibre is therefore compressed.

The gratings were placed in the seventh layer from the symmetry plane in a $[90/0/90/0_2/90/0/90]_s$ plate. Delaminations were created on the symmetry plane of the laminate. The lay-up ascertained that the segments above and below the delamination are symmetric, which prevents failure due to thermal residual stress induced curvature. The theoretical flexural rigidity of the beams equals $1.154 Nm^2$.

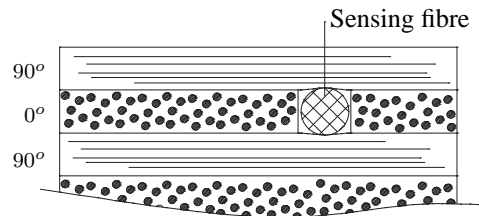


Figure 4.13: Cross-section of the top side of the laminate, showing the placement of the fibre bragg grating between two 90° layers.

One intact and five delaminated specimens were fabricated. Table 4.6 lists the various beam specimens. The delaminations were specifically located to validate the statement that each mode is affected differently by delamination location. From the analytical analysis in section 3.1 it followed that the effect of the delamination on the second resonance frequency is minimal for specimens with a delamination at .52 of the length. For the other specimens, with a delamination at .32 times the length, the effect is minimal on the third resonance frequency. The last specimen, U2.grow, will be used in stage C to monitor the effects of a growing delamination. The middle of delamination is located at a dimensionless distance \bar{a}_c from the clamped end and has a dimensionless length of \bar{b} . The parameters \bar{h}_2 gives the dimensionless thickness-wise location. Again this is summarized in appendix C.

Specimen ID	Specimen size			Del. parameters		
	L (mm)	w (mm)	h (mm)	\bar{a}_c	\bar{b}	\bar{h}_2
U2.000.00	455	20.1	2.31	na.	na.	na.
U2.052.02	455	20.1	2.32	.52	.2	.5
U2.052.03	455	19.9	2.32	.52	.3	.5
U2.032.02	455	20.0	2.32	.32	.2	.5
U2.032.03	455	20.0	2.32	.32	.3	.5
U2.grow	435	19.9	2.31	.32	.05	.5

Table 4.6: Specimen dimensions and configuration stage B.

4.4.4 Evaluation of the experimental results

Validation of the static test set-up

To validate the experimental static set-up, described in section 4.4.2, several tests were conducted on a $[0]_{16}$ carbon-polyetherimide test beam specimen of which the material properties are known. After several distinct tests a standard deviation of approximately .7% was obtained. Also the determined Youngs modulus corresponded well with the theoretical value. From this is concluded that the experimental set-up shows reproducible and reliable results.

Evaluation of strain measurements

Static measurements on three of the five specimens were conducted to investigate the general accuracy and resolution of the gratings for strain measurements. A 50kHz data acquisition system was used to investigate the resolution of the gratings. It was found that the signal was considerably corrupted with noise. The measured strain in the specimens showed, in the worst case, a standard deviation of $3.7\mu\epsilon$. The specimen with the best signal to noise ratio showed a standard deviation of $1.3\mu\epsilon$. Normally a standard deviation of $1.0p\epsilon$ is measured in similar fibre bragg gratings. These, however, are not embedded in a laminate. Possible causes of this high level of noise are discussed in section 4.4.5.

Table 4.7 lists the obtained results from the static tests. The obtained flexural rigidity, measured with force and laser displacement devices, correspond well with the theoretical value of $1.15Nm^2$. The strain was measured using a 1Hz data acquisition system. It can be seen, in table 4.7 that the measured strain deviates a lot from the theoretical case. A maximum difference of 27% is observed. The difference between validated and theoretical strain can have various causes, which are again discussed in section 4.4.5.

Specimen ID	STDEV noise ($\mu\epsilon$)	Measured rigidity (Nm^2)	Measured strain ($\mu\epsilon$)	Analytical strain ($\mu\epsilon$)	Difference (%)
U2.000.00	3.7	1.133	168.0	201.7	17
U2.052.02	2.3	1.161	163.1	224.1	27
U2.052.03	1.6	1.152	194.5	257.5	24

Table 4.7: Results from static experiments.

Evaluation of dynamic results

The dynamic analysis was performed in order to investigate the suitability of the 50kHz data acquisition system for fast digital signal processing and the capacity of the gratings to pick-up the different resonance frequencies. Since the data acquisition system was still in its development phase no software was available to perform a modal analysis, also the recording time was limited to one second. Therefore the quality of the obtained time signal was investigated visually. First the resonance frequencies of the specimens were determined with an accelerometer. Then the beam specimens were excited in their resonance frequencies and the time-strain signal was acquired. The obtained data was transformed by means of a fast fourier transform.

Table 4.8 shows the obtained results. It can be seen that the fibre bragg gratings is able to resolve the right frequencies. The upper graphs in figures 4.14 to 4.16 give the obtained fourier transform of the intact specimen vibrating in its resonance

Specimen ID	Driving frequency (Hz)	Obtained FBG frequency (Hz)
U2.000.00	11	11
-	368	369
-	910	910
U2.052.02	96	96
-	355	355
-	771	771
U2.032.02	87	87
-	591	591

Table 4.8: Results from dynamic experiments.

frequencies. In the lower graph the wavelength of the reflected light is plotted against the elapsed time. As stated in the introduction the shift in wavelength is coupled to the strain of the grating. From figure 4.16 can be seen that for higher vibration modes the strain becomes very small.

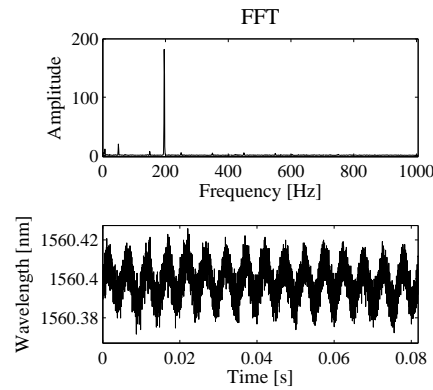


Figure 4.14: FFT and time signal for a driving frequency of 196Hz.

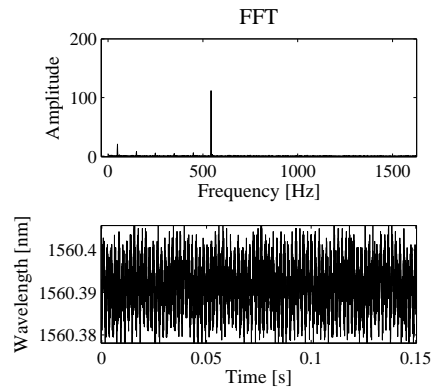


Figure 4.15: FFT and time signal for a driving frequency of 534Hz.

The driving frequency of 910Hz can still be found in the fourier plot, but it is a very weak signal. Also this FFT plot shows peaks at lower frequencies. The peaks are located at 50 to 550Hz with intervals of 100Hz. The same peaks are also observed in figure 4.15. However because of the fact that the strain, caused by the shaker vibration, is a lot higher for this vibration mode the lower frequency peaks are small compared to the driving frequency peak.

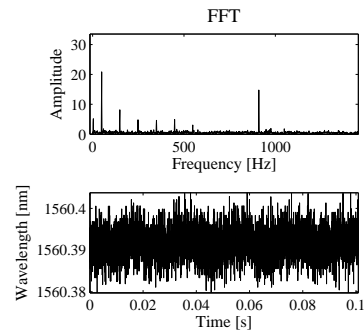


Figure 4.16: FFT and time signal for a driving frequency of 910Hz.

A detailed examination showed that in all signals these lower frequencies were represented. The origin of frequencies can be found in the AC/DC power conversion. After some an investigation the problem was solved.

The limiting factor in this testing phase was found to be the poor signal to noise ratio. The strain can not be distinguished from the background noise level. This plays a bigger role for higher vibration modes as the occurring strain becomes smaller. In stage A, where the response of the beam specimen was captured with strain gauges this problem was also observed. Earlier research in the suitability of the data acquisition system had shown that the system was able to capture the

signal reliably up to a driving frequency of 5kHz. However, further research in this field is desired.

4.4.5 Discussion

The possible use of fibre bragg gratings for dynamic health monitoring has been investigated in this experimental programme. The largest problem encountered lies in the poor signal to noise ratio. A standard deviation of $3.7\mu\epsilon$ was measured. This can be caused by several factors. Generally a standard deviation of $1.0p\epsilon$ is observed, however as stated these fibres are not embedded in a laminate. The production process of the laminate in which the fibres were embedded can have a severe influence on the signal strength. It is known that high temperatures can cause the grating marks to fade out, which results in an attenuation of signal strength. Since matrix material polyetherimide is consolidated during production at a temperature of $300^{\circ}C$ this might have had a bad influence on signal strength. An experiment, conducted during another research project, in which the signal strength was monitored during the consolidation of the matrix material confirms this theory.

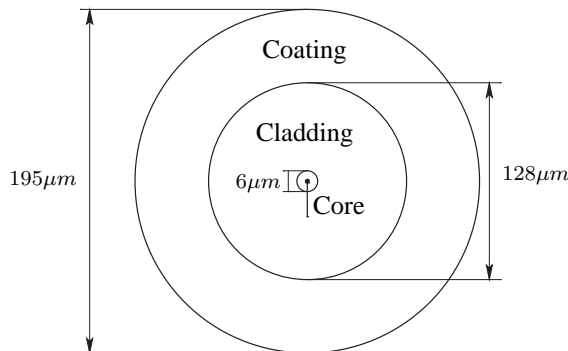


Figure 4.17: Dimensions of fibre bragg grating.

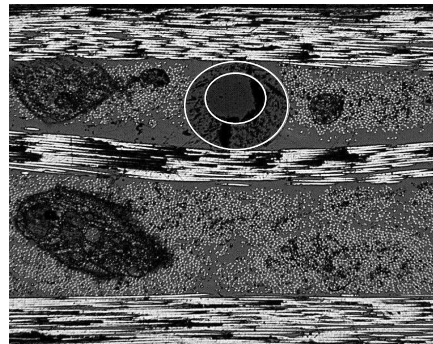


Figure 4.18: Micrograph of embedded fibre bragg grating (25x).

Also the applied pressure of 9 bar during the production process can have had a negative influence on signal strength. As stated before the sensing fibres are embedded between two 90° layers. Figure 4.17 indicates that the outer diameter of the fibre equals $195\mu m$. With a carbon-PEI layer thickness of approximately $150\mu m$ this effectively means that the grating is compressed between two layers. Micrographs of a cross-section of an embedded fibre, shown in figure 4.18, confirm this. The cross-section shows that the fibre has an elliptic form, while originally the fibre should show a circular cross-section. The drawn white ellipses show the position of the coating and cladding. It can be seen that they are not perfectly concentric. Figure 4.19 shows this in detail. Similar results were obtained for other specimens, i.e. figure 4.20. It is not known if this has a negative influence on accuracy or signal

strength. The dark areas in the micrographs are caused by water seeping through the voids in the laminate. Figure 4.20 shows that the ceramic coating of the fibre bragg grating is broken. Because the broken pieces are embedded by the matrix material it can be concluded that this occurred during the production phase of the laminate. It is unknown if such damage has a negative effect on signal strength and accuracy. Extended research in the influence of the production process on the quality of the fibres is therefore required.

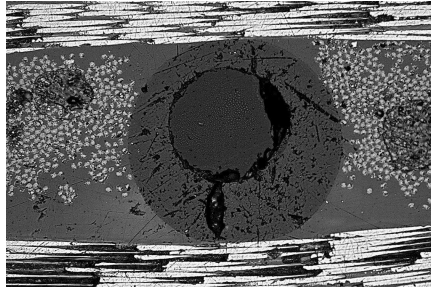


Figure 4.19: Micrograph of embedded fibre bragg grating (200x).

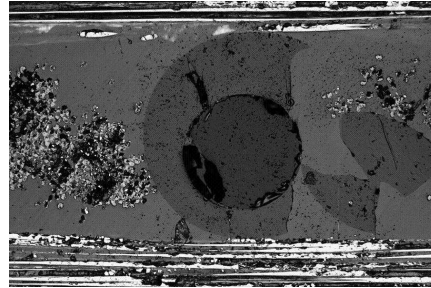


Figure 4.20: Micrograph of embedded fibre bragg grating (200x).

The difference between theoretical and experimental measured strain is the second problem encountered. The difference mounts up to 27%. The theoretical strain near the clamped end followed from:

$$\epsilon = \frac{3\delta \cdot t}{L^2} \quad (4.1)$$

In which δ is the displacement at the free end of the beam, L is the length of the beam and t the distance of the grating to the neutral plane. This equation assumes that the strain develops linearly over the thickness. For an ideal clamping condition, indicated in figure 4.21a, this might be the case. However, practically such a clamping condition is impossible. Figure 4.21b gives the used clamping condition. A finite element analysis in ANSYS evaluated the influence of the used clamping conditions. The results for both clamps are given in figure 4.21c and 4.21d. A clear difference in strain distribution is observed for the two cases. The analysis further showed that the used clamp can result in a difference of the strain near the gratings of at most 10%.

Another uncertainty in the strain measurements is caused by the fact that the exact axial location of the gratings is not known. During the placement of the sensing fibres an error of approximately 10mm can be introduced. This is caused by the fact that it is impossible to identify the gratings by naked eye. Additionally the grating has a length of 8mm over which the strain is measured.

However, because the mentioned causes cannot explain the large difference between measured and theoretical strain, of at most 27%, additional tests were performed. In order to investigate if embedding a fibre bragg grating has a negative

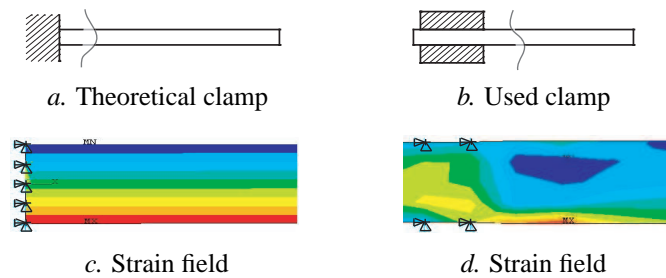


Figure 4.21: Finite element analysis of clamping condition.

influence on accuracy a tensile-strength test was conducted. For this purpose two specimens were fabricated. One unidirectional 16-ply carbon-PEI beam with a fibre bragg grating embedded on the symmetry plane. The other specimen was similar to the ones used in this stage and had a $[90/0/90/0/0/90/0/90]_s$ lay-up. In this specimen the fibre bragg grating was embedded in the seventh layer from the symmetry plane. Besides measuring the strain with the embedded fibre, this was also done with a fibre bragg grating glued to the surface of the test specimen. Additionally, the strain was measured by an external strain meter. The tests for both specimens showed that no differences at all were found in the different strain measurements. These tests show, as opposed to the previous tests, that the strain can very well be measured with an embedded fibre bragg grating. However, the strains that occurred during the bending test were significantly lower than the strain that arose during the tensile stress. Further research in order to explain the differences between theoretical and measured strain is required.

4.4.6 Conclusions and recommendations

Both static and dynamic experiments were conducted to investigate the possibilities of using fibre bragg gratings for dynamic health monitoring. The obtained results indicate a good perspective for future applicability of the fibre bragg gratings. The sampling rate of the data acquisition system is probably high enough to resolve frequencies up to 5kHz, however more research in this field is desired. One of the problems encountered was the lack of a software package to extract an averaged autospectrum of multiple measurements. However, the system is still in its development phase and sufficient improvement in this field can be expected. The largest problem at this moment is the low signal resolution and accuracy. Due to the low strain for higher vibration modes and high noise level it was impossible to resolve these higher resonance frequencies. The poor signal quality is known to be caused by the production process of the test specimens in which the fibres were embedded. It is recommended to concentrate future research in the following fields:

- To verify the accuracy of the fibre bragg gratings a four point bending test on a test specimen should be performed. The strain is then constant between

the two loading points. Also the problems described in the previous section with the clamping conditions are avoided this way.

- The effect of different processing conditions on general resolution and accuracy should be investigated thoroughly. It is known that high temperatures can cause the gratings to fade out. It has to be examined in what extend the applied temperature and pressure influences the accuracy and resolution.
- As an extension to the previous point it might be valuable to monitor the wavelength signal during the production process. The attenuation of signal strength can give insight in the influences of different production steps. While monitoring the changes in wavelengths can give interesting information about the development of residual stresses inside the laminate when cooling down.
- In order to test the potential a fibre bragg grating can be glued to the surface of a beam specimen. Signal attenuation due to the production process are avoided this way. The high accuracy allows an thorough investigation of the data acquisition system.
- Furthermore software should be developed for the data acquisition system to enable easy extraction of the resonance frequencies of test specimens.

4.5 Stage C: Validation of theoretical analysis

The goal of this stage was to validate the theoretical model provided in section 3.1. The specimens used in stage B were subjected to a modal analysis. It was observed in stage A that the experimental set-up with the shaker did not produce accurate results. The resonance frequencies of the specimens were therefore determined by measuring the response of the beam excited by a hammer-impact, as given in figure 4.11.

4.5.1 Testing scheme

The test specimens fabricated in stage B were all excited by a hammer-impact. The response was captured with an accelerometer. The found resonance frequencies were then compared to the ones calculated with the finite beam element model described in section 3.3.1. The finite element model was chosen as a reference because this provided an easy way of adding mass for the accelerometer. The flexural rigidity of the beam segments was determined as given in section 3.2.1. Furthermore the effect of a growing delamination was studied. A specimen containing a small delamination was manufactured and its resonance frequencies were determined. Then a razorblade was used to enlarge the delamination in a controlled

way prior to subsequent measurements. This way the effect of a delamination can closely be monitored.

4.5.2 Evaluation and discussion

Pre-delaminated specimens

Several hammer impact measurements were conducted and averaged. The data was used to obtain an autospectrum of the response. Figures 4.22 and 4.23 shows the response of respectively the intact and U2.052.02 specimen to the hammer-impact. The resonance frequencies can easily be identified by the peaks in the plots. A quick glance shows that the peaks in figure 4.22 appear to be steeper. The wider peaks in figure 4.23 are caused by an increase in damping, probably as a result of friction between the two delaminated segments. This subject, however, is not covered in this thesis. In table 4.9 the obtained resonance frequencies are compared to the ones calculated with the beam element model, provided in section 3.3.1. It can be seen that for the intact beam specimen the theory corresponds very well with the validated resonance frequencies. An averaged difference of 2.0% exists. However if the first resonance frequency, due to the high influence of the sampling rate, is excluded, an averaged difference of 0.8% is found. A similar result, an averaged difference of 0.4%, was observed in stage A, table 4.4. It can again be concluded that the results obtained by the hammer-impact are reliable. From table 4.9 it follows that the first and second resonance frequency for the intact specimen is lower than for the delaminated beams. The smaller theoretical resonance frequencies are caused by a differences in beam geometry. The intact specimen, U2.000.00 had a thickness of 2.31mm compared to 2.32mm for the delaminated specimens. This causes a reduction in flexural rigidity of 1.3%. This difference can be caused by the fact that the intact specimen, U2.000.00 was sawn from the edge of the laminated plate.

Further it can be seen that for the delaminated specimens the theoretical results

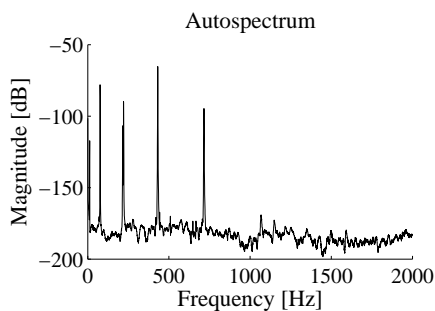


Figure 4.22: Autospectrum of intact specimen U2.000.00 excited by a hammer-impact.

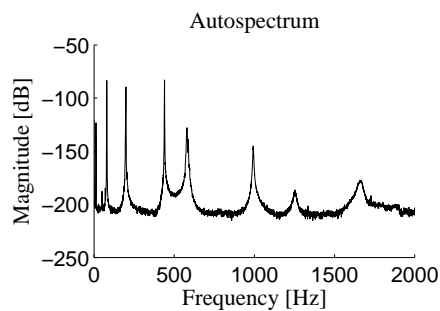


Figure 4.23: Autospectrum of delaminated specimen U2.052.02 excited by a hammer-impact.

show more deviation to the obtained values than for the intact specimen. An averaged deviation of 3.1% is found. The maximum difference of 10.2% is found for the fourth resonance frequency of specimen U2.052.03. The differences can be caused by several factors:

- The delaminated segments are modelled to stay in contact during vibration. This however is a requirement that is practically very difficult to satisfy. This also depends on the vibration mode considered.
- When contact occurs the theory demands that the delaminated segments are able to slide freely in relation to each other. However practically there will exist friction between the two segments. This friction can hinder the segments to slide, which then will result in an increase of flexural rigidity. The inserted kapton foil can have an additional negative effect on this friction. The foil thickness causes the contact pressure to increase with negative influence on friction forces. Also the friction coefficient of the foil can have a negative influence.
- In conjunction with previous point; the actual delamination, i.e. the region where the segments are able to slide, is probably smaller than the size of the inserted kapton foil. The kapton foil pushes the layers outwards, which results in a large contact pressure near the junction. This prevents the layers to slide freely near the junction and this effectively means that the delamination is probably shorter than intended.

It can be seen, despite the differences, from table 4.9 that the theoretical and validated results show a similar tendency.

In figure 4.24 it is again underlined to what extent delamination location influences frequency shifts of different modes. This figure plots the autospectra of two delaminated specimens. The delaminations were created on different locations. The first specimen, U2.052.03, has a delamination on .52 of the beam length. The lower graph in figure 4.24 indicates that for the second vibration mode the third derivative, and thus the shear force, is zero in this location. This means that the delamination has only a small influence on the second vibration mode. This also goes for the fourth vibration mode, as can be seen from figure 4.24. The delamination in the other specimen, U2.032.03, will have a small influence on the third resonance frequency. The delamination is located on a point of minimum shear force for this vibration mode. The upper graph of figure 4.24 shows the obtained autospectra of the two specimens. The graph shows that the second and fourth resonance frequency has shifted more for the U2.032.03 specimen than for the U2.052.03 specimen. The opposite is true for the third resonance frequency. This corresponds qualitatively very well with the theoretical analysis.

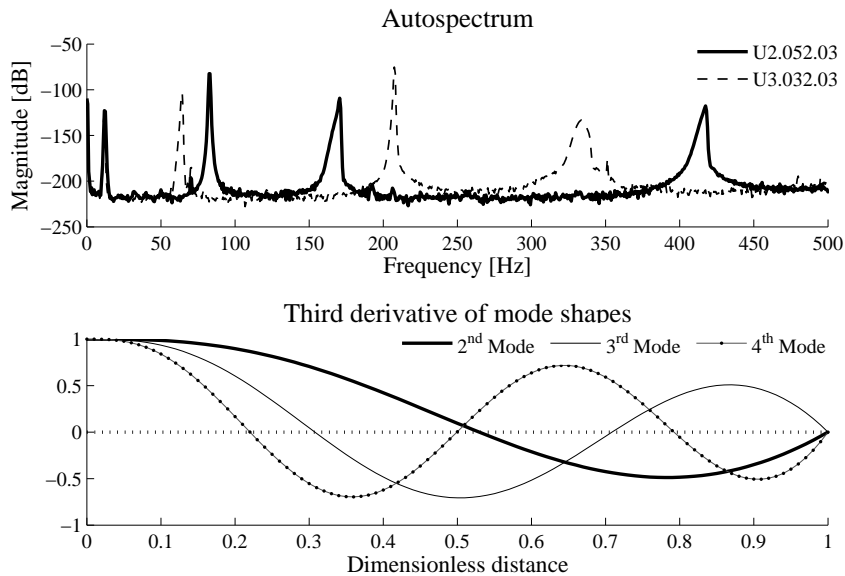


Figure 4.24: Influence of delamination location on resonance frequency shifts for different vibration modes.

Growing delamination

The effects of a delamination on the resonance frequencies is also investigated by enlarging a small delamination in between several modal analyses. This prevents unwanted frequencies shifts as a result of variations in specimen dimensions or material properties. The delamination was enlarged with a sharp razorblade. The effects of a delamination on the resonance frequencies can be monitored closely this way.

Figure 4.25 visualizes this effect. Several measured frequency response plots are plotted in this graph. As can be seen from the figure the effects of a growing delamination are most noticed for the higher vibration modes; the sixth and seventh resonance peak clearly shift to the lower values. For the lower vibration modes the effect is less significant. The sudden shift for the third and fifth resonance frequency for a delamination length of 142mm stands out. In table 4.9 the results are compared to the theoretical analysis. For a small, up to 42mm , delamination length the obtained theoretical results compare very well to the validated resonance frequencies. However as the delamination is enlarged the results show less comparison. Possible explanations were already listed above. One additional reason can be found in the fact that the delaminated surface was very rough. This is caused by the fact that the delamination was forced to grow with the razorblade. This can increase the occurring friction. Previous experiments were only conducted on a smooth predefined delamination surface.

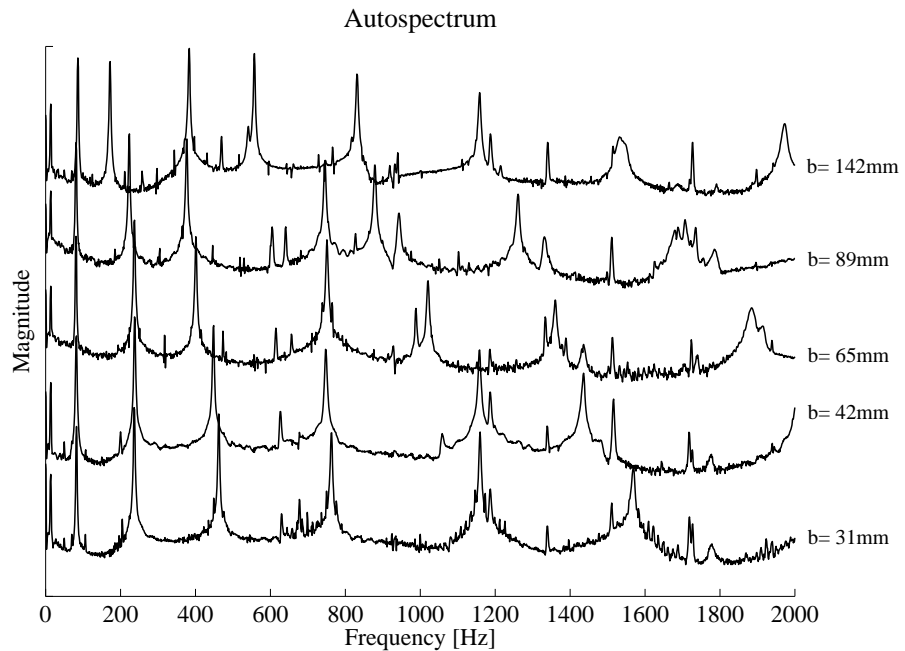


Figure 4.25: Effects of a growing delamination.

4.5.3 Conclusions and recommendations

From the results obtained in this experimental stage it can be concluded that the developed model gives a good indication of the effects of a delamination in vibrating beams. The theoretical and validated resonance frequencies show a similar trend. An average difference of 3.1% between theoretical and measured resonance frequencies of delaminated beams was found. This value was found for the pre-defined delaminations. Less comparison, 3.7%, is found when the delamination was forced to grow. This is probably caused by the newly created rough delamination surface. Because it is unknown in practice how much the measured resonance frequencies deviate from the theoretical model it is hard to use the model for damage localization. For instance, a difference of 3% on the measured second resonance frequency gives significant other results than the same difference on the third vibration mode. Also a more accurate model is desired to be able to predict the shifts in resonance frequencies better. The new model needs improvement in the following fields:

- Implement the effect of an opening delamination. As stated above the requirement that the delamination stays closed during vibration is hard to satisfy practically. The finite element model using contact elements can be extended for this purpose. This will, however, make the analysis far more time consuming since the vibration becomes non-linear.

Vibration Mode	U3.000.00		U3.052.02		S3.052.03		U3.032.02		S3.032.03	
	Theory	Validation	Theory	Validation	Theory	Validation	Theory	Validation	Theory	Validation
1 st	12.0	11	12.1	12	12.0	12	11.7	12	11.4	12
2 nd	77.2	76	77.9	80	77.5	83	73.4	74	65.9	65
3 rd	216.4	221	191.7	199	158.6	170	220.2	220	208.8	208
4 th	428.3	432	424.8	440	374.6	417	360.2	371	313.1	339
5 th	713.3	716	568.6	580	532.7	546	627.3	609	555.4	536
6 th	1071.4	1068	957.0	993	793.8	813	963.3	979	806.5	775
7 th	1502.1	na. [‡]	1248.3	1233	1175.6	1204	1247.9	1239	1183.4	1119

Vibration Mode	Del size: 31mm		Del size: 42mm		Del size: 65mm		Del size: 89mm		Del size: 142mm	
	Theory	Validation	Theory	Validation	Theory	Validation	Theory	Validation	Theory	Validation
1 st	13.03	13	13.0	13	12.9	13	12.7	13	12.5	13
2 nd	82.5	82	82.5	82	80.7	81	78.6	81	77.9	84
3 rd	235.3	236	234.8	237	226.5	237	187.3	223	164.4	208
4 th	458.2	462	446.2	449	389.9	401	369.7	373	355.5	383
5 th	758.7	764	747.1	748	733.7	751	591.1	746	551.1	557
6 th	1160.1	1160	1142	1159	939.4	1021	882.6	878	832.9	821
7 th	1545.9	1570	1445.7	1516	1392.9	1368	1209.8	1261	1169.4	1159

[‡] Unable to identify from autospectrum

Table 4.9: Comparison of theoretical and validated resonance frequencies of specimens with varying delamination parameters and with a growing delamination

- Implement the friction between the two delaminated segments. This also can best be achieved using the contact elements.

In order to validate the analytical and finite element models proposed in chapter 3 other beam specimens should be produced. The uncertainties regarding contact pressure and surface roughness should be avoided. To minimize these issues, specimens of for instance aluminium should be considered. Delaminations can then be created by gluing two aluminium beams. The glue will probably influence the measured damping coefficient but its influence on resonance frequencies will probably be small.

DISCUSSION AND APPLICATION

With the presented theoretical models the resonance frequencies of a delaminated beam can be determined. In this section it is discussed in what extend this model can be used to detect and locate originating delaminations.

5.1 Discussion

A general problem concerning dynamic 'health monitoring' consists of the sensitivity of dynamic parameters to environmental changes. In the literature survey it was already stated that these properties are highly influenced by changes in temperature or humidity. Kawiecki [16] reported that the resonance frequencies of a steel bridge showed variations up to 5% as a result of temperature changes only. This dependency relinquishes the use of *non-model* based techniques outside temperature and humidity controlled environments. A model or extensive database is required to distinguish damage or environmentally induced changes. In this light the application of such systems in for instance airplanes or wind turbine blades still has a long way to go. However in the field of quality control such problems play no role as a stable environment can easily be created. Dynamic 'health monitoring' could therefore be a strong short-term alternative to conventional quality check procedures.

An analytical and two finite element models were presented to determine the resonance frequencies of delaminated beam shaped specimens. The model proved that with the simple measurement of resonance frequencies, delaminations can be detected and located. An advantage of resonance frequencies over other dynamic parameters can be found in the fact that resonance frequencies show insignificant statistical variation. It was experimentally shown that the standard deviation between three measurements at distinct times was found to be less than 0.2%. This allows to detect changes of 1%, which makes resonance frequencies a very accurate parameter to model. For the proposed model however an averaged difference

between theory and validated resonance frequencies of 3.1% was found. It has to be added that this figure applies to the pre-delaminated specimens with a relatively smooth delaminated surface. For the specimen with the enlarged delamination an averaged difference of 3.7% was obtained. For the detection of damage these figures play no role. For the localization however this difference might prove problematic. As indicated in the theoretical model the location is determined by the combination of frequency shifts for various vibration modes. Only for the higher modes a frequency drop of more than 5% is expected. By taking more vibration modes into account the determined results will naturally become more reliable. In order to be able to use the lower vibration modes a more accurate model is required.

This thesis also investigated the possible application of fibre bragg gratings for health monitoring. The advantages over conventional methods to capture vibrations are obvious. The most notable can be found in the fact that fibre bragg gratings can easily be embedded in composite structures. This allows strain measurements inside the host material. Also embedding sensing fibres can be preferred over gluing strain gauges or accelerometers for practical reasons. Additionally, the matrix material will protect the sensors which allows application in harsh environments. Other advantages can be found in the ability of multiplexing, i.e. having multiple sensors on one fibre, and the high resistance against fatigue. In an experimental programme the fibre bragg gratings were evaluated. The main problem encountered was found to be the low signal to noise ratio. Together with the low strains for higher vibration modes, this made it impossible to identify the higher, over 1kHz, resonance frequencies. The data acquisition system itself has a sampling rate of 50kHz, which is certainly fast enough to resolve such frequencies. The poor signal to noise ratio is probably caused by the process conditions of the host material in which the fibres are embedded. The high temperature is known to have a negative influence on signal strength. Extensive research in this field is required.

Despite the low signal to noise ratio, fibre bragg gratings will certainly have a positive influence on the development of dynamic based health monitoring systems. The ability of embedding sensing fibres inside a composite together with the possibility of multiplexing gives a potentially strong measurement system. A network of gratings could be used to survey local strain development over a large area. Besides determining resonance frequencies, a network of sensors will then give the possibility to define mode shapes or determine cross-spectra between different gratings. New algorithms can be developed to make use of all this information simultaneously. Also the development of small lamb waves through the host material can be monitored for damage detection. The development of fibre bragg gratings thus provides new opportunities for dynamic health monitoring.

5.2 Application

The model proposed in section 3 determines the resonance frequencies of delaminated beams. Naturally, the opposite is desired for dynamic health monitoring, i.e. determining the delamination parameters from multiple measured resonance frequencies. In order to achieve this, the presented analytical solution can be rewritten to determine these three parameters (\bar{a}_c , \bar{b} , \bar{h}_2 , see appendix C). A total of three frequency shifts are required to resolve these unknowns. However, because this is a non-linear function, every small error introduced in the measured frequency shifts can result in large deviations. In an attempt to get around this problem, the model is used to construct a database with delamination parameters and their accompanying relative resonance frequency shifts. The fact that multiple shifts are taken into account means that errors in the measured resonance frequencies will have less influence on the found delamination parameters. The number of vibration modes included, determines the accuracy of the prediction. Also a larger database, with smaller increments in delamination parameters, allows a more accurate localization. The general idea is to compare relative resonance frequency shifts for an arbitrary specimen to the values in the database. The differences for each mode between the measured shifts and the database values are squared. By summing the squared differences for all modes some form of error function is obtained. The delamination parameters for which this sum is minimal can be seen as actual parameters.

This concept was tested with a database containing a total of 924 delamination cases. The first six resonance frequencies were considered. The frequency shifts for several arbitrary delamination parameters were then calculated and compared to the database. In case the exact input resonance frequencies were used, the database proved to be large enough to locate the damage in approximately 98% of the cases. However, if an error, e.g. caused by temperature changes, of 5% was introduced on one of the input frequencies it proved to be very difficult to resolve the delamination parameters. This corresponds very well with the statements made earlier. The model is, for now, not accurate enough to use it to locate a delamination. Also any error in the frequency measurements can have a serious influence on the obtained results. The short-term applicability of dynamic measurements for health monitoring should therefore be limited to controlled environments.

CONCLUSIONS AND RECOMMENDATIONS

This thesis investigated the possibilities of on line health monitoring based on dynamic behaviour. A literature survey described the research done in this field. Various techniques based on resonance frequencies, damping values or other modal parameters were discussed. It was chosen to investigate how the resonance frequencies of beam specimens are influenced by a delamination. An analytical model was investigated and extended to determine the resonance frequencies of a delaminated composite beam. In addition two finite element models were constructed. One of these is based on contact elements, which makes it applicable for future more complex analysis. The model was validated with carbon-PEI test specimens with varying delamination parameters. The model could be used to locate delamination based on shifts in the resonance frequencies. A neural network could for instance be used for this purpose. Further this thesis investigated the use of fibre bragg gratings for dynamic health monitoring; experiments concerned accuracy, resolution and data acquisition.

6.1 Conclusions

With respect to the various parts of this thesis, the following conclusions can be drawn:

General dynamic health monitoring

- Health monitoring based on variations in dynamic behavior is a potentially interesting technique. Damage can influence the material or geometrical properties of a structure. As a result the dynamic behaviour changes. Detected changes in modal parameters, like resonance frequencies, damping

values or mode shapes, are then probably caused by damage. Monitoring these parameters might prove interesting as an alternative for laborious 'scanning' non destructive damage detection methods.

- Damage detection algorithms can be divided in two groups, namely *model* and *non-model* methods. As stated in the literature survey *model* based techniques allow localization and quantification of occurring damage. The disadvantage of *model* based health monitoring can be found in the fact that it should be able to represent the actual damage with these models. This will not always be the case. *Non-model* based algorithms are harder to formulate.
- Shifts in resonance frequencies can very well be used as damage indicator. Damage can be detected at the moment it occurs. Also the potential damage location can be extracted by monitoring shifts of resonance frequencies of multiple modes. Resonance frequencies can easily and cheaply be obtained and do not require access to the whole structure under consideration. Also resonance frequencies show relatively little statistical variation.
- Damping is another potential interesting dynamic parameter to monitor. Damping seems to be more sensitive to damage, however no apparent relation exists.

Delamination detection

- The decrease in flexural rigidity as a result of a delamination is compensated by an internal bending moment. This moment is caused by the stretching and compressing of the delaminated segments. In case a delaminated beam is subjected to a pure bending moment this internal moment will fully compensate the loss in flexural rigidity. Only in case a shear force is present and the layers are free to slide, the effect of the delamination can be noticed.
- The decrease in flexural rigidity due to a delamination can be detected with more confidence and accuracy by monitoring shifts of resonance frequency than by a static analysis. Especially frequencies belonging to higher vibration modes are affected considerably.
- The shifts in frequencies are higher in case the delamination is located closer to the neutral plane. Also the length of the delamination has a positive effect on frequency shift.
- By measuring the shifts of resonance frequencies of different modes the axial location of the delamination can be determined. This is caused by the non-uniform shear stress distribution in a vibrating beam. If, for a particular vibration mode, the delamination is located in a region with low shear stress, the effect on resonance frequency for that mode will be minimal. This is caused by the fact that sliding of the delaminated segments will only occur in case a shear force is present.

Fibre bragg gratings

- Fibre bragg gratings can have a positive influence on the development of an applicable online health monitoring system. The ability to measure strain on multiple locations inside the host material offers a huge potential. A network of gratings provides a whole new range of opportunities for damage detection.
- The differences in accuracy and resolution between embedded and free fibre bragg gratings are a cause for concern. The poor signal to noise ratio prevented accurate measurements for higher modes. Research should concentrate on the influence of production parameters on signal strength and noise ratio.
- The tested 50kHz data acquisition system provides the ability to resolve resonance frequencies up to 5kHz confidentially. However the low signal to noise ratio prevented extensive research in this field.

6.2 Recommendations

Online health monitoring has a great potential and will in the future replace expensive routine check-ups. Fibre bragg gratings can play an important role. To aid in its development, the research on this subject should concentrate on the following fields:

- The current finite element model with the contact elements should be extended in order to allow the delamination to open and close during vibration. Also a friction coefficient between the layers should be added. With this new model delaminations can be detected with more accuracy. However, the opening and closing of the delamination results in non-linear vibration. This, however, will seriously complicate the analysis as the solution has to be obtained in the time domain.
- New algorithms should be developed which use the full potential of fibre bragg gratings. A network of gratings will be used to map the strain field in a host structure during vibration. The additional information can be used to extract mode shapes and cross-spectra between different gratings. A new algorithm should be able to use all this information for health monitoring.
- In order to use the gratings for health monitoring the problems regarding loss of accuracy and poor resolution should be solved. The influence of production parameters, like consolidation temperature and pressure, on embedded fibre bragg gratings has to be investigated. Embedding a sensing fibre should have no influence on its resolution or accuracy.

- Data acquisition system software has to be developed. New software should be able to extract autospectra or even frequency response functions from measured data. The system should be able to average a series of measurements.

BIBLIOGRAPHY

- [1] R. D. Adams, D. Walton, J.E. Flitcroft, and D. Short. Vibration testing as a non-destructive test tool for composite materials. *Composite reliability*, page 159, 1975.
- [2] R.D. Adams and D.G.C. Bacon. Dynamic properties of unidirectional fibre reinforced composites in flexure and torsion. *Journal of composite materials*, 7:53–67, 1973.
- [3] P. Cawley and R. D. Adams. A vibration technique for non-destructive testing of fibre composite structures. *Journal of composite materials*, 13:161–175, 1978.
- [4] P. Cawley and R.D. Adams. Improved frequency resolution from transient tests with short record lengths. *Journal of sound and vibration*, 64:123–132, 1979.
- [5] P. Cawley and R.D. Adams. The location of defects in structures from measurements of natural frequencies. *Journal of strain analysis*, 14(4):49–57, 1979.
- [6] R. Chandra, S.P. Singh, and K. Gupta. Damping studies in fiber-reinforced composites -a review. *Composite structures*, 46:41–51, 1999.
- [7] T.G. Chondros, A.D. Dimarogonas, and J. Yao. A continuous cracked beam vibration theory. *Journal of sound and vibration*, 215:17–34, 1998.
- [8] N.A. Chrysochoidis and D.A. Saravanos. Assessing the effects of delamination on the damped dynamic response of composite beams with piezoelectric actuators and sensors. *Smart materials and structures*, 13:733–742, 2004.
- [9] S.W. Doebling, C.R. Farrar, M.B. Prime, and D.W. Shevitz. Damage identification and health monitoring of structural and mechanical systems from changes in their vibration characteristics: A literature review. Technical Report LA-13070-MS, Los Alamos National Laboratory, May 1996.
- [10] C.R. Farrar and S.W. Doebling. An overview of modal-based damage identification methods. *Proc. of DAMAS Conference*, 1997.

- [11] P. Gudmundson. Eigenfrequency changes of structures due to cracks, notches or other geometrical changes. *Journal of mechanics, physics and solids*, 30(5):339–353, 1982.
- [12] F.J. Guild and R.D. Adams. The detection of cracks in damaged composite. *Journal of physics D: Applied physics*, 14(8):1651–1573, 1981.
- [13] F.J. Guild and R.D. Adams. A new technique for the measurement of the specific damping capacity of beams in flexure. *Journal of physics E: Scientific instruments*, 14:355–363, 1981.
- [14] S. Hassiotis and G.D. Jeong. Assessment of structural damage from natural frequency measurements. *Computers and structures*, 49(4):679–691, 1993.
- [15] H.H. Hu, B-T. Wang, C-H. Lee, and J-S. Su. Damage detection of surface cracks in composite laminates using modal analysis and strain energy method. *Composite structures*, 74:399–405, 2006.
- [16] G. Kawiecki. Modal damping measurement for damage detection. *Smart materials and structures*, 10:466–471, 2001.
- [17] H.Y. Kim. Vibration-based damage identification using reconstructed frfs in composite structures. *Journal of sound and vibration*, 259(5):1131–1146, 2003.
- [18] C. Kyriazoglou, B.H. Le Page, and F.J. Guild. Vibration damping for crack detection in composite laminates. *Composites part A: applied science and manufacturing*, 35:945–953, 2004.
- [19] B.T. Lee, C.T. Sun, and D. Liu. An assessment of damping measurement in the evaluation of integrity of composite beams. *Journal of reinforced plastics and composites*, 6:114–125, April 1987.
- [20] J. Lee. Free vibration analysis of delaminated composite beams. *Computers and structures*, 74:121–129, 2000.
- [21] P.M. Mujumdar and S. Suryanarayan. Flexural vibrations of beams with delaminations. *Journal of sound and vibration*, 128(3):441–461, 1988.
- [22] W.M. Ostachowicz and M. Krawczuk. Analysis of the effect of cracks on the natural frequencies of a cantilever beam. *Journal of sound and vibration*, 150(2):191–201, 1991.
- [23] A.K. Pandey, M. Biswas, and M.M. Samman. Damage detection from changes in curvature mode shapes. *Journal of sound and vibration*, 145(2):321–332, 1991.
- [24] D.P. Patil and S.K. Maiti. Experimental verification of a method of detection of multiple cracks in beams based on frequency measurements. *Journal of sound and vibration*, 281:439–451, 2005.

- [25] C.J. Pye and R.D. Adams. Detection of damage in fibre reinforced plastics using thermal fields generated during resonant vibration. *NDT International*, pages 111–118, 1981.
- [26] R.L. Ramkumar, S.V. Kulkari, and R.B. Pipes. Free vibration frequencies of a delaminated beam. In *Annual Technical Conference*, pages 1–5. Reinforced/Composites Institute, Society of plastics industry, 1979.
- [27] A. Rytter. *Vibration based inspection of civil engineering structures*. PhD thesis, Aalborg University, Denmark, 1993.
- [28] O.S. Salawu. Detection of structural damage through changes in frequency: a review. *Engineering structures*, 19:718–723, 1997.
- [29] R.P.C. Sampaio, N.M.M. Maia, and J.M.M. Silva. Damage detection using the frequency-response-function curvature method. *Journal of sound and vibration*, 226(5):1029–1042, 1999.
- [30] D.A. Saravanos and D.A. Hopkins. Effects of elaminations on the damped dynamic characteristics of composite laminates: Analysis and experiments. *Journal of sound and vibration*, 195(5):977–993, 1996.
- [31] C.T. Sun, B.T. Lee, and S.K. Chaturvedi. Composite material damping using impulse technique. In L. Rogers, editor, *Vibration Damping 1984; Workshop proceedings*, pages 1–24, November 1984.
- [32] L.H. Tenek, E.G. Henneke, and M.D. Gunzburger. Vibration of delaminated composite plates and some applications to non-destructive testing. *Composite structures*, 23:253–262, 1993.
- [33] F.G. Tomasel, H.A. Larrondo, and P.A.A. Laura. Detecion of cracks in cantilever beams: experimental set-up using optical tecniques and theoretical modelling. *Journal of sound and vibration*, 228(5):1198–1204, 1999.
- [34] S.H. Diaz Valdes and C. Soutis. Delamination detection in composite laminates from variations of their modal characteristics. *Journal of sound and vibration*, 228:1–9, 1999.
- [35] J.T.S. Wang, Y.Y. Liu, and J.A. Gibby. Vibration of split beams. *Journal of sound and vibration*, 84:491–502, 1982.
- [36] L. Warnet. *On the effect of residual stresses on the transverse cracking in cross-ply carbon-polyetherimide laminates*. PhD thesis, University of Twente, 2000.
- [37] L. Warnet and R. Akkerman. *Composite Course 2006*. University of Twente, 2006.
- [38] D. Wendtland. *Aenderung der Biegeeigenfrequenzen einer idealisierten Schaufel durch Risse*. PhD thesis, University of Karlsruhe, 1972.

- [39] M.M.F. Yuen. A numerical study of the eigenparameters of a damaged cantilever. *Journal of sound and vibration*, 103(3):301–310, 1985.
- [40] Y. Zou, L. Tong, and G.P. Steven. Vibration based model dependant damage (delamination) identification and health monitoring for composite structures -a review. *Journal of sound and vibration*, 230:357–378, 2000.

DATA ACQUISITION AND USED HARDWARE EQUIPMENT

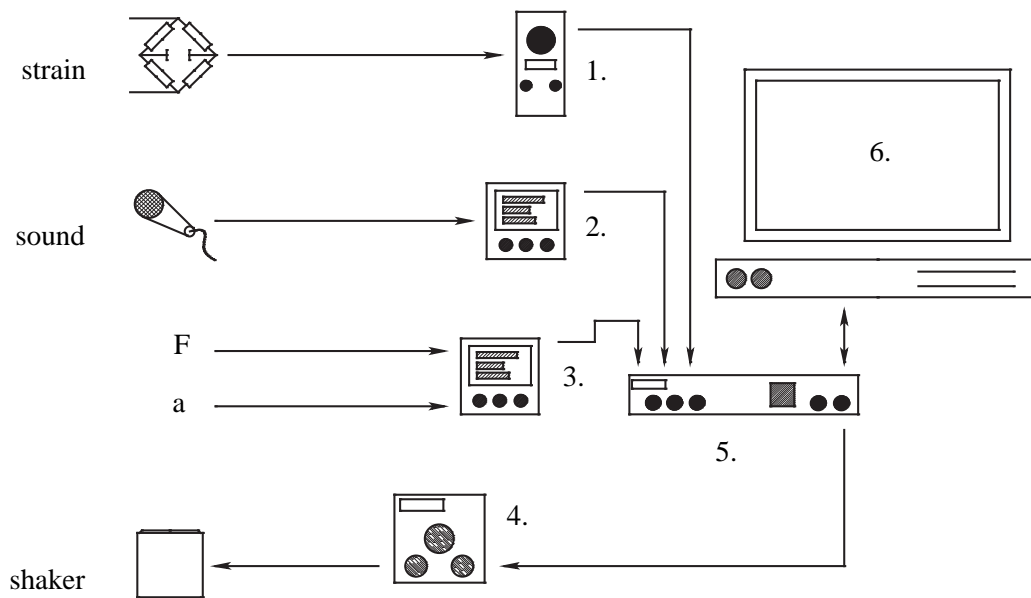


Figure A.1: Data acquisition scheme for the dynamic set-up.

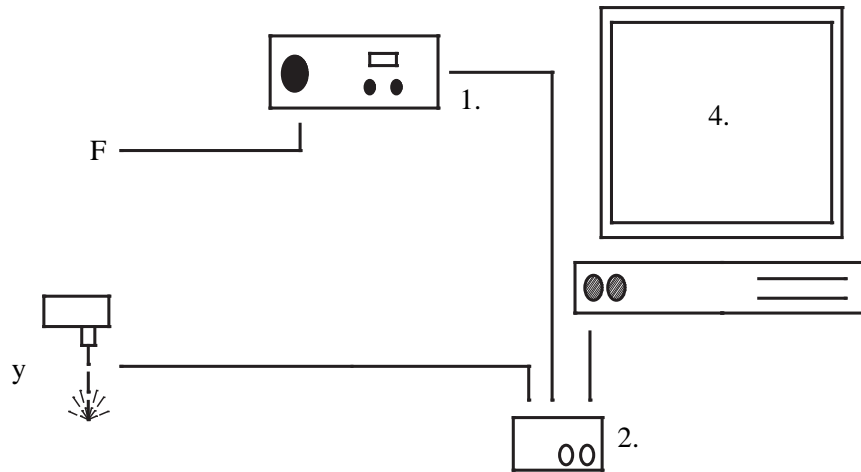


Figure A.2: Data acquisition scheme for the static set-up.

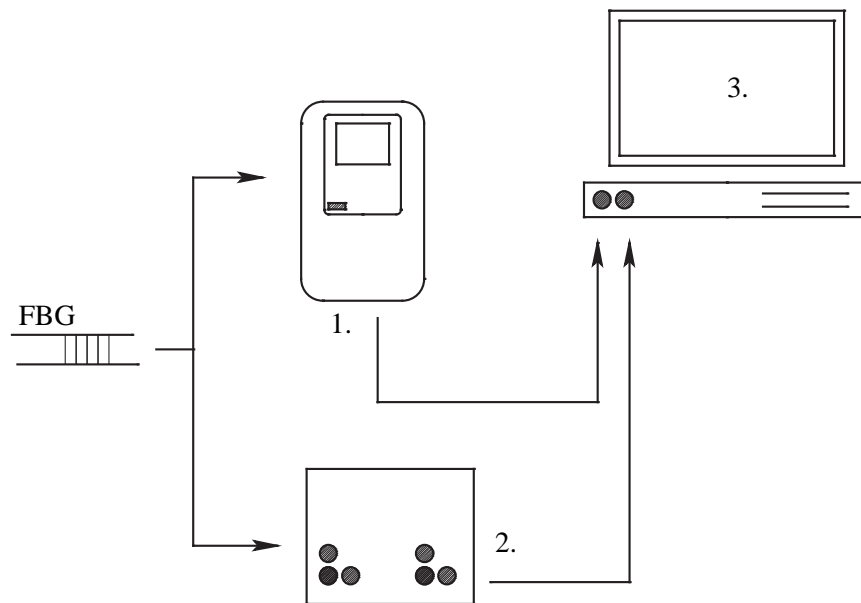


Figure A.3: Data acquisition scheme for the fibre bragg gratings.

N ^o	Hardware	Description
DYNAMIC SET-UP FIG. 4.1		
1	Shaker	B&K 4802
2	Force transducer	B&K 8203
3	Accelerometer	B&K 4517C-001
4	Strain gauges	TML 350 Ω , length 6mm
5	Fibre Bragg grating	FOS&S
6	Microphone	B&K 4192L
7	Spring	
DYNAMIC DATA ACQUISITION FIG. A.1		
1	Bridge amplifier	Fylde DC 500kHz
2	Charge condition amplifier	B&K Nexus
3	Charge condition amplifier	B&K Nexus
4	Power amplifier	B&K 2706
5	Digital sensor processor	Siglab 20-42
6	PC	
STATIC SET-UP FIG. 4.12		
1	Force cell	HBM 50N
2	Laser distance meter	Micro-epsilon non-contact
STATIC DATA ACQUISITION FIG. C.1		
1	Bridge amplifier	HBM AC amplifier
2	Data acquisition	NI USB-6008 Data Acq. Syst.
3	PC	
FBG DATA ACQUISITION FIG. A.3		
1	Slow data acquisition	SpectralEye 600
2	Fast data acquisition	50kHz Slope DAQ
3	PC	

Table A.1: Used measurement hardware.

SPECIMEN FABRICATION SCHEME

1. The needed amount of plies are cut out of a roll of pre-impregnated carbon-polyetherimide. Before the material can be used, they are put in a vacuum oven at 80°C for about 24 hours. The vacuum and high temperature makes sure that any moisture evaporates.
2. The plies are stacked, in the preferred lay-up, inside a mould. A sheet of polyamide is placed between mould and stacked pile to prevent the polyetherimide to stick to the mould. In case fibre bragg gratings are embedded, space is created by cutting a small strip out of the ply. The sensing fibre is fixed by sticking it to a ply with a polyamide adhesive tape. Delaminations are created by placing polyamide kapton foil at desired places. The foil prevents two plies to melt together and thus a delamination is formed. Meanwhile a press is heated to a temperature of 316°C¹.
3. The mould is closed and placed inside the press. A pressure of 2bar is applied for five minutes. The high temperature allows the polyetherimide matrix to melt. The relatively low pressure prevents that sensing fibre is crushed.
4. After the five minutes a pressure of 9bar is applied. During an additional five minutes the temperature of 316°C is maintained. Hereafter the temperature is gradually, in one hour, decreased to 20°C. The melted matrix material solidifies and binds the carbon fibres and fibre bragg gratings together.
5. The result is a laminated carbon-polyetherimide plate. Test specimens are sawn out of the plate and used in the experimental validation programme.

¹In case sensing fibres were embedded a consolidation temperature of 300°C was used. High temperatures can have a negative influence on signal strength.

SPECIMEN DIMENSIONS AND DELAMINATION PARAMETERS

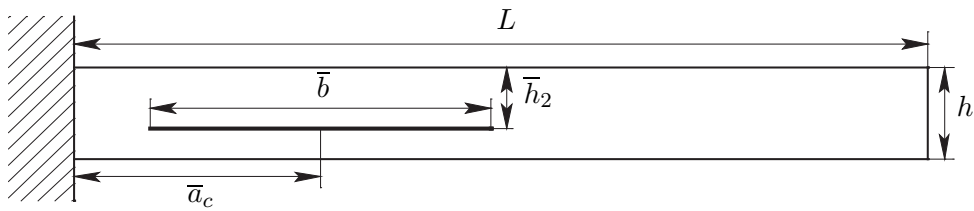


Figure C.1: Specimen and delamination parameters.

Specimen ID	Specimen size			Del. parameters			FBG
	L (mm)	w (mm)	h (mm)	\bar{a}_c	\bar{b}	\bar{h}_2	
U1.00.000	320	20.1	1.67	na.	na.	na.	no
U1.06.025	320	20.1	1.66	.5	.6	.25	no
U1.06.050	320	19.9	1.67	.5	.6	.5	no
U2.000.00	455	20.1	2.31	na.	na.	na.	yes
U2.052.02	455	20.1	2.32	.52	.2	.5	yes
U2.052.03	455	19.9	2.32	.52	.3	.5	yes
U2.032.02	455	20.0	2.32	.32	.2	.5	yes
U2.032.03	455	20.0	2.32	.32	.3	.5	yes
U2.grow	435	19.9	2.31	.32	.05	.5	no

Table C.1: Specimen dimensions and configuration.